Mechanisms and prevention of variable craniofacial defects in *Twisted gastrulation* mutant mice

A DISSERTATION
SUBMITTED TO THE FACULTY OF THE GRADUATE SCHOOL
OF THE UNIVERSITY OF MINNESOTA
BY

Charles John Billington, Jr.

IN PARTIAL FULFILLMENT OF THE REQUIREMENTS
FOR THE DEGREE OF
DOCTOR OF PHILOSOPHY

Anna Petryk, Advisor
Michael O'Connor, Co-advisor

February, 2013

© Charles Billington Jr. 2013

Acknowledgements

There are many people to thank without whom this thesis would simply not be here or without whom it would not be as good, or without whom I would not have made it through the researching and writing process. I will do my best to recognize some of them here.

A complete list of authors for this thesis could justifiably include many more names than just mine. In the case of colleagues involved with the research for chapters 2, 3, and 4 these authors have already been recognized as authors on publications associated with those projects. In the case of chapter 5 the following people should also be specifically credited for their assistance: Ashley Peterson, Brian Schmidt, Raphael Huntley, Kim Mansky, Raj Gopalakrishnan, and Anna Petryk.

I could not have done any of this work without my lab. Firstly and most importantly, I thank my advisor Anna Petryk. Her expectations of excellence, encouragement of my ideas and her (at times tried) patience with my difficulties and many missteps are deeply appreciated. I also owe a debt of thanks to some amazing lab staff, Brian Schmidt and Ashley Petersen, whose efforts made so many of my projects possible or at least much easier. I would also like to thank my fellow students BreAnne MacKenzie and especially Cynthia Forsman for insight and effort on projects in this work. I would also like to express appreciation for the efforts of Brandon Ng, Nate Burbach, Alison Riehle, Nevin Shenouda, Taylor Sulerud and Lauren Jelenchick, and the support of Jim Omlie, Claire Kuo and Rachel Heinze.

Our lab has worked closely with many other labs during my graduate education. Members of many other labs have helped directly with advice or assistance on the experiments or procedures reported in this thesis. Firstly, I owe great thanks to the lab of my co-advisor Michael O'Connor, where I particularly want to thank Mu Sun, Mary-Jane O'Connor, Aidan Petersen, Arpan Ghosh, Rachel Herder and Christina Brakken-Thal. In the lab of Vivian Bardwell and David Zarkower I would like to thank Tony Krentz, Michelle Hamline, Teng Zhang, Clint Matson, Mark Murphy, and Micah Gearhart. In the lab of Michael Georgieff, I appreciate the help of Erik Carlson, Stephanie Fretham, and Phu Tran. I owe an incredible depth of gratitude to the labs of Kim Mansky and Raj Gopalakrishnan where I have benefitted from the help of Eric Jensen, Ann Emery, Lan Pham, Aaron Broege, and Raphael Huntley. I also owe thanks to several other collaborators on various projects and want to thank Aaron Sarver, Lei Zhang, Jim Hodges, Anindya Bagchi, Thomas Mueller, Juliane Fiebig, Keiko Akagi, David Symer, Gunnar Schotta, and Wuming Gong. I'd like to thank the lab of Kaylee Schwertfeger and I also would particularly like to thank the members of the other Developmental Biology center labs, including particularly the members of the labs of Jeff Simon, Laura Gammill, Hiroshi Nakato, Yasu Kawakami and Tom Neufeld for their support over the years.

I want to take the opportunity to recognize the support staff at the University of Minnesota. In RAR, I particularly want to thank Brenda Koniar and Linda Kiey, as well as our several animal techs, who helped care for our mice. In the MCDB&G program I want to thank Sue Knoblauch and Tami Jauert for their administrative help throughout my time in MCDB&G. I also owe an amazing amount of thanks to the staff and faculty of the University of Minnesota Medical Scientist Training Program (MSTP) including Nick Berg, Tucker LeBien, Yoji Shimizu, and Susan Shurson for administrative and academic help and support. I'd also like to thank Cathy Carlson and Denis Clohisy and the Musculoskeletal Research Training Program as well as Ann Hagen and Mark Herzberg in the Minnesota Craniofacial Research Training program (MinnCResT). I was supported financially by the MSTP, the Musculoskeletal Research Training Program and MinnCResT throughout my time in graduate school and am very grateful for this support.

I want to thank the members of my committee for their insights and interest in my work and in my development as a scientist. Raj Gopalakrishanan, and Kim Mansky were an amazing source of advice and encouragement as well as close collaborators throughout my time in the PhD. York Marahrens assisted with some fascinating ideas and analysis trying to better understand the causes of phenotypic variation. Lisa Schimmenti was my teaching mentor and also provided some really helpful discussions on several aspects of the project. Kathleen Conklin served as my committee chair for both preliminary and final examinations and was a great source of support in the MCDB&G program. I'd like to thank my co-advisor Mike O'Connor. Finally, I thank once again and most importantly my primary advisor Anna Petryk. You have opened so many doors for me, at every chance you got and I cannot thank you enough.

On a more personal note, I thank my family: my mother and father, Susan and Charles Sr., and my sister, Beth, for their love and support over all these years. Their trenchant questions, encouragement and willingness to hear me digress at length on genetics, deformed baby mice, diets and assays helped shape this work and their support through the tougher parts of the process was invaluable. Finally and inestimably, thanks to my partner, friend, and biggest supporter, my intended wife, Jennifer. I couldn't have done it without you.

Dedication

This thesis is dedicated
In memory of Helen K. Berry and
In honor of Wilbur T. Billington.

My grandmother, Helen K. Berry, was a pioneer in care for children with genetic and metabolic diseases. She was trailblazer in genetics and biochemistry and a woman scientist in a time when this was rare. Her work looking at dietary modifications to prevent genetic disease seems particularly relevant in light of some of the results reported herein. Helen passed away a few months after this thesis was defended and is fondly remembered.

My grandfather, Wilbur T. Billington, graduated with his PhD from the University of Minnesota, 61 years before this thesis will complete my graduate education. He has given tireless effort in the cause of education. He is an exemplar of the idea that "*to whom much is given, of him much will be expected*." He is my role model and he is much loved.

Abstract

Craniofacial birth defects are associated with significant morbidity and mortality and can be highly variable in their severity and presentation. One key regulator of proper craniofacial development is the action of bone morphogenetic proteins (BMPs). Twisted gastrulation (TWSG1) modulates BMP signaling and the mutation of TWSG1 in mice results in a range of mild to severe birth defects, including forms of holoprosencephaly and dysgnathia. TWSG1 is a glycoprotein with sugar modifications which are essential for proper BMP binding and normal activity of TWSG1. In the mouse TWSG1 protein these sugars are attached in the region of the protein encoded by exon 4. The variable phenotypes resulting from exon 4 deletion (*Twsg1*$^{-/-}$) in mice are associated with distinct sets of transcriptional changes compared to wild type, even for apparently unaffected embryos. The action of p53 plays a key role in the manifestation of severe birth defects in *Twsg1*$^{-/-}$ mice, correlating with previously observed increases in apoptosis. Genetic deficiency of p53 is associated with reduced defects in *Twsg1*$^{-/-}$ mice. Some of the craniofacial defects in *Twsg1*$^{-/-}$ mice, specifically defects associated with the first branchial arch but not holoprosencephaly or midline defects, can be limited by maternal dietary supplementation with methyl donor compounds including folate, choline, betaine and vitamin B12. Previous pregnancy increases the risk of birth defects in *Twsg1*$^{-/-}$ mice. A mouse model of TWSG1 over-expression has been generated to further investigate the action of this gene and provide a reagent for future experiments examining the role of TWSG1 in development.

Table of Contents

List of Tables

List of Figures

Chapter 1: Background and significance

Craniofacial development and craniofacial disorders

In the United States, a child is born with a birth defect approximately every 4.5 minutes. Birth defects are the leading cause of infant mortality, accounting for 1 in 5 infant deaths (March-of-Dimes, 2010). Of babies born with defects, up to 1 in 3 have anomalies of the head and face (Trainor, 2010). These defects can be associated with significant impact on quality of life, both socially and functionally. Care for children with these defects can also be very costly. For example, up to $697 million is spent per year for therapy related to cleft lip and/or cleft palate alone in the United States. Better strategies are needed to limit the incidence of craniofacial birth defects.

Craniofacial defects typically arise very early in development between the second and fifth weeks of gestation in humans, often before pregnancy is even recognized. In the middle of the third week of development in humans (Larsen et al., 2001), and about embryonic day 7.5 (E7.5) in mice (Aoto et al., 2009; Lipinski et al., 2010), the prechordal plate forms anterior to the notochord of the neurulating embryo. This structure is responsible for helping pattern the midline of the developing head and brain, one of the most important signaling molecules for this being Sonic hedgehog (SHH) (Dale et al., 1997; Aoto et al., 2009).

Holoprosencephaly (HPE) originates from a failure of proper midline division in the forebrain and midline facial development during early embryogenesis. HPE is

among the most common disorders of early development, and is seen in up to 1 in 250 conceptuses, and 1 in 10,000 live births (Matsunaga and Shiota, 1977; Muenke and Beachy, 2000). HPE exhibits a range of phenotypes of varying severity with some individuals severely affected and others only minimally affected, with "microforms", if at all (Roessler et al., 1996; Ming and Muenke, 2002; Hehr et al., 2004).

In the beginning of the fourth week the neural tube begins to close. During this process neural crest cells (NCC) delaminate from the edges of the neural folds and migrate in streams to other points in the developing embryo. By the middle of the fourth week of development the branchial arches begin to form (Larsen et al., 2001). Branchial arch 1 (BA1) is an embryonic structure that will give rise to much of the lower half of the face. BA1 is made up of contributions from all three germ layers and, significantly a major portion of the mesenchyme of the branchial arches is NCC-derived. In BA1 the NCC come specifically from the caudal half of the midbrain and the first two rhombomeres of the hindbrain (Kontges and Lumsden, 1996)

Defects of BA1 can result in poor growth or absence of the jaw. When accompanied by ventral displacement of the ears, this is called otocephaly. Otocephaly can be seen in conjunction with HPE in very severe cases (Pauli et al., 1983; Tovitto and Rodriguez, 2007; Gekas et al., 2010; Chaoui et al., 2011). The most extreme form of otocephaly is aprosopia, non-formation of the face (Tovitto and Rodriguez, 2007).

Bone morphogenetic proteins (BMPs) are key signaling molecules during facial development. BMPs are involved in NCC formation, craniofacial skeleton

morphogenesis and palatal development (Nie et al., 2006) and cooperate with signals like SHH and Fibroblast Growth Factors (FGFs) to pattern the developing structures of the head.

Action of TWSG1, interaction with BMPs

Twisted gastrulation (Tsg, called TWSG1 in mammals) is a secreted BMP binding glycoprotein (Mason et al., 1994; Vilmos et al., 2001). TWSG1 acts through regulation of BMP signaling and has been proposed to have both agonistic (Mason et al., 1994; Oelgeschlager et al.; Oelgeschlager et al., 2003; Little and Mullins, 2004; Xie and Fisher, 2005) and antagonistic (Chang et al., 2001; Ross et al., 2001; Scott et al., 2001; Blitz et al., 2003; Gazzerro et al., 2005; Wills et al., 2006) actions on BMP signaling depending on the developmental context. Tsg was first discovered based on its impact on dorsal-ventral patterning in the early *Drosophila* embryo (Zusman and Wieschaus, 1985). The dorsal midline of the *Drosophila* embryo is patterned by a gradient of decapentaplegic (Dpp) (homologous with vertebrate BMPs 2 and 4) with peak signaling in the region that becomes an embryonic structure called the amnioserosa (Podos and Ferguson, 1999; Dale, 2000; Shimmi and O'Connor; Shimmi et al., 2005; O'Connor et al., 2006). Mutation of *tsg* was found to block the formation of the amnioserosa (Mason et al., 1994; Mason et al., 1997). This suggested that Tsg might help promote Dpp/BMP signaling. Set against this, a later study found that Tsg could potentiate the action of a Dpp inhibitor, Sog (homologous with vertebrate Chordin, CHRD) and that loss of function of this inhibitor had a similar phenotype to that of loss of Tsg (Yu et al., 2000).

This inhibitory role of TWSG, especially in cooperation with CHRD, was further characterized in vertebrate studies (Chang et al., 2001; Ross et al., 2001; Scott et al., 2001). The seeming paradox of TWSG1 being an inhibitor of BMPs while sometimes promoting BMP signaling was partially resolved by two hypotheses 1) that TWSG1 might facilitate transport of BMP ligands to sites of peak action as part of a morphogen gradient (Harland, 2001; Shimmi and O'Connor, 2003; Shimmi et al., 2005; O'Connor et al., 2006; Sawala et al., 2012) and 2) that while TWSG1 can form a BMP-inhibitory complex with CHRD, it can also facilitate cleavage of CHRD by the protease BMP1/Tolloid (Larrain et al., 2001; Oelgeschlager et al.; Xie and Fisher, 2005). Although TWSG1 may have pro-BMP activities in some contexts, evidence from mammalian cell culture systems, both in cell lines and in primary cultures (Graf et al., 2002; Gazzerro et al., 2005; Petryk et al., 2005; Schmidl et al., 2006; Sotillo Rodriguez et al., 2009; Tanno et al., 2009), supports the idea of TWSG1 as primarily an inhibitor of BMP signaling.

Mouse models of TWSG1 deficiency

Several mouse models of TWSG1 deficiency have been developed to investigate the role of TWSG1 in mammalian development and in adult tissues. Exon 2 of the gene, which contains the initial ATG-start of protein translation, has been deleted in two different models, and replaced either with a simple neomycin resistance (neo^R) cassette (Nosaka et al., 2003) or with a *LacZ-*neo^R transgene (Zakin and De Robertis, 2004). Another model has disruption of the *Twsg1* gene at exons 2 and 3 with a *LacZ-*neo^R

insertion (Gazzerro et al., 2006). Our lab has developed a model of TWSG1 deficiency by LoxP-flanking and deleting the fourth exon of the *Twsg1* gene (Petryk et al., 2004).

These models showed some common phenotypes in mixed or non-BL/6 backgrounds including small size and vertebral and skeletal defects (Canalis et al., 2003; Nosaka et al., 2003; Petryk et al., 2004; Zakin and De Robertis, 2004). The osteopenia (Nosaka et al., 2003; Zakin and De Robertis, 2004) observed in *Twsg1*$^{-/-}$ mice has been shown to result from overactive osteoclasts secondary to excess BMP signaling (Sotillo Rodriguez et al., 2009).

In the C57BL/6 background, *Twsg1*$^{-/-}$ mice exhibited a range of striking craniofacial malformations (Petryk et al., 2004). These mutations included midline facial and forebrain defects characteristic of HPE as well as jaw defects ranging from micrognathia to agnathia, consistent with otocephaly. Pups affected with severe midline defects also showed agnathia, similar to the agnathia-holoprosencephaly complex (Pauli et al., 1983). The most severely affected pups had anterior truncation (aprosopia) and showed no development of anterior facial structures. Our lab has also observed cleft lip and palate in *Twsg1*$^{-/-}$ mice (*cf. infra,* Chapter 4). The craniofacial defects in *Twsg1*$^{-/-}$ mice showed incomplete penetrance with only 44% of homozygous mice showing craniofacial abnormalities. These mice also showed variable expressivity with a range of phenotypes being observed. The variation of phenotypes was visible as early as E9.5 where embryos were observed to have midline defects and mandibular arch defects of differing severity (MacKenzie et al., 2009). The similarity of the phenotypes seen in

Twsg1$^{-/-}$ mice to those seen in mice deficient for the BMP inhibitors CHRD and Noggin (NOG) (Anderson et al., 2002) suggests that TWSG1 acts as a BMP antagonist in promoting forebrain development.

TWSG1 deficiency was associated with reductions in *Shh* expression in the rostral ventral neural midline at embryonic day E9.5 (Petryk et al., 2004). Malformed *Twsg1*$^{-/-}$ embryos showed loss of expression of *Msx1* and *eHand* (*Hand1*), ventrally shifted and reduced expression of *Bmp4* and *Msx2*, and ectopic expansion of *Fgf8* and *Barx1* across the midline of a fused BA1. On a cellular level, premature BA1 fusion was associated with massively increased apoptosis (MacKenzie et al., 2009), consistent with the idea that ectopic and increased apoptosis is a potential mechanism of birth defects (Sulik et al., 1988). Mice deficient for CHRD and NOG show similar increases in BA1 apoptosis indicating that ectopic BMP signaling can drive this increase in cell death (Stottmann et al., 2001).

Single gene inheritance with multifactorial determination of phenotype as a conceptual framework for understanding the craniofacial defects of *Twsg1*$^{-/-}$ mice

The variable expressivity and incomplete penetrance seen in craniofacial abnormalities such as defects of BA1, those in the HPE spectrum, or in orofacial clefting, suggests that these disorders are the result of multiple factors working together to generate the phenotype (Fraser, 1970; Murray, 2002; Dixon et al., 2011). In classical Mendelian genetics, inheritance is determined allelically, while in multifactorial inheritance the manifestation of a phenotype is due to complex interactions of genetic and

environmental factors. A given genetic defect may predispose an individual or family to certain birth defects, but the occurrence of the full effect of that predisposition is dependent on the combined action of genes at other loci and environmental factors (Nora, 1968; Nussbaum et al., 2007). The hypothesis of complex or multifactorial etiology rather than simple single gene inheritance has a long history in craniofacial defects including all of the major craniofacial defects seen in the *Twsg1* mutant mouse.

HPE presents an excellent example of a disease which can have multifactorial inheritance leading to variable penetrance and expressivity. Underlying this multifactorial inheritance is a wide range of genetic and environmental causes for HPE (Roessler and Muenke, 1999; Muenke and Beachy, 2000; Muenke and Cohen, 2000; Cohen and Shiota, 2002). For example, even when a family has a genetic defect known to be highly predisposing for HPE, phenotypes range from apparently unaffected or minimally affected, all the way to profoundly affected (Roessler et al., 1996; Hehr et al., 2004). The vast range of causes associated with HPE that could act together as contributing factors, combined with the range of phenotypes seen, has led to a multiple hit hypothesis for the etiology of HPE (Ming and Muenke, 2002).

Otocephaly is much rarer than HPE or clefting in humans but, based on evidence from animal models dating as far back as the 1920s (Utkus et al., 2001) has also been proposed as having a multifactorial etiology, in at least some cases. Significantly, in three different mouse models for otocephaly, the *Twsg1*$^{-/-}$ mouse (Petryk et al., 2004), the *Otx2*$^{-/-}$ mouse (Matsuo et al., 1995) and the *Pgap1*$^{-/-}$ mouse (Juriloff et al., 1985), the

C57BL/6 strain is an important permissive factor for otocephalic defects, with other inbred mouse strains being largely resistant. This strain dependence immediately suggests the action of other genetic loci, fixed in the strain, in exacerbating the molecular triggers leading to defects in each of these mice. Some of the other modifying loci in the BL/6 strain have begun to be characterized for the *Otx2* mouse (Hide et al., 2002). The action of other genes as modifiers of the phenotypes for each of these genes supports a multiple hit hypothesis for the mechanism of otocephalic defects in mice.

Taken together, these lines of evidence relating to the different types of defects seen in *Twsg1* deficient mice suggest a model where the defects in these mice are multifactorial in origin, with mutation of *Twsg1* predisposing to defects while other genetic and environmental factors act on that predisposition. The predisposition is based on a single gene (as in Mendelian inheritance) while the realization of the phenotype is subject to modification by other genetic and environmental factors (as in multifactorial inheritance). This interaction of a genetic lesion with other factors, in combination with the wide range of severity and phenotypes affecting nearly every aspect of craniofacial development make the *Twsg1* deficient mouse an invaluable model. The model's inherent susceptibility to defects allows it to provide information not only about the molecular underpinnings of how craniofacial defects are actually realized, but also about the genetic and environmental factors that contribute to the prevention or actualization of those defects.

Objective, rationale, summary

The objective of this thesis project has been to uncover the molecular mechanisms underlying the phenotypes associated with *Twsg1* mutation, and to identify contributing factors for and ways to ameliorate these phenotypes.

The rationale of these lines of investigation in the *Twsg1* deficient mouse lies in the potential to develop preventive therapeutic interventions for craniofacial defects. If the factors which drive a predisposition towards an actual defect can be uncovered and eliminated, or conversely, if protective factors can be identified this will suggest preventive interventions to limit the incidence or severity of craniofacial defects.

This thesis examines some of the molecular consequences and modifying factors of *Twsg1* mutation. It begins in the second chapter with the impact of mutation on the interaction between TWSG1 and BMPs and uncovers a role for protein glycosylation in that interaction. Next, in chapter 3, it explores the patterns of gene transcription changes underlying different BA1 phenotypes in *Twsg1*$^{-/-}$ animals. Drawing on these data it demonstrates a genetic strategy for reducing defects. Chapter 4, examines the modifying effects of diet and parity as they impact the incidence and types of craniofacial defects of the *Twsg1*$^{-/-}$ mouse. Finally, the last chapter describes the generation and initial characterization of a transgenic mouse with increased *Twsg1* expression to be used as a model in future studies. The thesis is organized around the pursuit of the following specific aims:

Specific Aims:

Aim 1: Investigate the role of *Twsg1* exon 4 in the interaction with BMP.

Aim 2: Characterize the transcriptional changes in BA1 and the underlying molecular and cellular alterations associated with variable *Twsg1*$^{-/-}$ phenotypes.

Aim 3: Investigate the role of maternal diet and maternal parity in modifying the frequency of *Twsg1*$^{-/-}$ phenotypes.

Aim 4: Develop a conditional mouse model of *Twsg1* overexpression.

Chapter 2: Glycosylation of Twisted gastrulation is required for BMP binding and activity during craniofacial development.

Introduction

Twisted gastrulation (TWSG1 in mammals, Tsg in non-mammals) is one of several key regulators of bone morphogenetic proteins, including BMP2, BMP4, and BMP7, in the extracellular space (Chang et al., 2001; Ross et al., 2001; Scott et al., 2001; Blitz et al., 2003; Zakin et al., 2005). TWSG1 is highly evolutionarily conserved and mutations in *Drosophila*, *Xenopus*, and *Danio rerio* Tsg disrupt normal dorsal-ventral patterning (Mason et al., 1994; Oelgeschlager et al., 2000; Ross et al., 2001; Scott et al., 2001). In mice, mutations in TWSG1 result in a range of craniofacial defects, including micrognathia and agnathia, due to abnormal development of the first branchial arch (mandibular arch), as well as cyclopia and other midline facial defects (Petryk et al., 2004; Zakin and De Robertis, 2004; MacKenzie et al., 2009; Billington et al., 2011a).

The presumed biochemical basis of these craniofacial defects is impaired binding of TWSG1 to BMPs. Previous work in *Xenopus* has identified the importance of a set of conserved cysteines and a conserved tryptophan within the N-terminus of xTsg for binding (and inhibiting) BMPs. The C-terminus was shown to play a role in xTsg's interaction with chordin and BMP-promoting activity (Oelgeschlager et al., 2000; Oelgeschlager et al., 2003), most likely through facilitation of Chordin (CHRD) cleavage (Larrain et al., 2001). Deletion of exon 4 (coding exon 3), which removes neither the cysteine-rich domain nor the C-terminus, produces similar craniofacial and skeletal phenotypes to those resulting from targeting the first and second coding exons

(exons 2 and 3) (Nosaka et al., 2003; Zakin and De Robertis, 2004; Gazzerro et al., 2006), raising the possibility that exon 4 encodes a region of the TWSG1 protein with important biochemical properties.

That Tsg is a glycoprotein has been known since the early stages of characterization of this protein (Mason et al., 1994). Despite this history, little research has actually investigated the role of glycosylation in TWSG1 function. There are two common types of glycosylation, N- and O-linked. In N-linked glycosylation, sugar chains are linked to asparagine residues and are generally seen in an Asn-X-Ser/Thr triplet (where X is not proline) (Neuberger and Marshall, 1968; Gavel and von Heijne, 1990; Spiro, 2002). In O-glycosylation sugar modifications occur on serines or threonines (Spiro, 2002). In this report we demonstrate a role for exon 4-encoded sequences as the exclusive site of N-glycosylation of mTWSG1 and show that the glycosylation of mTWSG1 is critical for mediating BMP binding and activity of mTWSG1.

Materials and Methods

Animal care

Use and care of the mice in this study was approved by the University of Minnesota Institutional Animal Care and Use Committee. Wild type mice were in the C57BL/6 background.

Protein sequence analysis

TWSG1 homolog protein sequences were downloaded from NCBI for M*us musculus*, *Rattus norvegicus*, *Homo sapiens*, *Bos taurus*, *Canis lupus familiaris*,

Monodelphis domestica, *Gallus gallus*, and *Xenopus laevis*. Protein sequences were aligned using ClustalW in the MacVector (MacVector, Cary, NC) program. Protein phylogeny was calculated using MacVector's phylogeny tool. Glycosylation sites were predicted in each protein using EnsemblGly (http://turing.cs.iastate.edu/EnsembleGly/) (Caragea et al., 2007) and confirmed using NetNGlyc 1.0 (http://www.cbs.dtu.dk/services/NetNGlyc/).

Plasmids

All plasmids for expression of mTWSG1 in HEK 293 cells were constructed in the C-terminal FLAG-tagged expression vector pCMVTag4c (Stratagene, Santa Clara CA). A full-length wild type *Twsg1* ORF and a *Twsg1* ORF lacking exon 4 were each cloned into this vector using *EcoRI* and *XhoI* to create pCMVTag-Twsg1^{WT} and pCMVTag-Twsg1$^{\Delta ex4}$. Constructs with glycosylation site mutations (pCMVTag-Twsg1^{N80Q}, pCMVTag-Twsg1^{N146Q}) were generated from the wild type construct using the QuickChange site directed mutagenesis kit (Stratagene) employing the following primers N80Q F: 5'-atgtgcaaccctcggcagtacagcgacaccccg, N80Q R: 5'-cggggtgtcgctgtactgccgagggttgcacat, N146Q F: 5'-ccagctgcaccaccaacaggtgtctgttcccagc, N146Q R: 5'-gctgggaacagacacctgttggtggtgcagctgg). The double glycosylation site mutant was generated from the N80Q plasmid, adding the N146Q mutation to generate pCMVTag-Twsg1^{QQ}. A glycosylation site at Asn51 was restored into mouse TWSG1 using the primers P53S F: 5'-tggagaagggaactgcagctgctgtaaggagtgc and P53S R: 5'-gcactccttacagcagctgcagttcccttctcca. Following mutation, plasmids were assessed by restriction digests to confirm mutation (*RsaI* for N80Q, *AflIII* for N146Q, *PstI* for

P53S) and sequenced to confirm no other changes had been introduced.

For production of recombinant proteins in *E. coli* the cDNA mature parts of mTWSG1 and xTsg were cloned into the expression vector pET28b(+) (Novagen, Darmstadt) via the restriction sites *NdeI* and *BamHI*, resulting in proteins carrying an N-terminal His6-Tag, which can be proteolytically removed using the protease thrombin. The expression construct for recombinant xTsg from insect cell expression was derived by cloning the mature part of xTsg into a modified version of the transfer vector pBAC-3 (Novagen, Darmstadt) using the restriction sites *BamHI* and *XhoI*. The resulting construct for xTsg harbors a gp64 signal peptide for secretion into the medium and an N-terminal His6-Tag, which can be removed by thrombin proteolysis. The cDNAs encoding for mTWSG1 and xTsg were obtained from imaGenes (Berlin) and the correctness of all cloned cDNAs was verified by sequencing.

Recombinant protein preparations

The *E. coli* strain BL21(DE3) was used for bacterial protein expression. Transformed cells were grown in shaking flasks in LB-Medium (Melford, Chelsworth) at 37°C and 130rpm, selection of transformed cells was achieved using 30µg/ml kanamycin. Gene expression was induced at an optical density of OD_{600} = 0.6 by adding isopropyl-1-thio-β-D-galactopyranoside (IPTG) to a final concentration of 1 mM and protein expression was continued for 4h and 37°C. Cells were harvested by centrifugation (6000xg, 15 min, 4°C) and the pellet was resuspended in TBSE buffer (10mM Tris-HCl pH 8.0, 150mM NaCl, 1mM EDTA). The recombinant proteins mTWSG1 and xTsg were

expressed in insoluble form as so-called inclusion bodies. To isolate the proteins, 10g bacterial cells were lysed on ice by sonication (Bandelin Sonopuls HD3200, 10min, 150W). The suspension was centrifuged to harvest the insoluble protein fraction. Inclusion bodies were purified by mechanical washing and centrifugation using TBS buffer (10mM Tris-HCl pH 8.0, 150mM NaCl) with and without 1% Triton X-100. To extract the recombinant Tsg proteins the inclusion bodies were dissolved in 20 volumes (v/w) 100mM Na-Phosphate, 10mM Tris-HCl pH 8.0, 6M Guanidinium chloride (GuCl) and the mixture was stirred for 12h at 20°C. After centrifugation to remove insoluble impurities the supernatant was subjected to metal affinity chromatography (IMAC) using Ni^{2+}-NTA resin (Amocol Bioprocedures Ltd., Teltow). Tsg protein was eluted employing a step gradient and 100mM Na-Phosphate, 10mM Tris pH 8.0, 6M GuCl, 300mM imidazole. Tsg-containing fractions were pooled, dialyzed against 50mM Tris-HCl pH 8.0, 6M GuCl, 5mM EDTA and concentrated to a protein concentration of 5mg/ml. Refolding of Tsg was carried out by rapid dilution using the conditions reported for preparation of BMP2 from *E. coli* (Ruppert et al., 1996). The solution containing refolded Tsg was dialyzed against 50 volumes 20mM HEPES pH 8.0, 300mM NaCl and Tsg was purified first by an IMAC chromatography step under non-denaturing conditions. Tsg-containing fractions were pooled and dialysed against 50 volumes 20mM HEPES pH 7.4, 500mM NaCl. As a final purification step size exclusion chromatography was performed to separate monomeric Tsg protein from accompanying dimeric and oligomeric species (Superdex 75 16/60 prep grade, GE Healthcare, Freiburg).

Recombinant xTsg protein from a eukaryotic source was generated by transient expression in baculovirus-transfected insect cells. The virus was prepared by co-transfection of the transfer vector pBAC3 containing the mature part of xTsg along with linearized virus DNA, using the BacVector-3000 DNA Kit (Merck KGaA, Darmstadt) into *Sf9* insect cells according to the manufacturer`s instructions. Recombinant virus was identified and picked by a plaque-assay and protein expression was tested from six clones during virus amplification. A high-expression virus clone was then amplified in *Sf21* insect cells to a titer of $\geq 10^7$ - 10^8 pfu/ml.

For protein production, HighFive insect cells (BTI-TN-5B1-4, gift of R. Grabherr, VIBT, Vienna, Austria) were used, which were grown as adherent cell cultures in IPL-41 medium supplemented with 1% Penicillin/Streptomycin (LONZA, Köln) and 1% Lipid Medium Supplement (Sigma-Aldrich, München) at 27°C. For large-scale expression HighFive cells were transferred to RollerBottles (Greiner Bio-One, Frickenhausen) and adapted to suspension culture. $8x10^5$ cells/ml were infected with recombinant baculovirus at a multiplicity of infection of 5 and protein expression was continued for additional 4-5 days. The cell suspension was clarified by centrifugation (6,000g, 20min, 4°C) and the protein-containing supernatant was dialyzed against 20mM Tris-HCl pH 7.9, 500mM NaCl, 20mM imidazole for IMAC purification. Pure xTsg was eluted in a step gradient using 20mM Tris-HCl pH 7.9, 500mM NaCl, 300mM imidazole. Tsg-containing fractions were pooled, dialyzed twice against 50 volumes 20mM HEPES pH 7.4, 500mM NaCl and frozen at -20°C until further use.

Cell culture, protein isolation and deglycosylation

HEK293 cells were cultured in Dulbecco's minimum essential media supplemented with 10% fetal bovine serum and 1% 100X Anti-Anti antibiotic-antimycotic (GIBCO, Carlsbad, CA). Cells were transfected using Lipofectamine with PLUS reagent (Invitrogen, Carlsbad, CA) in media without serum or antibiotics and lysed to isolate proteins after 16 hours. Proteins from transfected cells were isolated in lysis buffer (50mM Tris-HCl, 125mM NaCl, 1% NP-40 Substitute (BioChemika #74385), and 0.5% sodium deoxycholate) with the addition of Complete protease inhibitor (Roche, Indianapolis, IN). Lysates were spun for 10 minutes at 10,000g to pellet cell debris. Supernatant fractions were analyzed using SDS-PAGE with and without deglycosylation. Transfection product proteins, insect cell xTsg, and *E. coli* mTWSG1 and were deglycosylated using PNGase F (New England Biolabs (NEB), Ipswich, MA) according to manufacturer's instructions. Recombinant mouse TWSG1 from murine myeloma cells (R&D systems, Minneapolis, MN) was deglycosylated using PNGaseF or protein deglycosylation mix (NEB) according to manufacturer's instructions. Blots of FLAG tagged proteins were probed with 1:1000 Rabbit Anti-DYKDDDDK in 0.1% casein/PBS (Cell Signaling, Danvers MA). Untagged recombinant proteins were visualized using a rabbit antibody custom generated (Open Biosystems, Thermo Fisher Scientific) against the peptide EGDTQLNWNIVSFPVAEE (mTWSG1 aa.108-125) at 1:250 in 0.1% casein/PBS. All blots were pre-blocked in 0.1% casein/PBS.

Immunoprecipitation

HEK293 cells were transfected with FLAG-tagged WT, QQ or Δex4

constructs while one plate was left untransfected. Cells were lysed after 16 hours in 250ul of 140mM NaCl, 0.4 mM TrisHCl pH 8.0, 1% Glycerol, 1% NP40 Substitute, 2% BSA with protease inhibitor cocktail. Lysates were spun at 10000g for 10 minutes and supernatant was combined with EZview anti-FLAG M2 affinity beads (Sigma, St. Louis MO) as well as 100 ng recombinant BMP2 (R&D). IP beads, BMP ligand and lysate were allowed to interact for 6 hours at 4˚C in a rotary shaker. IP beads were washed four times in 280mM NaCl, 0.4 mM TrisHCl pH 8.0, 1% Glycerol, 1% NP40 Substitute. Samples were eluted by boiling 5 min in sample loading buffer (62.5 mM Tris-HCl pH6.8, 2% SDS, 10% glycerol 0.002% bromophenol blue) and analyzed by SDS PAGE immunoblotting. Duplicate blots of immunoprecipiated samples were probed with Rabbit Anti-DYKDDDDK (Cell Signaling) (1:5000) or with anti-BMP2 (R&D) (1:5000). Blots were blocked in 5% BSA and primary antibodies were probed in 5% dry milk.

Surface plasmon resonance analysis

In vitro interaction analysis employing Surface Plasmon resonance (SPR) was performed using a ProteON XPR36 system (Biorad Laboratories Inc., Technion, Haifa, Israel). Recombinant BMP2 derived from *E. coli* expression was immobilized onto a ProteOn GLC-chip (Biorad Laboratories Inc., Technion, Haifa, Israel) via amino coupling. The alginate polymer surface was first activated with a freshly prepared mixture of 100mM 1-Ethyl-3-[3-dimethylaminopropyl]carbodiimide hydrochloride (EDC) and 25mM N-hydroxysulfosuccinimide (Sulfo-NHS). Then recombinant human BMP2 was immobilized on flow cells 1 and 2 by perfusing a solution of 200nM BMP2 in 10mM sodium acetate pH 4.0 over the activated alginate surface until protein

densities of 100-200 (low density coating) and 400-500RU (medium density coating) on the biosensor surface were obtained. Non-glycosylated xTsg and mTsg from *E. coli* as well as glycosylated xTsg from insect cells were perfused as analytes over the biosensor surface. Six different analyte concentrations were used in a one-shot kinetic measurement setup. All measurements were performed at 25°C in HBST buffer (10mM HEPES pH 7.4, 500mM NaCl, 0.005% Tween20, Sigma) using a flow rate of 100µl/min. The association phase was set to 240s, the dissociation phase was measured for 660s. The BMP2 biosensor surface was regenerated using a short pulse 30s of perfusion with 10mM glycine pH 1.5. The correct function of the BMP2 biosensor was tested using perfusion with the BMP type I receptor BMPRIA and the values obtained were compared to reported binding affinities in the literature (Heinecke et al., 2009).

To account for bulk face effects a control flow cell (without BMP2 coating) was subtracted from all measurement flow cells. Interaction data were evaluated using the software ProteON Manager 2.1.2 Version 2.1.2.05. Apparent equilibrium binding constants K_D were derived from the kinetic rate constants for association k_a and dissociation k_d by the equation $K_D=k_d/k_a$. All measurements were performed in duplicate.

Mandibular explants

Embryos were collected at embryonic day 10.5 (E10.5). Organ culture of mandibular processes was performed according to previously reported protocols (Jaskoll et al., 2005; Melnick et al., 2005). Briefly, the mandibular component of the first branchial arch was isolated by microdissection and explanted into a culture system using

serum-free chemically defined BGJb medium supplemented with 0.1 mg/ml ascorbic acid (Sigma) and 1% penicillin/streptomycin (Cellgro, Manassa VA). Explants were allowed to develop at 37°C and 5% CO2 for 1 hour before bead placement. Beads were soaked in either 1% BSA/PBS, 100ng/µl BMP4 (R&D systems), 50 ng/µl mTWSG1 (R&D Systems), 50 ng/µl xTsg derived from insect cell expression or 50 ng/µl mTWSG1 produced by bacterial expression in *E. coli* and placed in the distal region of the explant with microforceps. Explants were cultured for additional 24 hours following bead placement. *In situ* hybridization for *Msx2* was performed as previously published (MacKenzie et al., 1992; Sasaki and Hogan, 1993)

Results

Twisted gastrulation proteins have evolutionarily conserved glycosylation sites, mapping in rodents to exon 4

Analysis of the mouse TWSG1 protein sequence using the EnsemblGly software predicts two putative N-linked glycosylation sites, at asparagines Asn80 and Asn146. No O–linked glycosylation sites were predicted (Caragea et al., 2007). Other vertebrate TWSG1/Tsg protein sequences were also analyzed. All other tetrapods also have the two putative glycosylation sites corresponding to those predicted in mice (Figure 1) A third putative glycosylation site at Asn51 is widely conserved in other organisms (Vilmos et al., 2001; Oelgeschlager et al., 2004) and has been shown in Xenopus to be an active site of in vivo glycosylation (Oelgeschlager et al., 2003). This site is not present in either mice or rats, where a consensus serine is substituted by proline, altering the N-X-S/T glycosylation sequon. Given that this site is widely conserved throughout other

tetrapods, we infer that a mutation specifically in the rodent lineage lead to a loss of this site. Interestingly, phylogenetic analysis of the protein sequences for these selected tetrapods recapitulated the expected species phylogeny with the rodents grouping together, the marsupial as an outgroup to the other mammals and avian and amphibian representatives on a more distant branch.

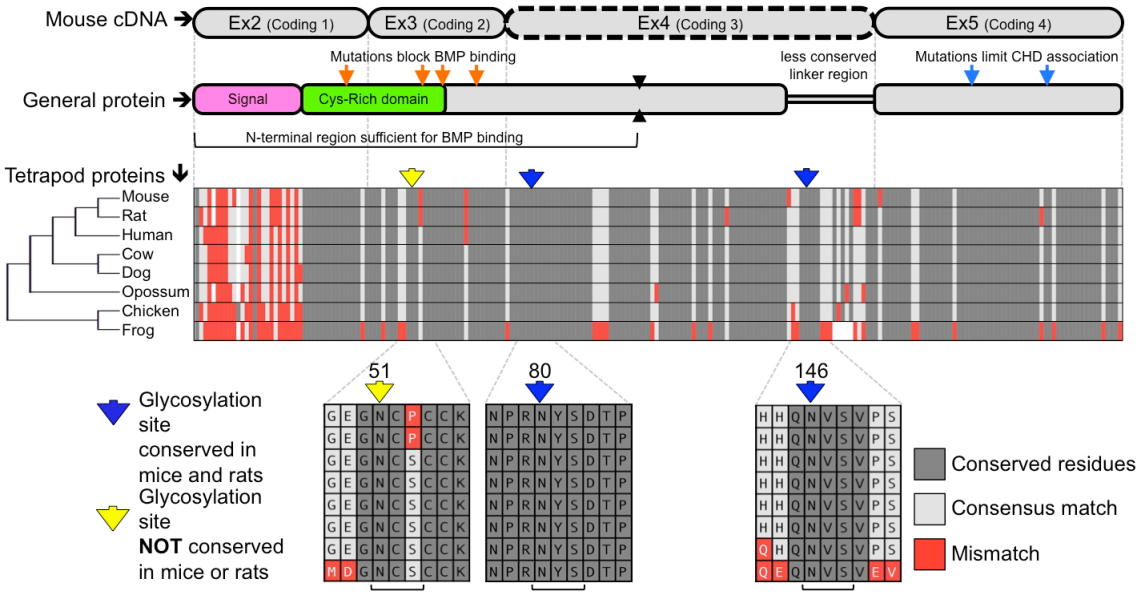

Figure 1: Twisted gastrulation is a conserved glycoprotein with predicted conserved and non-conserved glycosylation sites.

The splicing map of the mouse cDNA sequence is shown at the top. The 4th exon, deleted in a mouse knockout with craniofacial defects (Petryk et al., 2004), is indicated by a dashed line.

A general mapping of the known functional regions of TWSG is indicated below the spliced message. The signal peptide cleaved in the mature protein is indicated in pink. In green is the cysteine-rich domain thought to be important for BMP binding (Oelgeschlager et. al., 2000). Mutations studied in Xenopus experiment which ablated binding with BMP or association with Chordin are indicated in orange or light blue respectively (Oelgeschlager et. al., 2003). An N-terminal fragment necessary and sufficient for BMP binding is indicated below the general diagram, with the break between N and C termini indicated with black arrowheads (Oelgeschlager et. al. 2000).

ClustalW aligned proteins from various tetrapods are shown to highlight the high degree of conservation of the Twisted gastrulation protein and to show the locations of conserved and non-conserved glycosylation sites. A protein phylogenetic tree is shown at left, which also correlates with species phylogeny. The N-glycosylation sequons are indicated in context below with brackets at the bottom indicating the N-X-S sequons, while arrows in yellow or blue at the top indicate the asparagines to which sugars can be linked.

Most notably, both predicted glycosylation sites in mouse TWSG1 (Asn80 and Asn146) are in the region encoded by exon 4, suggesting that deletion of this exon in rodents would completely ablate the glycosylation of any truncated protein product.

Mutational analysis confirms putative glycosylation sites

Our analysis of mTWSG1 sequences suggested that mTWSG1 is exclusively N-glycosylated. We tested this by first deglycosylating the protein using a cocktail of endoglycosidases that is able to remove both N- and O-linked glycosylation from recombinant mTWSG1 (data not shown). We also deglycosylated the protein using PNGaseF, which specifically removes N-glycosylation directly at the asparagine-carbohydrate linkage, and observed an equivalent increase in electrophoretic mobility (Figure 2A). This indicated that, as predicted, mTWSG1 is solely N-glycosylated.

Although two N-glycosylation sites are predicted in mTWSG1, they have not been previously confirmed experimentally. The only mutational analysis performed to confirm a glycosylation site on a Tsg molecule had been done in xTsg at the site not conserved in rodents. Therefore, we mutated each of the putative rodent glycosylation sites, replacing asparagine with glutamine as had been done on other glycoproteins (Barbosa et al., 1987; Yamaguchi et al., 1991; Buller et al., 1994), reasoning that this would prevent glycosylation without disrupting the overall protein structure (Figure 2).

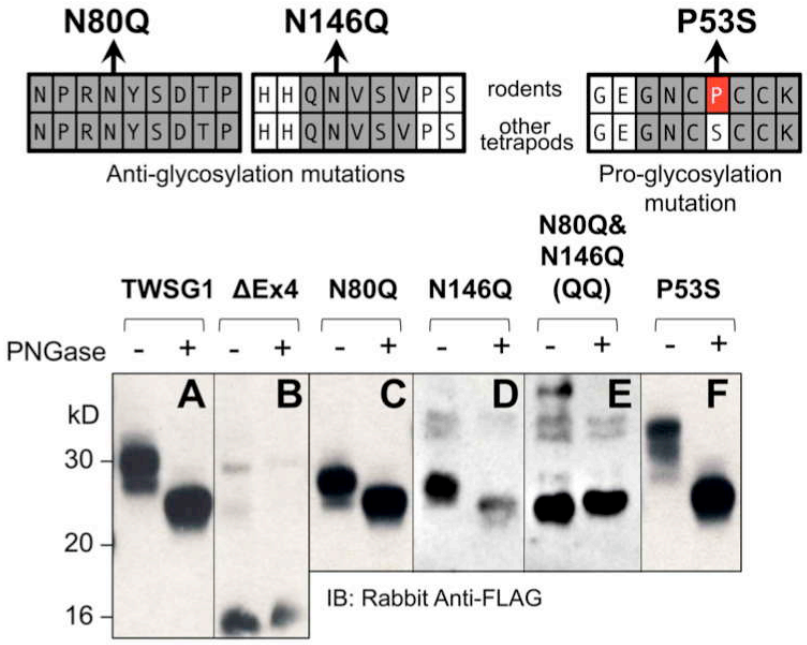

Figure 2: Twisted gastrulation in rodents is N-glycosylated at 2 residues, both in exon 4. (Top) Locations of mutations that remove or add glycosylation at conserved sites are shown with reference to the sequences in rodents and other tetrapods. (A) Wild type mTWSG1 is glycosylated and runs on SDS PAGE as a doublet of about 27 kD and 30 kD. (B) Exon 4-deleted mTWSG1 is not glycosylated. (C) The N80Q mutation removes one glycosylation site but is still glycosylated. (D) The N146Q mutation removes one glycosylation site but is still glycosylated. (E) When the N80Q and N146Q mutations are combined the resulting QQ-TWSG1 is not glycosylated. (F) Mutation of a proline in mTWSG1 to the consensus serine restores a third glycosylation site.

As expected, expression of an exon 4 deletion mutant construct (TWSG1$^{\Delta ex4}$) showed no change in protein mobility with PNGaseF treatment, indicating the expected lack of glycosylation (Figure 2B). Mutating either Asn80 or Asn146 alone to glutamine increased electrophoretic mobility compared to the wild type protein (Figure 2C,D). Notably, whereas the wild type protein runs on SDS PAGE as a doublet of roughly 27 and 30 kD, the mutant forms no longer show the 30 kD band and instead run as doublets of ~25 and 27kD. These single mutant proteins showed further increased mobility, to a

single band at ~25kD, the molecular weight predicted for the unmodified amino acid sequence, when treated with PNGaseF, suggesting that they were still glycosylated, although to a lesser degree than the wild type protein. When both mutations were combined, no change in mobility with PNGase treatment was observed and a single band was observed at ~25 kD, indicating a complete lack of glycosylation in the double mutant (Figure 2E).

Based on data for xTsg in which glycosylation at Asn52 has been shown to occur (Oelgeschlager et al., 2003), we hypothesized that if the consensus serine at position 53 were restored in rodent TWSG1, Asn51 of mTWSG1 would also be a glycosylation site. As predicted, when Pro53 was mutated in the mouse sequence to serine, a decrease in electrophoretic mobility was observed, and a triplet of bands appeared on SDS-PAGE analysis at 27, 30 and 33 kD (Figure 2F). The glycosylability of this restored site strongly suggests that other tetrapods, including humans, have three active glycosylation sites on TWSG1.

The observation that the number of bands in SDS PAGE analysis roughly correlates with the number of glycosylation sites suggests that, at least in this in vitro system, there can be an equilibrium between fully and partially or non-glycosylated forms of the protein.

Lack of glycosylation limits BMP binding

Since TWSG1's primary known function is to modulate BMP activity in the extracellular space, we tested if glycosylation affected the binding of TWSG1 to

BMPs. We also wanted to confirm that the exon 4 deletion, presumed to be defective for BMP binding, actually did prevent binding of TWSG1 to BMPs.

Immunoprecipitation of BMP2 by the wild type TWSG1, but not by the Δex4 mutant protein nor the QQ double glycosylation mutant, indicates that neither of these mutant proteins is able to bind BMP2 (Figure 3A). Immunoprecipitation experiments were also performed using BMP4 protein and showed similar results (Figure 3B)

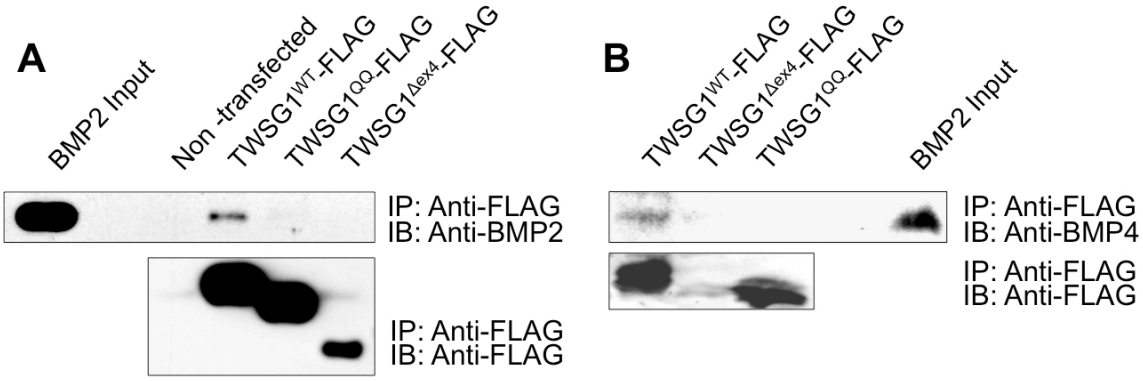

Figure 3: Immunoprecipitation indicates that glycosylation and exon 4 are necessary for BMP binding.

Immunoprecipitation (IP) was performed with anti-FLAG and immunoblots (IB) were probed with either anti BMP2 (top) or anti FLAG (bottom); (A) BMP2 immunoprecipitates with wild type but not glycosylation defective TWSG1QQ or exon 4 deleted TWSG1Δex4. (B) BMP4 immunoprecipitates with wild type but not glycosylation defective exon 4 deleted TWSG1Δex4. Or TWSG1QQ

Glycosylation of TWSG1 recombinant proteins varies markedly by cellular source

Cells derived from different species have variable abilities to glycosylate proteins. For example, in gram-negative bacteria glycosylation is an extremely rare event, with *E. coli* only having two glycoproteins, AIDA-I and the TibA adhesin, both of which are potential virulence factors (Lindenthal and Elsinghorst, 1999; Benz and Schmidt,

2001). To allow for the heterologous expression of O- or N-glycosylated proteins from bacteria, a very complex setup is required using either coexpression of certain UDP-GlcNac epimerase and transferase enzymes (Henderson et al., 2011) or the transfer of the glycosylation machinery of another bacterium, i.e. from the ε-proteobacterium *Campylobacter jejuni* into *E. coli* (Wacker et al., 2002). Thus mammalian glycoproteins are usually obtained in unglycosylated form when expressed in *E. coli*. On the other hand, insect cells are able to glycosylate these proteins although they may do so with slightly different sugar moieties and generally reduced saccharide chain complexity (Jarvis et al., 1998; Tomiya et al., 2004). Here N-glycosylation usually displays a high-mannose type unless engineered insect cells are used, which can mimic mammalian-type glysosylation. Following a common approach for investigating the role of sugar modifications on proteins (Walsh and Jefferis, 2006), we exploited this naturally occurring variation in glycosylation modification to test the biochemical and biological properties of mTWSG1.

We expressed TWSG1/Tsg in *E. coli*, which do not glycosylate the protein, as well as in HighFive insect cells, which should glycosylate the protein, and also used a commercially available preparation of mTWSG1 produced in murine myeloma cells for comparison. When we treated TWSG1/Tsg proteins with PNGaseF and analyzed them by electrophoresis, we were able to confirm differences in glycosylation (Figure 4). Murine TWSG1 made in murine cells was fully glycosylated. Xenopus Tsg made in the HighFive insect cell line was also N-glycosylated, although this glycosylation may differ in the kinds or size of sugar moieties compared to mammalian glycosylation, since the shift

in electrophoretic mobility was less than the apparent mobility shift observed upon deglycosylation of mTWSG1 from murine cells. Murine TWSG1 made in *E. coli* was not glycosylated and hence showed no change in mobility with PNGaseF treatment.

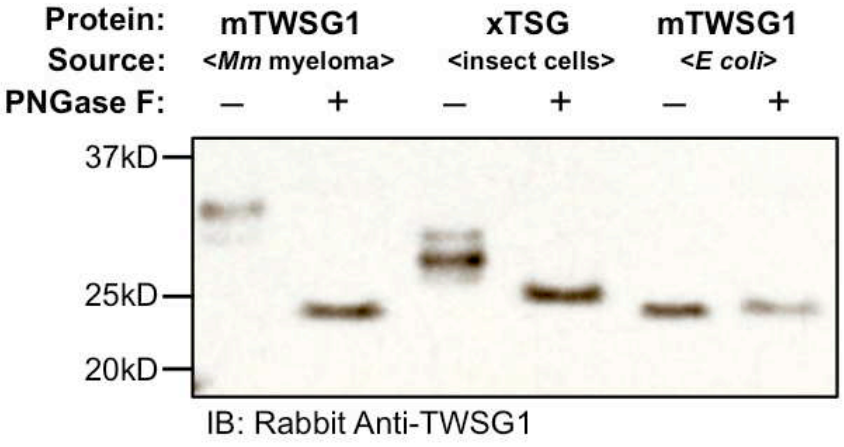

Figure 4: TWSG1 glycosylation varies depending on host source.
mTWSG1 made in murine myeloma cells is markedly glycosylated as indicated by the increase in mobility with PNGaseF treatment. Xenopus Tsg made in insect cells is also glycosylated but shows a smaller mobility shift. Murine TWSG1 made in E. coli is not glycosylated and shows no shift in mobility after treatment with PNGaseF.

Lack of glycosylation decreases the affinity of the BMP-TWSG1 interaction

Our immunoprecipitation data suggest that TWSG1 can bind BMP2/4 only when glycosylated. However, Surface Plasmon Resonance (SPR) analysis allows for a more precise quantification of this change in affinity. To measure the affinity of the Tsg proteins for BMP2, the ligand BMP2 was immobilized on a biosensor chip surface by amino coupling. Varying concentrations of xTsg or mTWSG1 proteins made in insect cells or E. coli, respectively, were allowed to perfuse over the BMP2 biosensor surface and association and dissociation kinetics were measured (Figure 5). Quantitative analysis

of the sensorgram reveals that glycosylated xTsg has a 3-4 fold slower dissociation rate compared to non-glycosylated xTsg derived from *E. coli* (Table 1, Figure 5A,B) and also a 3-fold faster association. The change in association and dissociation kinetics results in an approximately 10-fold increased affinity of N-glycosylated xTsg compared to the non-glycosylated form for BMP2. The difference in affinity and binding kinetics becomes most apparent by a overlay of two SPR sensorgrams of insect cell derived xTsg and *E. coli* derived xTsg at identical protein concentrations (Figure 5C).

Ligand	k_{on} [$M^{-1}s^{-1}$]	k_{off} [s^{-1}]	K_D [nM]
xTsg from insect cells	$11\pm0.8x10^{4}$	$2.0\pm0.5x10^{-4}$	2.5
xTsg from *E. coli*	$3.8\pm1x10^{4}$	$7.1\pm0.5x10^{-4}$	20.2
mTWSG from *E. coli*	$4.4\pm0.3x10^{4}$ ($10.7\pm3x10^{4}$)[a]	$7.6\pm1.3x10^{-4}$ ($2.0\pm0.3x10^{-2}$)	39.6 (301)

Table 1: Tsg affinity for BMP2 varies depending on host source.
[a]values in parenthesis denote low affinity interaction of the biphasic interaction between mTWSG1and BMP2

Despite large efforts mTWSG1 could not be obtained from insect cell expression, however mTWSG1 could be produced in sufficient quantities in *E. coli* using the same expression and purification scheme as used for the production of xTsg. Measuring the interaction of BMP2 and mTWSG1 from *E. coli* via SPR revealed also a fast dissociation rate constant. In contrast to the interaction of xTsg and BMP2 the binding of mTWSG1 to

BMP2 exhibited a biphasic binding kinetics, which could not be analyzed by a simple 1:1 Langmuir type interaction model (Figure 5D). Instead one interaction showed a fast association (on-rate) and a fast dissociation (off-rate) whereas the other interaction exhibited a slow on- and a slow off-rate. From the latter kinetics binding parameters could be deduced that were very similar to the ones determined for xTsg derived from *E. coli* (Table 1). Although we have no explanation why mTWSG1 shows two different binding kinetics for binding to BMP2 the comparison of mTWSG1 and xTsg produced in *E. coli* clearly suggests that the presence of the carbohydrate leads to a significant increase in binding affinity for BMP2.

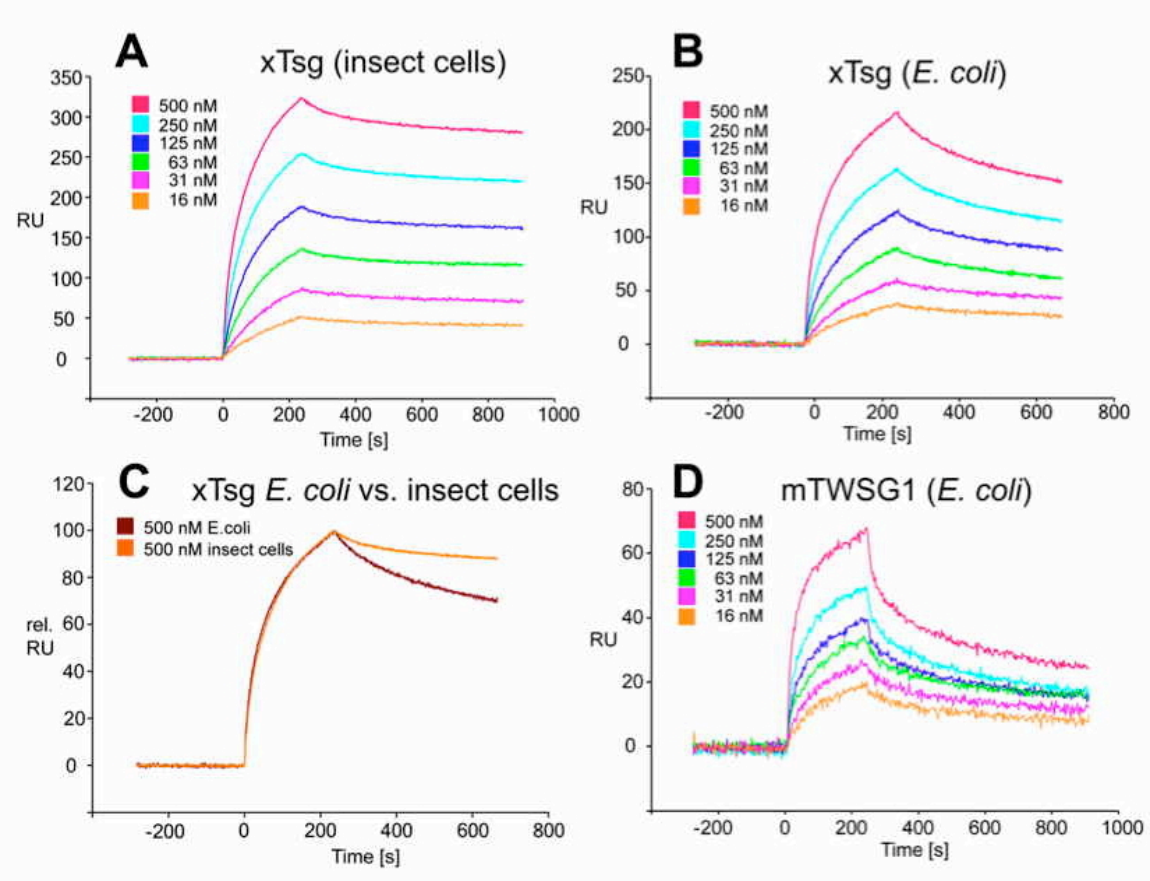

Figure 5: Surface Plasmon Resonance (SPR) interaction analysis of BMP2 binding to recombinant Tsg proteins derived from different sources.
Binding of recombinant Tsg proteins to a BMP2 biosensor was analyzed using SPR. BMP2 was immobilized on a GLC chip via amino coupling. Indicated concentrations of Tsg proteins were perfused over the biosensor surface, injection started at time point 0 with a duration of 240s (association phase) after which only buffer was again perfused for 660s to record the dissociation of Tsg from BMP2. (A,B). The BMP2 biosensor was perfused with varying concentrations of (A) xTsg derived from expression in insect cells or (B) xTsg produced in *E. coli*. (C) The different dissociation rate constants between xTsg protein derived from either a eukaryotic or a prokaryotic host is apparent from an overlay of two normalized SPR sensorgrams recorded for the interaction of different xTsg proteins (500nM concentration) with BMP2. (D) The interaction of mTWSG1 derived from *E. coli* expression reveals a biphasic interaction with BMP2. The binding kinetics following a slow association and a slow dissociation yields an equilibrium binding constant very similar to that of xTsg produced in bacteria.

TWSG1 proteins have different biological activity depending on expression system and glycosylation

To demonstrate the biological effect of glycosylation loss, we chose a mandibular explant system, which has been used previously to examine the activity of BMPs and BMP binding proteins (Ekanayake and Hall, 1997; Tucker et al., 1998; Mina et al., 2002). Expression of the gene *Msx2* was used as a reporter to assay of the effect of TWSG1/Tsg on BMP signaling in these explants.

As previously shown (Semba et al., 2000), treatment with BMP4 strongly induced *Msx2* expression (Figure 6A). When a bead soaked with glycosylated mTWSG1 (expressed in murine cells) was placed in the *Msx2* expression zone the TWSG1 was able to suppress *Msx2* expression indicating local inhibition of BMP signaling (Figure 6B) Glycosylated xTsg from insect cells was similarly able to suppress *Msx2* expression, indicating the competency of N-glycosylated protein from a different species and a heterologous expression system to inhibit BMP signaling (Figure 6C). On the other hand, mTWSG1 derived from *E. coli* expression, which is not glycosylated, showed no repression of *Msx2*, suggesting that it is unable to inhibit BMP signaling (Figure 6D). Thus, glycosylation appears to be essential for TWSG1's BMP binding and BMP inhibitory functions in this tissue assay.

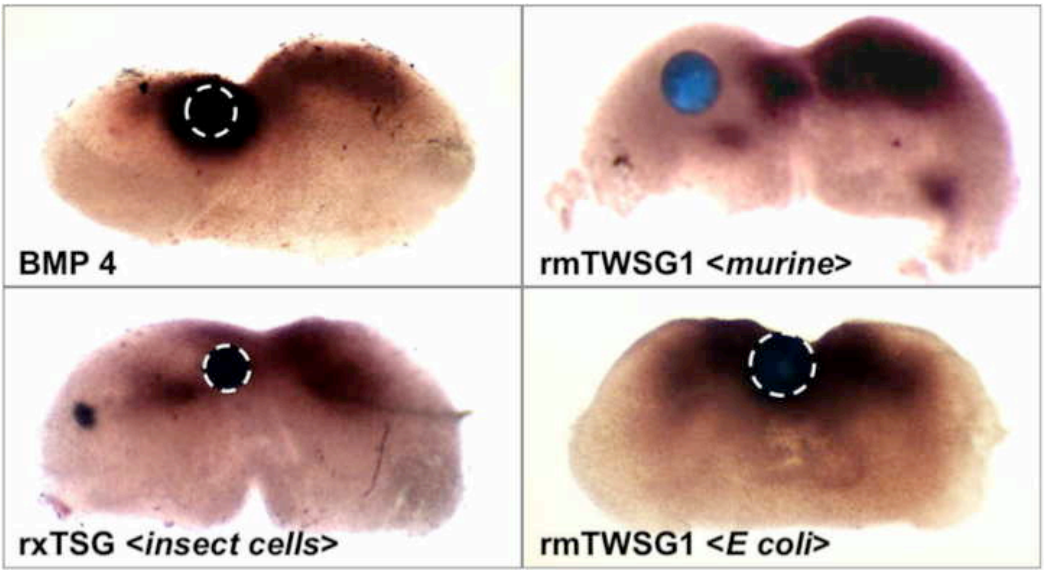

Figure 6: TWSG1 biological activity varies depending on host source.
Mandibular explants were treated with beads soaked in ligand solutions for 24 hours. In situ hybridization was performed to examine the expression of *Msx2*. Bead placements are indicated with dashed white lines where less visible due to dark *Msx2* staining. Bead treatments were: (A) BMP4, showing induction of *Msx2*, (B) mTWSG, expressed in murine myeloma cells, showing suppression of *Msx2* and indicating inhibition of BMP signaling, (C) Xenopus TSG derived from insect cell expression, with the same result, and (D) mTWSG1 expressed in *E. coli*, which shows no effect on *Msx2* expression, indicating a lack of impact on BMP signaling.

Discussion

Although mTWSG1 protein has been presumed to be glycosylated since its initial characterization, the role of glycosylation in mTWSG1 activity has not been studied in much detail. We report here, for the first time, that TWSG1 binding to BMPs is dependent on N-glycosylation. We also show that reduced BMP binding correlates with diminished TWSG1 BMP inhibitory activity.

Our data complement those previously published (Oelgeschlager et al., 2003) in which mutation of a glycosylation site in xTsg led to a stronger biological effect than that of the wild type protein. When serine 54 of xTsg (corresponding to proline 53 in mice)

was mutated to alanine, the electrophoretic mobility of the protein was increased. In addition, this S54A mutant showed enhanced ventralizing activity compared to wild type xTsg, which the authors attributed to increased diffusability of the protein in the tissue. Based on our results, it is also possible that BMP binding may have been compromised by reduced glycosylation. We predict that this would limit BMP binding but may not interfere with the ability of Tsg to stimulate CHRD cleavage. This model is consistent with other results reported by Oelgeschlager et. al. (2003), in which they showed that N-terminal mutations of xTsg that were unable to bind BMPs still retained BMP promoting activity via the C terminus of the protein, that resulted in enhanced ventralization. These explanations are not mutually exclusive and diffusability differences of variable TWSG1 glycoforms could represent an exciting new line of investigation.

Our findings raise the possibility that TWSG1's BMP modulatory activity may be dependent on, or regulated by, glycosylation and highlight the importance of sugar modifications in extracellular signaling interactions. Given that several other extracellular BMP modulating proteins are also predicted glycoproteins, for example CHRD (Gumienny and Padgett, 2002), CV2/BMPER (Kamimura et al., 2004), Noggin (Groppe et al., 2002), and the DAN family of BMP binding proteins (Stanley et al., 1998; Avsian-Kretchmer and Hsueh, 2004), glycosylation may play a wider role in extracellular BMP regulation than presently recognized. The role of glycosylation in interactions of other proteins will have to be verified however. For example, Xenopus Lefty, which plays a role in Nodal signaling analogous to the role of TWSG1 in BMP signaling, is also a glycoprotein but does not require glycosylation for normal function (Westmoreland

et al., 2007). In addition to the BMP binding proteins, glycosylation of the ligand itself is also likely to play a role in regulation of extracellular signaling as illustrated by the absolute requirement of N-glycosylation for the specific interaction of BMP6 with its BMP type I receptor Alk2 (Saremba et al., 2008). Likewise, given the important role of the metalloproteinase Tolloid/Xolloid/BMP1 in regulating BMP action in combination with TWSG/Tsg and CHRD (Larrain et al., 2001), it is interesting that glycosylation has been identified as regulating the activity of the metalloproteinase MT1-MMP (Wu et al., 2004) and even more interesting that glycosylation has been identified as a regulator of BMP1 secretion and stability (Garrigue-Antar et al., 2002)

TWSG1 made in cells of various species may have differential glycosylation or complete lack of glycosylation. Given the correlation reported here between protein source, glycosylation, BMP binding activity and biological activity, we suggest that experiments using recombinant BMP modulating proteins should carefully consider the source and glycosylation status of these proteins. It is also interesting to speculate whether glycosylation of TWSG1 or other proteins may be regulated at a tissue specific level, allowing fine-tuning of protein activity in various contexts.

The exon 4 deletion mutant, which led us to this line of inquiry, is deficient for normal TWSG1 activity and a lack of glycosylation may contribute to this deficiency and the ensuing craniofacial phenotypes. In the mandibular explant system, application of exogenous glycosylated mTWSG1 resulted in a reduction of Msx2 expression, consistent with TWSG1's role as a BMP antagonist. The interactions between TWSG1 and BMPs in

vivo, however, are more complex. Functional TWSG1 serves to establish a BMP signaling gradient in the developing mandibular arch. Deletion of exon 4 disrupts the interactions between TWSG1 and BMPs, which, in affected embryos, results in loss of the BMP gradient, more diffuse BMP signaling, and ectopic apoptosis (MacKenzie et al., 2009). Correspondingly, the expression of the BMP target gene *Msx2* is shifted ventrally at E9.5 and then mostly lost by E10.5 (MacKenzie et al., 2009; Billington et al., 2011a). We believe that loss of expression of *Msx2* as well as other BMP target genes by E10.5 is due to the loss of a proper BMP gradient and the resultant apoptosis of the distal tissues of the mandibular arch. While TWSG1 antagonizes BMP signaling within the mandibular arch in the explant culture system, we suggest that in vivo the BMP limiting action of TWSG1 can act to actually maintain proper BMP signaling levels in mandibular development and that this action is dependent on glycosylation of TWSG1.

Our results highlight the importance of a better understanding of both the various signaling molecules in craniofacial development as well as their potential post-translational modifications. The complex extracellular regulation of BMPs has been compared to a baroque "court of intrigue" (Bier, 2008) based on all the surprising and nuanced interactions of the many players in BMP signaling. Our study adds to this complexity by highlighting the role of post-translational modifications.

Chapter 3: The molecular and cellular basis of variable craniofacial phenotypes and their genetic rescue in *Twisted gastrulation* mutant mice

Introduction

Phenotypic variation is a well-known phenomenon in a number of developmental abnormalities. For example, patients with Treacher-Collins syndrome or holoprosencephaly (HPE) have an extremely wide range of clinical manifestations (Hansen et al., 1996; Roessler et al., 1996; Muenke and Cohen, 2000). In HPE, the most severe defects, such as cyclopia, are usually incompatible with life, while others including hypotelorism or microphthalmia represent milder forms (Ming et al., 2002). However, the molecular basis for such reduced penetrance and variable severity, even in the context of the same mutations on the same genetic background, has remained unclear.

Differences in genetic background and environmental influences are thought to be two major drivers of transcriptional variation, leading to phenotypic variation or reduced penetrance in both humans and mice (Champy et al., 2008; Butchbach et al., 2009). The contribution of epigenetic phenonema, including DNA methylation and histone modification, has also been increasingly recognized to be an important mechanism underlying variability in genetic expressivity, particularly in the case of imprinted genes (Peaston and Whitelaw, 2006; Dindot et al., 2009). For example, craniofacial manifestations of the Silver-Russell syndrome correlate with the degree of methylation at the H19-(Insulin-like Growth Factor) IGF2 locus (Bruce et al., 2009). This underscores

the importance of a better understanding of the basis of phenotypic variation of craniofacial malformations and identification of mammalian models that would facilitate such insights. An advantage in using inbred mouse models to study such phenotypic variation is that both strain differences and environmental differences can be controlled.

We previously reported that disruption of *Twisted gastrulation* (*Twsg1*), a modulator of BMP signaling, in mice leads to a spectrum of craniofacial defects on an isogenic, inbred C57BL/6 background (Petryk et al., 2004; MacKenzie et al., 2009). Within a single litter, some mice are born with normal craniofacial structures; some have mild defects, such as micrognathia and microphthalmia; and still others have profound craniofacial abnormalities including anterior truncation, cyclopia, agnathia, and HPE. While some of this variation could be attributed to a variable extent of apoptosis and thus variable loss of first branchial arch 1 (BA1) derivatives (MacKenzie et al., 2009), the underlying molecular mechanisms are not entirely understood. Manifestation of craniofacial defects is highly strain background-dependent and appears in about 40% of *Twsg1*$^{-/-}$ mice on the C57BL/6 background. In early generations after derivation of the mutant allele on the C57BL/6 background, some as yet undiscovered modifier gene/s could partially account for the observed variation. However, this variation has persisted despite serial backcrossing of the mutant alleles onto the isogenic strain background. The ongoing occurrence of extreme differences in phenotypes, even within the same litter, raises the question of how phenotypic variation might occur despite virtually no differences in inherited genes. The *Twsg1* mutant mouse model provides an excellent,

well-controlled experimental system in which to study the molecular mechanisms underlying the resulting phenotypic variation and reduced penetrance.

In this study, we have analyzed transcriptional changes that are associated with development of distinct classes of craniofacial phenotypes in *Twsg1* mutant mice. We anticipated that these differentially expressed transcripts would include previously unknown effectors of the mutant phenotype as well as genes that may compensate for the loss of TWSG1 and account for incomplete penetrance of *Twsg1* mutation. In particular, we were interested in identifying transcriptional differences between unaffected and affected mutants that would shed light on potential mechanisms that allow an organism to cope with a predisposition to disease.

Materials and Methods

Mice and tissue collection

Generation and genotyping of mice deficient for TWSG1 (Petryk et al., 2004), p53 (Donehower et al., 1992) as well as transgenic *Sox10-cre* mice that express Cre recombinase in neural crest cells (NCC) (Matsuoka et al., 2005) have been previously reported. To generate mice with NCC-specific deletion of *Twsg1* (*Twsg1*$^{flox/flox}$*;Sox10-cre*), mice carrying a conditional allele of *Twsg1*, with exon 4 (coding exon 3) flanked by *loxP* sites (*Twsg1*$^{flox/flox}$, MGI: *Twsg1*^{tm1Aptr}), were mated to *Sox10-cre* mice (MGI: *Tg(Sox10-cre)1Wdr*) to generate *Twsg1*$^{flox/WT}$*; Sox10-cre*, which were then mated to *Twsg1*$^{flox/flox}$ mice. Mice simultaneously deficient for both p53 and TWSG1 were produced by intercrossing *Twsg1*$^{-/-}$ (MGI: *Twsg1*$^{tm1.1Mboc}$) and *p53*$^{-/-}$ mice (MGI:

Trp53^{tm1Brd}). All strains were on C57BL/6 background. Presence of a spermatic plug was counted as day 0.5 post conception (E0.5). *Twsg1*$^{-/-}$ embryos were classified as previously published as class A (phenotypically the same as wild type), class B (moderately affected), and class C (severely affected) (MacKenzie et al., 2009). For microarray analysis, mandibular prominences of BA1s from mutants of various phenotypic classes and WT embryos at E10.5 were dissected by cutting the BA1 at the junction between the maxillary and mandibular components using alkali etched tungsten needles. BA1s were flash-frozen in liquid nitrogen and stored at -80˚C. Both maxillary and mandibular prominences were dissected at E11.5 to confirm deletion of exon 4 of *Twsg1* in NCC-derived tissues. This embryonic stage was chosen to allow the analysis of individual samples in case of variable efficiency of *Cre*-mediated recombination. Use and care of the mice in this study was approved by the University of Minnesota Institutional Animal Care and Use Committee.

RNA isolation

Frozen tissue samples were thawed in Trizol reagent (Invitrogen, Carlsbad, CA) and pooled according to the phenotypic class. RNA was purified using RNeasy micro kit spin columns (Qiagen, Valencia, CA). Five biological replicates of each mutant class and of WT (each representing a pool of 4-7 arches) were analyzed to achieve adequate statistical power for this microarray analysis (Pavlidis et al., 2003). Pooling was necessary to allow collection of sufficient RNA for microarray analysis (Bobola et al., 2003; Feng et al., 2009).

Microarray analysis

Microarray analysis was performed at the Kimmel Cancer Center Cancer Genomics Core Facility, Thomas Jefferson University (Philadelphia, PA). Total RNA (50 ng) was used to prepare amplified cDNA using the WT-Ovation Pico RNA amplification system (NuGen Technologies, Inc., San Carlos, CA). Sense transcript cDNA (ST-cDNA) was generated from 3 μg of amplified cDNA. Finally, 5.0 μg ST-cDNAs were labeled using FL-Ovation cDNA biotin module v2 (NuGen Technologies, Inc.) (Linton et al., 2009). Affymetrix GeneChip mouse exon 1.0 ST arrays (Affymetrix, Santa Clara, CA) were used following manufacturer's recommendations. Samples were hybridized overnight, scanned and processed using Command Console Software. Background correction and normalization were done using Robust Multichip Average (RMA) with Genespring v10.0 software (Agilent, Palo Alto, CA, USA).

Bioinformatics analysis

mRNA expression profile data were condensed using RMA to generate raw expression values log base 2. Two group T-tests were used to assess significance in pairwise comparisons between groups with correction for a false discovery rate (FDR) of 10% or less (Benjamini and Hochberg, 1995). For inclusion in WT vs. C and A vs. C analyses, genes were also required to have an absolute value of fold change ≥1.5. Heatmaps were generated using Cluster3.0 and JavaTreeview. Expression profiles were clustered in both supervised and unsupervised methods to identify molecular patterns present in the data. Ingenuity Pathways Analysis (IPA; Ingenuity® Systems,

www.ingenuity.com) was used to identify biological functions regulated by differentially expressed genes.

Quantitative PCR

Reverse transcription was carried out with the Thermoscript RT kit (Invitrogen) priming with random hexamers, followed by quantitative PCR (Q-PCR, MX3000p, Agilent, LaJolla, CA) using expression assays from Applied Biosystems (Foster City, CA) for *Bambi* (Mm03024088_g1), *Bmp4* (Mm00432087_m1), *Bmpr1b* (Mm03023971_m1), *Cyp26a1* (Mm00514486_m1), *Dkk1* (Mm00438422_m1), *Gpr50* (Mm00439147_m1), *Peg3* (Mm00493299_s1), *Plagl1* (Mm00494250_m1), *Satb2* (Mm00507337_m) or using published primer sequences with SYBR green RT^2 master mix (SABiosciences, Valencia, CA) for *Dlk1*, *Igf2* (Varrault et al., 2006), and *Msx2* (Berdal et al., 2009). To detect *Twsg1*, the following primers were used (forward: 5'-CTGAACTGGAACATCGTCTC-3', reverse: 5'-GCAGTCATCAAAGTAAACCAC-3'). *Trp53inp1* was detected with primers from the MGH primer bank (Spandidos et al., 2010) (PrimerBank ID 11230806a1; forward: 5'-AAGTGGTCCCAGAATGGAAGC-3', reverse: 5' –GGCGAAAACTCTTGGGTTGT-3'). All samples were normalized to expression of *Gapdh* (forward: 5'-TGCACCACCAACTGCTTAG-3', reverse: 5'-GATGCAGGGATGATGTTC-R for SYBR green assays; Applied Biosystems 4352339E for TaqMan assays). Assays were run in triplicate using N≥3 pooled cDNA samples per probe.

In situ hybridization

In situ hybridization was performed by standard methods (Sasaki and Hogan, 1993). cDNA probe fragments for *Plagl1* (Tsuda et al., 2004), *Peg3* (Kuroiwa et al., 1996) and *Satb2* (FitzPatrick et al., 2003) were amplified from a cDNA library obtained from E10.5 embryos and cloned into the pCRII-TOPO vector (Invitrogen). A probe for *Dkk1* was a gift from Dr. William Shawlot (Finley et al., 2003). *Msx2* probe was previously published (MacKenzie et al., 1992). Clones were transcribed to generate digoxigenin labeled probes using a DIG RNA labeling kit (Roche). At least 2-3 embryos were evaluated in each phenotypic class per probe.

Western blotting

E10.5 embryos were isolated from pregnant females set up in timed matings, in ice-cold Tris buffered saline with EDTA (50 mM TrisHCl pH7.4, 150mM NaCl, 1mM EDTA). Embryos were homogenized in lysis buffer (Tris buffered saline with 1% TritonX-100), centrifuged for 10 min at 10,000 g at 4˚C, and supernatants were electrophoresed in a 10% polyacrylamide gel using the NextGel system (Amresco, Solon, OH). Proteins were transferred to ImmobilonFL PVDF membranes (Millipore, Billerica, MA) and probed with an anti p53 mouse monoclonal antibody at 1:1000 (clone 1C12, #2524, CellSignaling, Beverly, MA). The immunoblot was imaged with HRP conjugated anti mouse IgG secondary at 1:2500 (Promega, Madison, WI) and peroxide/luminol chemiluminescence with the SuperSignal West Pico kit (Pierce/Thermofisher, Rockford, IL). For loading control, blots were re-probed with mouse monoclonal anti-GAPDH (AM4300, Ambion, Foster City, CA) and imaged with goat anti-mouse secondary

conjugated to IR800 fluorophore on the LICOR Odyssey system (Lincoln, NE). Three samples per phenotypic class were analyzed.

Statistical analyses

Student's t-tests and Pearson's correlations of Q-PCR data were performed in Prism 4 (GraphPad Software, LaJolla, CA). Significance was set at $p<0.05$. The incidence of Mendelian ratios and normal vs. abnormal phenotype incidence for *Twsg1*;*p53* mice were compared using Chi-squared analyses and Chi-squared goodness of fit tests.

Results

Transcriptional changes correlate with classes of phenotypic severity

We previously classified *Twsg1*$^{-/-}$ embryos based on the severity of the phenotype into three classes at E9.5 (MacKenzie et al., 2009). Similarly, at E10.5, class A (unaffected) mutant embryos are morphologically indistinguishable from normal, wild type (WT) embryos, while class B embryos exhibit partial midline fusion of the mandibular components of BA1, and class C embryos have severe midline fusion (Figure 7A). To determine if these phenotypic classes are associated with differences between their transcriptomes, we used mouse exon microarrays to analyze total RNAs isolated from BA1 samples at E10.5. Differences in gene expression between the classes increased with increasing phenotypic severity, and thus were greatest in the most severely affected (class C) embryos (Figure 7B).

Hierarchical clustering analysis was performed on the transcript expression profiles of a set of 127 genes exhibiting the greatest differences in expression between any two pools (Figure 7C). This analysis clearly distinguished class C phenotypic samples from WT and class A samples. In fact, the clustering algorithm placed class A embryos just as distantly from WT as class C from WT, implying that gene expression differences in class A embryos, albeit not as pronounced as in class C, may be sufficient to compensate for the *Twsg1*$^{-/-}$ genetic predisposition. Class B samples, representing an intermediate phenotype, clustered with either class A or class C. These results demonstrate that the variable morphological features of individual embryos with the same genetic mutations in *Twsg1* on the same genetic background are associated strongly with distinct transcriptional profiles.

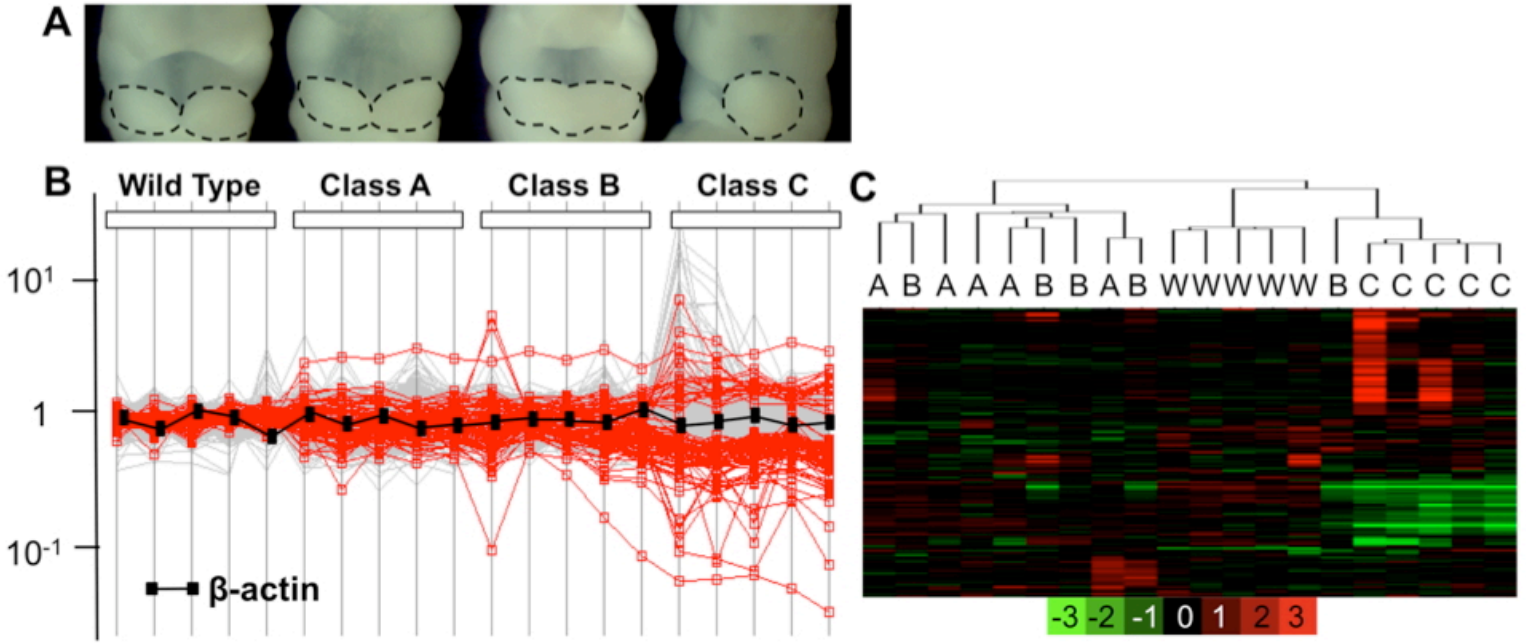

Figure 7: Association between phenotypic classes and expression differences
(A) Morphological differences between phenotypic classes of E10.5 embryos are displayed. Dotted lines outline the mandibular components of BA1. (B): Gene expression levels are expressed on a log10 scale (y-axis) vs. an average of WT samples (Y=1) for a given gene. Each vertical line represents a biological replicate from given phenotypic classes (WT, A, B, or C). Genes that are differentially expressed between WT and class C, based on a fold change of 1.5 fold or greater and a false discovery rate of 10% or less, are highlighted (red). Compared with WT gene expression levels, variation is greatest in the most severely affected embryos (class C). (C) Unsupervised hierarchical clustering of array data. Class C samples are clearly separated from WT and class A samples. Class B represents an intermediate phenotype, clustering alternatively with either A or C. The log2 scale of the expression values is shown in the key at the bottom.

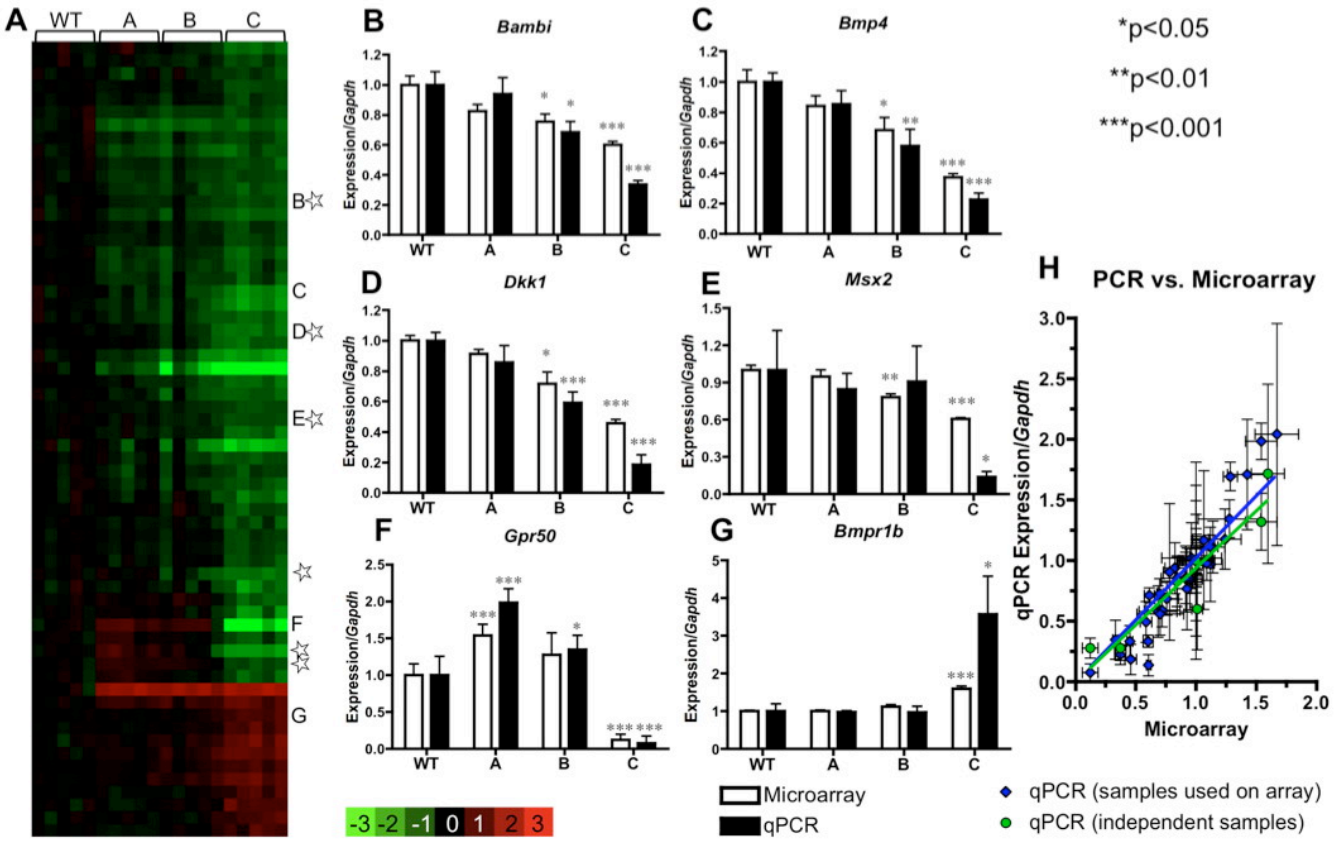

Figure 8: Gene expression differences between wild type and severely affected mutants.
(A) A heatmap displays gene expression changes compared to the average of WT. Genes with expression changes >1.5 fold and with a false discovery rate of <10% are presented as rows. Each column represents a biological replicate. (B-G) Q-PCR confirmation; ⋆genes confirmed by in situ hybridization in Fig. 4; *significance in comparison with WT. (H) Scatter plot showing close correlation between microarray data and Q-PCR data for genes in panels B-G (blue) and independent RNA samples (green) for Gpr50, Bmp4 and Bmpr1b.

Table 2: Genes showing significant change between WT and C or between A and C phenotypic classes.

Name	Description	Affy-ID	WTvC only	Both	AvC only	A/WT Relative expression	A to WT p-value	B/WT Relative expression	B to WT p-value	C/WT Relative expression	C to WT p-value	C/A Relative expression	A to C p-value
Angpt1	angiopoietin 1	6835353	X			0.748	0.0065	0.68	0.0018	0.627	0.0009		
Bambi	BMP and activin membrane-bound inhibitor homolog (Xenopus laevis)	6858465	X			0.828	0.0505	0.756	0.0158	0.605	0.0002		
Bmp5	bone morphogenetic protein 5	6990569	X			0.667	0.0016	0.583	0.0017	0.56	0.0006		
Ccdc80	coiled-coil domain containing 80	6841160	X			0.795	0.0059	0.744	0.0040	0.59	0.0002		
Cd59a	CD59a antigen or CD59b antigen (Cd59b)	6879646	X			0.531	0.0002	0.519	0.0002	0.544	0.0002		
Cox7a2l	cytochrome c oxidase subunit VIIa polypeptide 2-like or predicted gene, EG629383	6804268	X			2.84	0.0000	2.79	0.0000	3.18	0.0000		
Cyp51	cytochrome P450, family 51, subfamily A, polypeptide 1	6935927	X			0.865	0.0089	0.847	0.0260	0.661	0.0001		
Ddc	dopa decarboxylase (aromatic L-amino acid decarboxylase)	6786045	X			0.761	0.0071	0.696	0.0084	0.632	0.0005		
Enpp1	ectonucleotide pyrophosphatase/phosphodiesterase 1	6772802	X			0.755	0.0052	0.709	0.0047	0.624	0.0002		
Fgf9	fibroblast growth factor 9 (glia-activating factor)	6819442	X			0.861	0.2950	0.857	0.1720	0.66	0.0008		
Hmgcr	3-hydroxy-3-methylglutaryl-Coenzyme A reductase	6815305	X			0.935	0.2750	0.922	0.2830	0.664	0.0002		

Hmgcs1	3-hydroxy-3-methylglutaryl-Coenzyme A synthase 1 (soluble) or LOC100040592, similar to Hmgcs1 protein	7005797	X			0.907	0.0893	0.88	0.0657	0.648	0.0000		
Id1	inhibitor of DNA binding 1, dominant negative helix-loop-helix protein	6882315	X			0.891	0.0293	0.882	0.1010	0.599	0.0006		
Id2	inhibitor of DNA binding 2, dominant negative helix-loop-helix protein	6799462	X			0.922	0.0919	0.861	0.0191	0.615	0.0000		
Id3	inhibitor of DNA binding 3, dominant negative helix-loop-helix protein	6917809	X			0.919	0.3810	0.815	0.0356	0.628	0.0008		
Itm2a	integral membrane protein 2A	7018847	X			0.811	0.0984	0.798	0.0531	0.652	0.0007		
Krt14	keratin 14	6791408	X			0.751	0.0001	0.734	0.0139	0.596	0.0011		
Lgi2	leucine-rich repeat LGI family, member 2	6938171	X			0.866	0.0060	0.817	0.0010	0.664	0.0002		
Lrig3	leucine-rich repeats and immunoglobulin-like domains 3	6771476	X			1.09	0.0174	1.19	0.0100	1.52	0.0000		
Mid2	midline 2 or eukaryotic translation initiation factor 2C, 2 (Eif2c2)	7014171	X			0.886	0.0297	0.772	0.0014	0.613	0.0000		
Nell2	NEL-like 2 (chicken)	6838171	X			0.743	0.4070	0.666	0.0017	0.513	0.0000		
Nr2f1	nuclear receptor subfamily 2, group F, member 1	6814557	X			1.37	0.0147	1.4	0.0143	1.79	0.0001		
Pcdh7	protocadherin 7	6931001	X			0.753	0.4350	0.71	0.3480	0.562	0.0002		
Pitx2	paired-like homeodomain 2	6901280	X			0.836	0.0016	0.822	0.0083	0.639	0.0000		
Sc4mol	sterol-C4-methyl oxidase-like	6982921	X			0.716	0.0004	0.724	0.0055	0.538	0.0000		
Sox2	SRY (sex determining region Y)-box 2	6896695	X			0.708	0.0008	0.699	0.0189	0.593	0.0016		

A930038C07Rik	A930038C07Rik	6946750		X		0.8860	0.1030	0.6970	0.0328	0.3550	0.0000	0.4010	0.0000
Alx1	ALX homeobox 1	6776603		X		0.87	0.4430	0.506	0.0204	0.238	0.0000	0.274	0.0000
Asb4	ankyrin repeat and SOCS box-containing protein 4	6943873		X		1.13	0.0656	1.12	0.2120	0.541	0.0001	0.479	0.0000
AW551984	AW551984	6994790		X		0.8800	0.4710	0.7360	0.1020	0.5230	0.0011	0.5940	0.0037
Bmp4	bone morphogenetic protein 4	6824266		X		0.841	0.1590	0.676	0.0177	0.373	0.0000	0.443	0.0000
Bmpr1b	bone morphogenetic protein receptor, type 1B	6909941		X		1.01	0.8110	1.11	0.0693	1.59	0.0000	1.58	0.0000
Cyp26a1	cytochrome P450, family 26, subfamily a, polypeptide 1	6869522		X		0.929	0.4170	1.1	0.2800	1.68	0.0004	1.81	0.0000
Dclk1	doublecortin-like kinase 1	6897599		X		1	0.9810	1.11	0.0423	1.64	0.0002	1.64	0.0001
Dgkk	diacylglycerol kinase kappa	7009748		X		1.06	0.6430	0.833	0.1090	0.484	0.0001	0.455	0.0001
Dkk1	dickkopf homolog 1 (Xenopus laevis) or predicted gene, EG546723 or protein phosphatase 1, regulatory (inhibitor) subunit 2 (Ppp1r2)	6872615		X		0.914	0.0776	0.703	0.0136	0.456	0.0000	0.498	0.0000
Dlk1	delta-like 1 homolog (Drosophila)	6797978		X		1.24	0.0286	0.996	0.9670	0.579	0.0006	0.468	0.0001
Dok5	docking protein 5	6883533		X		0.776	0.0062	0.654	0.0101	0.349	0.0000	0.45	0.0000
E130114P18Rik|D130039L10Rik|A130013F12Rik	E130114P18Rik or D130039L10Rik or A130013F12Rik	6923584		X		0.9080	0.0959	0.9870	0.8430	0.5670	0.0008	0.6250	0.0016
Ebf1	early B-cell factor 1	6780443		X		1.12	0.0703	1.32	0.0127	1.89	0.0000	1.68	0.0000
Figf	c-fos induced growth factor	7015007		X		1.08	0.1660	0.945	0.5930	0.418	0.0010	0.386	0.0004
Gata3	GATA binding protein 3	6884642		X		0.96	0.3670	0.727	0.0223	0.508	0.0000	0.529	0.0000
Gpr50	G-protein-coupled receptor 50	7011861		X		1.55	0.0007	1.25	0.1490	0.11	0.0000	0.0714	0.0000

Isl1	ISL1 transcription factor, LIM/homeodomain	6816288		X		0.741	0.0059	0.481	0.0029	0.308	0.0000	0.416	0.0000
Kazald1	Kazal-type serine peptidase inhibitor domain 1	6869981		X		0.796	0.0161	0.668	0.0101	0.508	0.0000	0.638	0.0002
Lrrc17	leucine rich repeat containing 17	6929132		X		0.928	0.4640	0.832	0.2240	0.478	0.0002	0.515	0.0005
Lrrn1	leucine rich repeat protein 1, neuronal	6948878		X		0.948	0.2760	1.03	0.6500	1.51	0.0008	1.6	0.0007
Mme	membrane metallo endopeptidase	6898010		X		0.867	0.2080	0.726	0.0205	0.569	0.0001	0.656	0.0017
Mstn	myostatin	6749461		X		0.995	0.9520	1.04	0.6960	1.57	0.0015	1.58	0.0004
Msx2	homeobox, msh-like 2 or LOC100046255, similar to homeobox protein	6813259		X		0.946	0.4250	0.781	0.0016	0.608	0.0000	0.643	0.0000
Nr2f2	nuclear receptor subfamily 2, group F, member 2	6968201		X		1.11	0.1270	1.3	0.0021	1.84	0.0000	1.66	0.0002
Nsdhl	NAD(P) dependent steroid dehydrogenase-like	7011907		X		0.934	0.4330	0.921	0.3470	0.603	0.0002	0.646	0.0011
Peg3	paternally expressed 3	6972750		X		1.29	0.0016	1.14	0.0925	0.613	0.0000	0.476	0.0000
Plagl1	pleiomorphic adenoma gene-like 1	6766046		X		1.07	0.3900	0.682	0.0274	0.452	0.0000	0.424	0.0000
Pmp22	peripheral myelin protein	6781612		X		0.857	0.0712	0.625	0.0093	0.532	0.0000	0.621	0.0000
Rasgef1b	RasGEF domain family, member 1B	6940303		X		0.86	0.0594	0.686	0.0006	0.475	0.0000	0.553	0.0001
Rgs5	regulator of G-protein signaling 5	6755055		X		0.598	0.0007	0.216	0.0028	0.0581	0.0000	0.0972	0.0000
Satb2	special AT-rich sequence binding protein 2	6758862		X		1.42	0.0016	0.928	0.6590	0.331	0.0000	0.233	0.0000
Scd1	stearoyl-Coenzyme A desaturase 1	6873271		X		0.891	0.1400	0.783	0.0006	0.476	0.0000	0.535	0.0002

Sema3e	sema domain, immunoglobulin domain (Ig), short basic domain, secreted, (semaphorin) 3E or hypothetical protein LOC100044162	6928880		x		0.886	0.0112	1.08	0.2240	1.5	0.0010	1.7	0.0001
Speer4a	spermatogenesis associated glutamate (E)-rich protein 4a or spermatogenesis associated glutamate (E)-rich protein 4b (Speer4b)	6936791		x		0.931	0.5190	0.827	0.2270	0.438	0.0009	0.47	0.0006
Stom	stomatin	6886039		x		1.04	0.5280	0.967	0.7580	0.605	0.0002	0.584	0.0000
Tbx3	T-box 3	6933913		x		1.22	0.0261	0.939	0.4410	0.557	0.0006	0.457	0.0000
Zcchc5	zinc finger, CCHC domain containing 5	7018819		x		0.911	0.3740	0.694	0.0074	0.584	0.0000	0.641	0.0018
Zic4	zinc finger protein of the cerebellum 4 or RIKEN cDNA B130024G19 gene (B130024G19Rik)	6961396		x		1.1	0.3260	1.21	0.0885	1.96	0.0002	1.79	0.0002
2610017I09Rik|LOC100044386	2610017I09Rik or LOC100044386	6758223			x	0.8210	0.0946	1.0400	0.6850	1.3200	0.0127	1.6100	0.0010
9330120H11Rik	9330120H11Rik	6968842			x	0.8230	0.1380	0.8290	0.2280	1.3600	0.0358	1.6500	0.0014
A930001N09Rik	A930001N09Rik	6849466			x	0.8070	0.0102	0.8860	0.0697	1.2300	0.0065	1.5300	0.0000
Acta2	actin, alpha 2, smooth muscle, aorta	6872765			x	0.827	0.0002	1.06	0.3320	1.43	0.0002	1.73	0.0000
Capsl	calcyphosine-like	6828663			x	0.631	0.0003	0.647	0.0008	1.03	0.6550	1.64	0.0000
Cldn8	claudin 8	6847680			x	0.744	0.0035	0.839	0.1530	1.28	0.0125	1.72	0.0001
Cobll1	Cobl-like 1	6887286			x	0.726	0.0086	0.885	0.1360	1.14	0.0962	1.57	0.0004

Dab1	disabled homolog 1 (Drosophila)	6915993			x	0.757	0.0275	0.84	0.1210	1.18	0.0206	1.56	0.0025
Dhcr24	24-dehydrocholesterol reductase	6916089			x	1.18	0.2060	1.03	0.7750	0.753	0.0257	0.639	0.0003
E330013P04Rik	E330013P04Rik	6870841			x	0.7710	0.0164	0.9670	0.6610	1.4100	0.0045	1.8300	0.0003
Elovl6	ELOVL family member 6, elongation of long chain fatty acids (yeast)	6901316			x	1.14	0.0783	1.06	0.3200	0.746	0.0036	0.654	0.0003
Enpp2	ectonucleotide pyrophosphatase/phosphodiesterase 2	6835759			x	0.784	0.0039	1.01	0.9160	1.31	0.0206	1.67	0.0006
Enpp3	ectonucleotide pyrophosphatase/phosphodiesterase 3	6772810			x	0.86	0.0087	0.993	0.9140	1.4	0.0002	1.63	0.0000
Epha4	Eph receptor A4	6759905			x	1.11	0.1360	1.09	0.3200	0.653	0.0029	0.59	0.0010
Etv5	ets variant gene 5	6844558			x	1.17	0.2360	1.21	0.0863	0.631	0.0032	0.541	0.0007
Evi1	ecotropic viral integration site 1	6903875			x	1.21	0.0101	1.16	0.0313	0.791	0.0039	0.655	0.0000
Eya4	eyes absent 4 homolog (Drosophila)	6772736			x	1.19	0.1160	1.06	0.5730	0.687	0.0011	0.578	0.0003
Fabp7	fatty acid binding protein 7, brain	6768075			x	0.58	0.0145	0.79	0.3350	1.21	0.3250	2.09	0.0009
Foxf1a	forkhead box F1a	6979570			x	1.08	0.4460	0.805	0.0277	0.697	0.0056	0.645	0.0006
Frem1	Fras1 related extracellular matrix protein 1	6922890			x	1.1	0.1260	1.02	0.7380	0.706	0.0000	0.643	0.0000
Grik2	glutamate receptor, ionotropic, kainate 2 (beta 2)	6773802			x	0.824	0.0569	1.02	0.8750	1.46	0.0032	1.77	0.0000
Hgf	hepatocyte growth factor	6928939			x	0.809	0.0079	0.866	0.0965	1.28	0.0122	1.58	0.0002
Igf2	insulin-like growth factor 2	6972317			x	1.12	0.1280	0.916	0.2730	0.703	0.0006	0.628	0.0000

Lce3b	late cornified envelope 3B or late cornified envelope 3C (Lce3c)	6899456			x	1.68	0.0010	1.55	0.0111	0.962	0.7710	0.571	0.0002
Leprel1	leprecan-like 1	6844806			x	1.06	0.5160	0.867	0.0496	0.7	0.0020	0.661	0.0037
Lhx8	LIM homeobox protein 8	6910727			x	1.35	0.0006	1.25	0.0221	0.559	0.0166	0.413	0.0016
Lix1	limb expression 1 homolog	6848947			x	1.02	0.7910	0.983	0.8390	0.632	0.0019	0.619	0.0023
Lyz1	lysozyme 1 *or* lysozyme 2	6777310			x	0.729	0.0031	0.742	0.0083	1.09	0.4880	1.500	0.0058
Meg3	maternally expressed 3	6797969			x	1.34	0.0048	1.14	0.1490	0.707	0.0003	0.528	0.0000
Mgst1	microsomal glutathione S-transferase 1	6950582			x	0.746	0.0134	0.764	0.0345	1.16	0.1360	1.56	0.0015
Olfml3	olfactomedin-like 3	6907784			x	1.17	0.0320	0.939	0.4970	0.687	0.0015	0.584	0.0000
Olfr1505	olfactory receptor 1505 *or* olfactory receptor 1502 (Olfr1502)	6868243			x	0.689	0.0027	0.87	0.2810	1.06	0.5840	1.54	0.0041
Pcolce2	procollagen C-endopeptidase enhancer 2	6991538			x	1.07	0.2230	0.88	0.0368	0.683	0.0006	0.639	0.0002
Prrx2	paired related homeobox 2	6876081			x	1.08	0.2260	1.09	0.1970	0.687	0.0047	0.634	0.0007
Ptch1	patched homolog 1	6813844			x	1.16	0.1010	0.853	0.1720	0.767	0.0245	0.663	0.0003
Slc2a3	solute carrier family 2 (facilitated glucose transporter), member 3	6957051			x	0.778	0.0423	0.97	0.8040	1.25	0.0375	1.61	0.0003
Tbx22	T-box 22	7013222			x	1.29	0.1780	1.32	0.1130	0.479	0.0062	0.37	0.0011
Tcfap2b	transcription factor AP-2 beta	6747919			x	0.756	0.0152	0.99	0.9200	1.32	0.0175	1.75	0.0005
Tdg	thymine DNA glycosylase	6769343			x	0.754	0.0949	0.819	0.2140	1.23	0.1960	1.64	0.0034
Trp53inp1	transformation related protein 53 inducible nuclear protein 1	6911679			x	0.823	0.0023	0.826	0.0083	1.25	0.0227	1.51	0.0004
Unc5c	unc-5 homolog C (C.elegans)	6901898			x	1.03	0.6020	0.931	0.3360	0.675	0.0001	0.658	0.0000

Table 3: Human and mouse craniofacial phenotypes associated with genes showing altered expression in *Twsg1*$^{-/-}$ mice.

Name	WTvC only	Both	AvC only	Associated human syndrome features (OMIM)	Mouse knockout phenotype (MGI)	Relative expression			
						A/WT	B/WT	C/WT	C/A
Alx1		x			short mandible and maxilla, abnormal calvaria, facial clefting	0.87	0.51[a]	0.24[c]	0.27[c]
Bmp4		x		Microphthalmia/anopthalmia (OMIM #607932), orofacial clefting (OMIM #600625)	shortened frontal and nasal bones, agnathia	0.84	0.68[a]	0.37[c]	0.44[c]
Bmp5	x				small ears, small skull, short nasal bone, short mandible, short maxilla, abnormal hyoid	0.67[b]	0.58[b]	0.56[c]	0.84
Bmpr1b		x			short snout	1.01	1.11	1.59[c]	1.58[c]
Cyp26a1		x			branchial arch hypoplasia, abnormal facial/head morphology, microcephaly	0.93	1.1	1.68[c]	1.81[c]
Dkk1		x			absent mandible, maxilla, nasal bone, abnormal calvaria and BA1 morphology, microcephaly	0.91	0.70[a]	0.46[c]	0.50[c]
Dlk1		x		Facial malformations (OMIM 176290)		1.24[a]	1.0	0.58[c]	0.47[c]
Evi1			x		abnormal branchial arch morphology	1.21[a]	1.16[a]	0.79[c]	0.66[c]
Eya4			x		abnormal palate morphology	1.19	1.06[a]	0.69[c]	0.58[c]
Gata3		x			abnormal craniofacial bone morphology	0.96	0.73[a]	0.51[c]	0.53[c]
Igf2			x	Silver Russell Syndrome (OMIM #180860), micrognathia, cleft palate (Bruce et. al 2009)	variable cleft palate with (maternal) uniparental disomy 7	1.12	0.92	0.70[c]	0.63[c]
Isl1		x			abnormal branchial arch morphology	0.74[b]	0.48[b]	0.30[c]	0.42[c]
Lhx8			x		cleft palate	1.35[c]	1.25*	0.56*	0.41[b]
Lrig3	x				abnormal craniofacial morphology, short snout	1.09[a]	1.19[b]	1.52[c]	1.39[c]
Msx2		x		Craniosynostosis type 2 (OMIM #604757)	abnormal craniofacial development, cleft palate, short snout, abnormal calvaria, teeth, middle ear ossicles	0.95	0.78[b]	0.61[c]	0.64[c]
Pitx2	x			Axenfeld-Rieger syndrome (OMIM #180500), eye abnormalities, dental and maxillary hypoplasia	abnormal Meckel's cartilage, mandible, maxilla, teeth, cleft palate	0.84[b]	0.82	0.64[c]	0.76[c]
Prrx2			x		micrognathia, abnormal maxilla, Meckel's cartilage, middle ear ossicles, hyoid, ears, teeth, cleft palate	1.08	1.09	0.69[c]	0.63[c]
Ptch1			x	Holoprosencephaly (OMIM #610828)	Abnormal craniofacial morphology, abnormal mandible, BA1	1.16	0.85	0.77[a]	0.66[c]

Satb2		X		Isolated cleft palate (OMIM #119540)	micrognathia, premaxilla hypoplasia, abnormal nasal capsule, microcephaly, cleft palate, tooth abnormalities, short snout	1.42 [b]	0.93	0.33 [c]	0.23 [c]
Sema3e		X		CHARGE syndrome (OMIM #214800), facial dysmorphism, external ear abnormalities		0.89 [b]	1.08	1.5 [b]	1.7 [c]
Sox2	X			microphthalmia/anopthalmia (OMIM 184429)	abnormal palate morphology	0.71 [c]	0.7 [a]	0.59 [b]	0.84
Tbx22			X	X-linked cleft palate (OMIM #303400) with or without ankyloglossia	abnormal calvaria, cleft palate	1.29	1.32	0.48 [b]	0.37 [b]

Alx1, ALX homeobox 1; *Bmp4*, bone morphogenetic protein 4; *Bmp5*, bone morphogenetic protein 5; *Bmpr1b*, bone morphogenetic protein receptor, type 1B; *Cyp26a1*, cytochrome P450, family 26, subfamily a, polypeptide 1; *Dkk1*, dickkopf homolog 1 (Xenopus laevis) or predicted gene, EG546723 or protein phosphatase 1, regulatory (inhibitor) subunit 2 (*Ppp1r2*); *Dlk1*, delta-like 1 homolog (Drosophila); *Evi1*, ecotropic viral integration site 1; *Eye4*, eyes absent 4 homolog (Drosophila); *Gata3*, GATA binding protein 3; *Igf2*, insulin-like growth factor 2; *Isl1*, ISL1 transcription factor, LIM/homeodomain; *Lhx8*, LIM homeobox protein 8; *Lrig3*, leucine-rich repeats and immunoglobulin-like domains 3; *Msx2*, homeobox, msh-like 2 or LOC100046255, similar to homeobox protein; *Pitx2*, paired-like homeodomain 2; *Prrx2*, paired related homeobox 2; *Ptch1*, patched

Identification of molecular and cellular effectors of craniofacial phenotype in *Twsg1* mutants

To study the association between phenotypic variability and differential gene expression in more detail, we first focused upon samples representing the most divergent morphological classes, i.e. WT vs. class C embryos. Microarray analysis identified 65 genes (represented by 66 exon probe sets, including two sets for *Rgs5*) with significantly different, reproducible patterns of expression between these classes (Figure 8A and Table 2). While most of these full-length transcripts (82%) are downregulated in class C embryos, 12 transcripts (18%) are increased. To validate results from microarrays, we performed Q-PCR on selected, differentially expressed transcripts. The results closely corroborated those from microarrays ($r=0.9541$, $p<0.0001$) (Figure 8 B-G). This high degree of reproducibility of the microarray data was confirmed further using independently isolated mRNAs, by re-measuring expression levels of G-protein-coupled receptor 50 (*Gpr50)*, *Bmp4*, and BMP receptor, type 1B *(Bmpr1b)* by Q-PCR (Fig 8H). Again, a high concordance between microarray and Q-PCR results exists across the different phenotypic classes ($r=0.9321$, $p=0.0003$) (Figure 8H).

Among those genes that are differentially expressed between WT and class C mutants, 15 are known to be associated with craniofacial defects in mice and/or humans (Table 3), as annotated by Mouse Genome Informatics (MGI) and Online Mendelian Inheritance in Man (OMIM). Several encode ligands (*Bmp4*, *Bmp5*), receptors (*Bmpr1b*) and downstream targets of BMP signaling (*Msx2*; *Pitx2)* (Schlange et al., 2002; Du and Yip, 2009), which is consistent with the known role of TWSG1 in modulating BMP

signaling (Ross et al., 2001). Beyond confirming an expected role for BMPs in *Twsg1*$^{-/-}$ phenotypes, transcriptome analysis facilitated identification of additional candidate effectors of the craniofacial phenotype in *Twsg1*$^{-/-}$ mice. For example, there is an inverse correlation between *Dkk1* expression and increasing phenotypic severity. Other genes showing a similar pattern to *Dkk1* include *Alx1* (Zhao et al., 1996), *Gata3* (Pandolfi et al., 1995), *Isl1* (Pfaff et al., 1996), or *Pitx2* (Sclafani et al., 2006), each known to play various roles in BA1 development, palate and craniofacial bone morphology.

The genes that are differentially expressed between class C and WT regulate a number of biological processes that are important for normal craniofacial morphogenesis (Table 4; top 12 molecular and cellular functions represented by at least 3 molecules are shown based on the p value), including apoptosis, which was identified previously as a key cellular process that is altered in *Twsg1*$^{-/-}$ mice (MacKenzie et al., 2009). In addition, a significant number of differentially expressed genes have been linked by Ingenuity Pathway Analysis (IPA; Ingenuity® Systems, www.ingenuity.com) to "small molecule biochemistry" and "lipid metabolism," highlighting the importance of cholesterol biosynthesis and metabolism of fatty acids and acyl-CoA in normal craniofacial development (Muenke and Beachy, 2000).

Table 4: Predicted biological processes underlying craniofacial phenotype in *Twsg1*$^{-/-}$ mice.

Molecular and Cellular Functions	Highest P-value	List of molecules
Cellular Movement Migration of neurons	2.54E-06	ANGPT1, BMP4[n], DCLK1[n], EBF1[n], FGF9, FIGF, GATA3[n], HMGCR, ID1, ID2, ID3, ISL1, MME, MSX2, NR2F1[n], NR2F2[n], PITX2, PMP22, SATB2[n], SEMA3E
Cellular Development	2.54E-06	ANGPT1, BMP4, BMPR1B, CYP26A1, DLK1, EBF1, ENPP1, FGF9, FIGF, GATA3, ID1, ID2, ID3, ISL1, MSTN, MSX2, NR2F1, PITX2, PMP22, SATB2, SOX2, TBX3,
Cellular Function and Maintenance	1.58E-05	BMP4, BMP5, BMPR1B, GATA3, ID1, ID2, NR2F1
Cellular Growth and Proliferation	1.58E-05	ANGPT1, BMP4, BMP5, BMPR1B, DLK1, FGF9, FIGF, GATA3, ID1, ID2, ID3, HMGCR, ISL1, MSTN, MSX2, PITX2, PMP22, PLAGL1, SOX2, TBX3
Gene Expression	1.58E-05	ALX1, TBX3, ISL1, GATA3, PITX2, ID2, BMPR1B, PLAGL1, SATB2, MSX2, DCLK1, SOX2, NR2F1, ID3, EBF1, MSTN, ID1, NR2F2, BMP4
Cell Cycle	1.5E-04	ANGPT1, BMP4, BMPR1B, FGF9, FIGF, ID1, ID2, ID3, SOX2, PITX2, PLAGL1, TBX3
Cell Signaling BMP signaling pathway	6.6E-04	ANGPT1, BMP4[b], BMPR1B[b], DOK5, ID1[b], MSX2[b]
Cell-To-Cell Signaling and Interaction	1.1E-03	ANGPT1, BMP4, BMPR1B, FIGF, ID1, ID3, PCDH7
Lipid Metabolism	2.5E-03	BMP4, CYP26A1, CYP51A1, DLK1, FGF9, HMGCR, NSDHL, SCD
Small Molecule Biochemistry	2.5E-03	ANGPT1, CYP26A1, CYP51A1, DDC, DLK1, ENPP1, FGF9, GATA3, HMGCR, KRT14, NSDHL, SCD, BMP4
Cell Death	3.49E-03	BMP4, BMPR1B, DLK1, ID1, ID2, ISL1, MME, MSX2
Cell Morphology	6.81E-03	ANGPT1, BMP4, DCLK1, EMA3E, ENPP1, FIGF, GATA3, ID1, ID3, MSX2, NR2F1, PLAGL1, PMP22, SDLK1

[b]molecules involved in BMP signaling pathway, [n]molecules involved in migration of neurons

To determine whether NCC are the cellular effectors of the craniofacial phenotype in *Twsg1*$^{-/-}$ mice, we generated mice with NCC-specific deletion of *Twsg1* (*Twsg1*$^{flox/flox}$*;Sox10-cre*). *Sox10-cre* mice express Cre recombinase in NCC, as early as a premigratory stage, and in NCC derivatives, specifically the pharyngeal region (Matsuoka et al., 2005; Muller et al., 2008). The phenotype of these mice recapitulated the phenotype of global deletion of *Twsg1* (MacKenzie et al., 2009), but the effect was dependent on the efficiency of Cre-mediated deletion of exon 4 of *Twsg1* (Figure 3). A reduction of *Twsg1* level to less than 0.2% of the wild type expression in BA1 at E11.5 resulted in embryonic craniofacial defects, including premature fusion of the mandibular components of BA1, midline fusion of the frontonasal prominences and non-septation of the telecephalic vesicles.

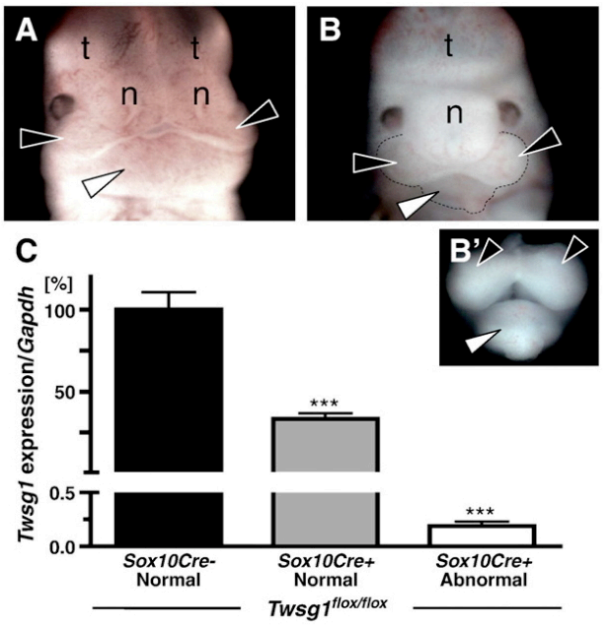

Figure 9: The frequency of craniofacial defects in mice with neural crest cell-specific deletion of *Twsg1*.
The frequency of craniofacial defects in mice with NCC-specific deletion of Twsg1. *Twsg1*$^{flox/flox}$; *Sox10-cre* + embryos included both (A) normal appearing embryos (black arrowheads point to the maxillary components of BA1; white arrowhead to the mandibular component; n, nasal prominences; t, telencephalic vesicles) and (B) embryos with craniofacial abnormalities, including fusion of the mandibular arches, nasal processes, and telencephalic vesicles (B′) Dissection of the mandibular and maxillary components of BA1 highlights hypoplasia and midline fusion of the mandibular prominences that characterizes the severe Twsg1 phenotype. (C) Expression levels of *Twsg1*, measured using primers to exon 4 and 5 were compared between *Twsg1*$^{flox/flox}$*;Sox10-cre-* and *Twsg1*$^{flox/flox}$*;Sox10-cre+* depending on the presence or absence of external craniofacial abnormalities. A reduction of *Twsg1* levels to less than 0.2% of the wild type expression in BA1 at E11.5 resulted in craniofacial defects. Both maxillary and mandibular prominences were collected. Q-PCR was performed using individual mRNA samples. Three embryos per genotype were analyzed.

Transcriptional changes between class A and class C mutants and their functional significance

Class A and class C embryos share the same genetic mutation in *Twsg1* but differ in the absence or presence of craniofacial defects. Therefore we extended our analysis to genes that are differentially expressed between these classes of mutants, as they may provide new insights into mechanisms underlying variable disease expressivity. We identified 80 genes that were differentially expressed between affected and unaffected *Twsg1*$^{-/-}$ embryos (Table 2), including 41 additional transcripts that were not identified in the WT vs class C comparison. The number of genes that showed opposite trends in class A vs class C (Figure 10A) significantly increased compared to the class C vs WT comparison (Figure 8A) by using this approach. To highlight such changes, we grouped these differentially expressed genes into various expression patterns: P1 includes genes downregulated in class C; P2 genes upregulated in class A and downregulated in class C; P3 the reverse trend of P2; and P4 genes upregulated in class C (Figure 10A).

Microarray results indicating differential gene expression between phenotypic classes A and C were validated further by both Q-PCR (Figure 10B-F) and *in situ* hybridizations (Figure 11). Despite their normal external appearance, class A mutants show a marked increase in expression for *Plagl1*, *Satb2* and *Peg3* (Figure 5 G-O). Other anatomic expression sites for these genes outside BA1 were not affected in the various classes of embryos, indicating a BA1-specific effect (data not shown).

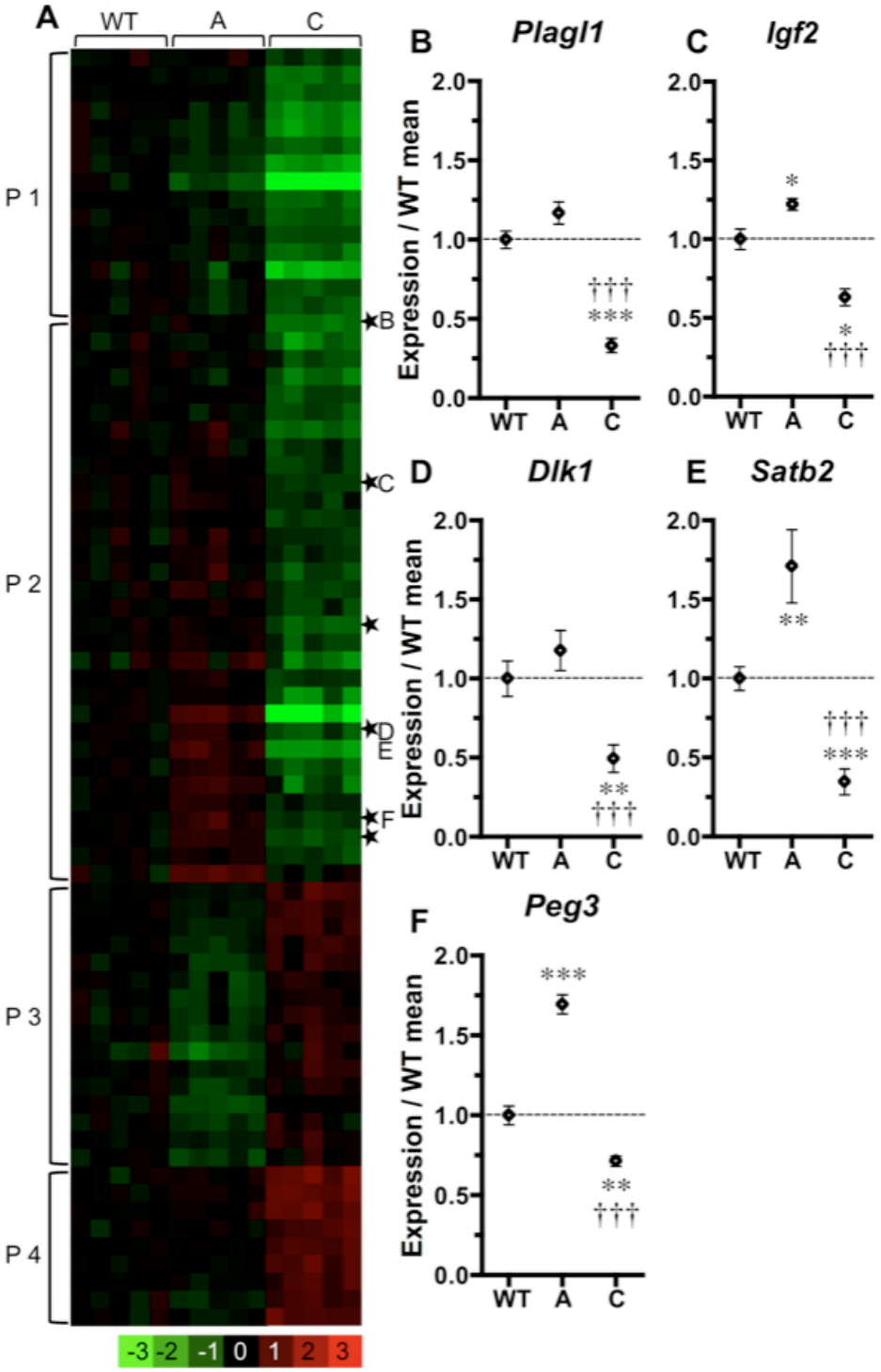

Figure 10: Gene expression differences between unaffected and severely affected mutants. (A) A heatmap of expression changes in various phenotypic classes was compared to the average of WT. Genes with expression changes >1.5 fold and with a false discovery rate of <10% are presented as rows. ★Imprinted genes. (B-F) Q-PCR confirmation. Significance levels in comparison with WT (*) or with class A (†); three symbols represent p<0.001; two, p<0.01; one, p<0.05.

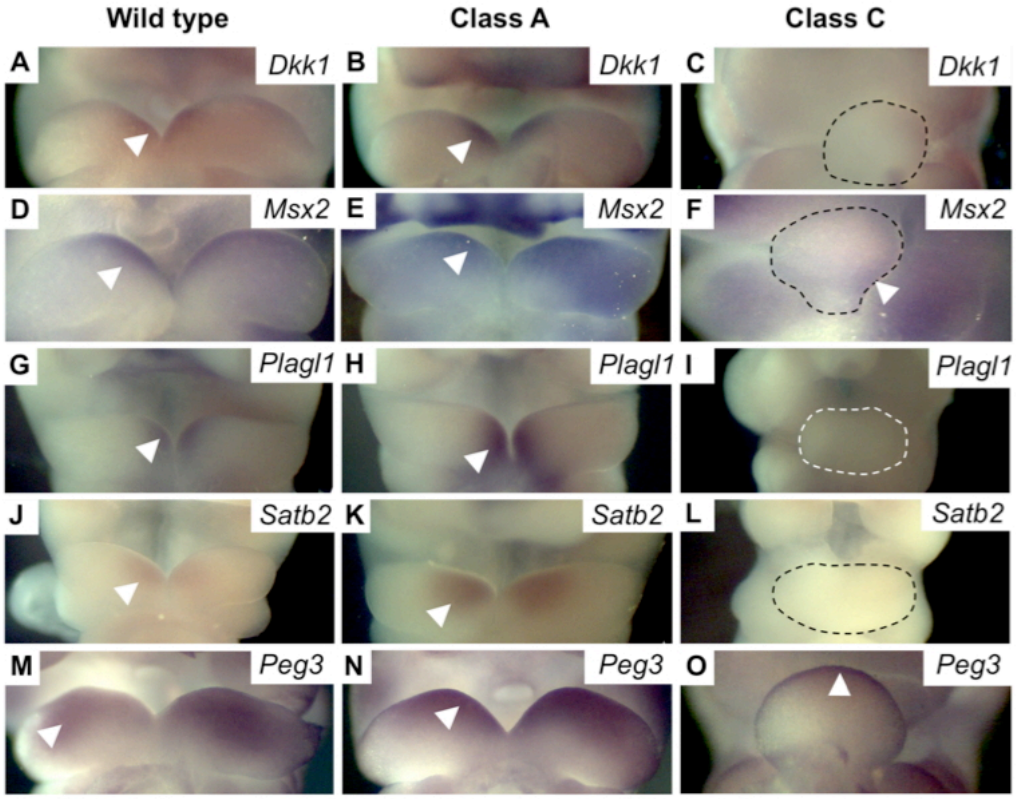

Figure 11: Validation of differential gene expression by *in situ* hybridization. Photomicrographs of embryos from different phenotype classes, probed by *in situ* hybridization for (A-C) *Dkk1* and (D-F) *Msx2*, show similar expression levels between WT and class A, but profoundly decreased expression in class C. (G-I) *Plagl1*, (J-L) *Satb2* and (M-O) *Peg3* show increased expression in class A and markedly decreased expression in class C. These represent various patterns of differential gene expression as described in the text. Arrowheads indicate expression domains within BA1.

The ontological categories of genes whose expression levels differ between class A and class C are shown in Table 5. Again, apoptosis is among the key biological processes. *Tumor protein 53-induced nuclear protein 1* (*Trp53inp1*) was identified among a set of genes that play a role in regulating apoptosis, which are uniquely altered between affected and unaffected mutants. Additional biological processes were identified as distinguishing between affected and unaffected embryos, including cellular assembly and organization, carbohydrate metabolism, and DNA replication, recombination, and repair.

Table 5: Predicted biological processes regulated by genes uniquely altered between class A and class C mutants.

Molecular and Cellular Functions	Highest P-value	List of molecules
Cellular Movement	1.1E-02	DAB1, ENPP2, EPHA4, ETV5, FABP7, FOXF1, HGF, IGF2, UNC5C
Cell-To-Cell Signaling and Interaction	1.32E-02	ENPP3, FABP7, GRIK2, HGF, IGF2
Cellular Growth and Proliferation	1.6E-02	DHCR24, ENPP2, ENPP3, EVI1, FABP7, FOXF1, HGF, IGF2, PRRX2, PTCH1, TFAP2B, TP53INP1, UNC5C
Cellular Assembly and Organization*	1.71E-02	DAB1, ENPP2, EPHA4, FABP7, HGF, IGF2, PTCH1, TFAP2B,
Small Molecule Biochemistry	1.71E-02	DHCR24, ENPP2, ENPP3, ELOVL6, FABP7, HGF, IGF2, TP53INP1,
Cellular Development	1.71E-02	FABP7, FOXF1, HGF, IGF2, LHX8, UNC5C
Carbohydrate Metabolism*	1.71E-02	ENPP2, HGF, IGF2, TP53INP1
Cell Death	1.71E-02	DHCR24, GRIK2, HGF, IGF2, MGST1, TFAP2B, TRP53INP1, UNC5C
Cellular Function and Maintenance	1.71E-02	EPHA4, EVI1, FABP7, HGF, IGF2
Lipid Metabolism	1.71E-02	DHCR24, ELOVL6, ENPP2, FABP7, HGF
Molecular Transport*	1.71E-02	ENPP2, FABP7, HGF, IGF2, TP53INP1
Gene Expression	1.84E-02	ETV5, EVI1, FOXF1, HGF, IGF2, TBX22, TFAP2B
DNA Replication, Recombination, and Repair*	1.84E-02	ENPP3, HGF, IGF2, PTCH1

*Processes identified as significant based on class C vs class A comparison, but not class C vs wild type comparison

Among the differentially expressed transcripts that were not identified in class C vs WT embryo comparisons, but were identified in comparisons of class A vs. C

embryos, seven play known roles in craniofacial development in mice and/or humans (*Evi1, Eya4, Igf2, Lhx8, Prrx2, Ptch1, Tbx22*) (Hoyt et al., 1997; ten Berge et al., 1998; Zhao et al., 1999; Braybrook et al., 2001; Ming et al., 2002; Depreux et al., 2008; Bruce et al., 2009) (Table 3). Interestingly, each of these genes groups in expression pattern P2. While each transcript showed less than 1.5-fold decrease in expression in class C compared to WT, the difference from class A was accentuated by a small increase in their expression in class A mutants. Since many of these genes may serve similar functions during craniofacial development, it is plausible that additive effects of these small changes may compensate for the loss of TWSG1 during BA1 morphogenesis, and protect class A embryos against manifestation of disease. Other genes, including imprinted genes, also are upregulated in class A and downregulated in class C, suggesting that they either are co-regulated within gene networks important for craniofacial development or may play a direct role in craniofacial development (Feng et al., 2009).

Genetic deletion of *p53* reduces incidence of craniofacial defects in *Twsg1*$^{-/-}$ mice

Further comparison of class A vs. C differentially expressed transcripts identified genes that are downregulated in class A and upregulated in class C. This pattern (P3) was not observed in the comparison between WT and class C mutants except for *Sema3e*. Among them was a p53-inducible gene, *Trp53inp1* (Tomasini et al., 2003). The pattern of *Trp53inp1* expression in the different phenotypic classes suggested that increased p53 activity could play a role in mediating the phenotype. Western blotting on whole embryos demonstrated that p53 levels were, in fact increased in severely affected homozygous mutants (class C) with lower levels of p53 in unaffected homozygous mutants (class

A), or WT embryos (Figure 12A). Q-PCR analysis of *Trp53inp1* transcript levels confirmed microarray data indicating upregulation of this gene in class C embryos with a trend toward reduction in class A embryos compared to WT (Figure 12B).

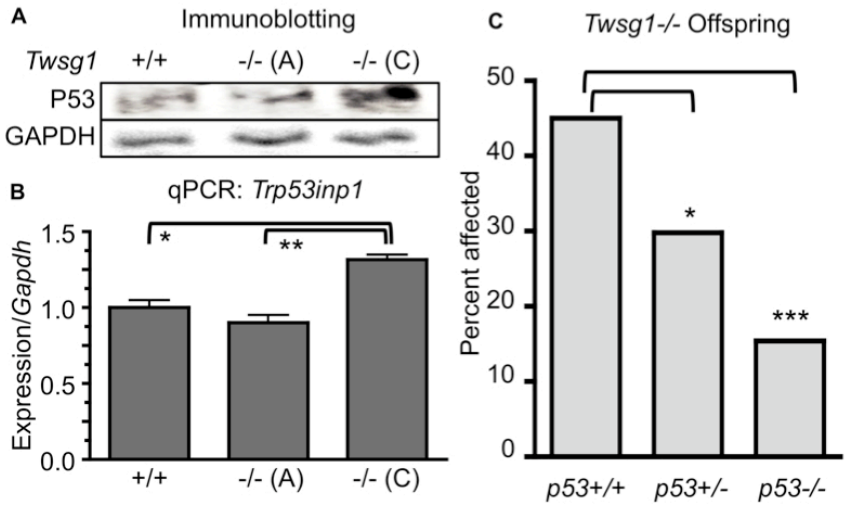

Figure 12: Suppression of craniofacial defects *Twsg1*$^{-/-}$ mice by a genetic deletion of *p53*. (**A**) Western blotting for p53 using whole E10.5 embryos indicates increased p53 protein levels in *Twsg1*$^{-/-}$ class C, compared to *Twsg1*$^{-/-}$ class A or WT embryos. GAPDH levels were consistent across these samples (**B**) Q-PCR measurement of *Trp53inp1* transcript levels confirms microarray data indicating upregulation of this gene in class C embryos with a trend toward reduction in class A embryos (**C**) Decreasing incidence of craniofacial defects among *Twsg1*$^{-/-}$ pups is associated with reduced *p53* gene dosage. *p<0.05, **p<0.01, ***p=0.001.

Based on upregulation of p53 and *Trp53inp1* in class C embryos that show the highest degree of apoptosis in BA1, and since suppression of p53 prevents the neurocristopathy of Treacher-Collins syndrome through inhibition of NCC apoptosis (Jones et al., 2008), we hypothesized that a similar phenotypic rescue might be observed after a genetic deletion of p53 on the *Twsg1*$^{-/-}$ background.

Progeny from *Twsg1*$^{+/-}$*p53*$^{+/-}$ intercrosses or *Twsg1*$^{+/-}$*p53*$^{+/-}$ × *Twsg1*$^{-/-}$*p53*$^{+/-}$ matings were analyzed (both neonates and embryos at E17.5) for the presence of external craniofacial defects. The rate of recovery of *Twsg1*$^{-/-}$*p53*$^{+/-}$ and *Twsg1*$^{-/-}$*p53*$^{-/-}$ genotypes is consistent with the predicted distribution based on Mendelian inheritance. The frequency of *Twsg1*-related craniofacial defects significantly decreased with a reduction of p53 gene dosage from 44% in *Twsg1*$^{-/-}$*p53*$^{+/+}$ pups (N=675) (Sun et al., 2010) to 30% in *Twsg1*$^{-/-}$*p53*$^{+/-}$ (N=47, p=0.04) and 15% in *Twsg1*$^{-/-}$*p53*$^{-/-}$ littermates (N=39, p=0.001) (Figure 12C). While craniofacial defects were prevented to a large degree by a loss of two copies of p53, there was also a high degree of perinatal death among *Twsg1*$^{-/-}$*p53*$^{-/-}$ neonates (up to 66%), suggesting involvement of other organ systems. As previously published, we observed that homozygous deletion of p53 leads variably to exencephaly (Sah et al., 1995). This phenotype appeared independently of *Twsg1* genotype.

Imprinted genes are overrepresented among genes that are upregulated in class A and downregulated in class C mutants

The various expression patterns defined for groups of differentially expressed genes may help identify a common regulatory mechanism for each group. Interestingly, we found that group P2, with an increase or a trend toward increase from WT in class A and a decrease in expression in class C mutants, is highly enriched in imprinted genes. Using a list of imprinted loci (Morison et al., 2001; Morison et al., 2005), we identified 68 transcript clusters corresponding to imprinted loci in the array of 16755 transcript clusters. Of these 68, six are differentially regulated between class A and class C: *Plagl1* (Figure 10B), *Igf2* (Figure 10C)*, Dlk1* (Figure 10D)*, paternally expressed 3 (Peg3)*

(Figure 10F), *ankyrin repeat and SOCS box-containing protein 4 (Asb4),* and *maternally expressed 3* (*Meg3)*. This proportion of imprinted genes is much higher than predicted by chance, as indicated by a χ^2 analysis yielding a p-value of $< 2.92*10^{-23}$. To confirm the enrichment of imprinted genes, a more stringent approach was also taken. In this case, we estimated the number of imprinted genes to represent 2.5% of the mouse genome (Luedi et al., 2005). Finding six imprinted genes represented in the 81 differentially expressed transcript clusters was again significant, with a p value of <0.0046.

Discussion

Differential gene expression is associated with *Twsg1*$^{-/-}$ phenotypic severity

Transcriptional profiling has been used previously to identify genes important in normal development of individual facial prominences (Feng et al., 2009) as well as downstream targets of mutated genes (Jeong et al., 2008). Mouse knockouts with variable phenotypes present a particular challenge and an opportunity to gain insights into the basis of this variability. For the first time, we undertook an effort to correlate phenotypic severity of craniofacial defects with changes in the transcriptome, based on the premise that both unaffected and affected *Twsg1*$^{-/-}$ mutants would show changes in gene expression compared to WT mice and to each other.

We observed reproducible transcriptional profiles that cluster into distinct groups, and are strongly associated with the observed phenotypic categories in *Twsg1*$^{-/-}$ mice. This observation strongly suggests that these transcriptional patterns help to define the

distinct morphological and functional groups of *Twsg1*$^{-/-}$ mice. Among the genes that are differentially expressed between class C and WT BA1, about 20% are associated directly with known human or mouse craniofacial defects. Others may represent new candidate genes that may contribute to human craniofacial diseases. Most of these genes are downregulated in class C mutants; since they regulate development of similar craniofacial structures, their loss of expression helps to explain observed craniofacial defects in *Twsg1* mutants. As an example, significantly reduced *Dkk1* expression could contribute to the anterior truncation phenotype (Mukhopadhyay et al., 2001) of some *Twsg1*$^{-/-}$ mice.

We were able to distinguish transcript differences not only between WT and affected mutants, but also between unaffected and affected *Twsg1*$^{-/-}$ mutants. This led to three main conclusions. First, class A *Twsg1*$^{-/-}$ embryos, despite appearing normal on a morphological level, are not "normal" on a molecular level. Second, genes that are differentially expressed between the genetic mutants and the WT embryos, but not differentially expressed between phenotypic class A vs. class C mutants, presumably do not play a role in development of the severe mutant phenotype. Third, genes that are differentially expressed between class A and class C mutants may provide clues about possible compensatory mechanisms that prevent class A mutants from developing craniofacial defects. In particular, upregulation of craniofacial genes which regulate development of BA1, palate, maxilla, nasal capsule, and teeth (*Evi1, Eya4, Igf2, Lhx8, Prrx2, Ptch1, Satb2*, and *Tbx22*) in class A mutants may compensate for the loss of

TWSG1 function during craniofacial morphogenesis.

A role for a stress response in craniofacial pathology

It has been suggested that NCC are particularly sensitive to cellular stress during embryogenesis and that suppression of p53 can prevent craniofacial defects in a murine model of Treacher-Collins syndrome (Jones et al., 2008), *Tcof1*$^{+/-}$ mice. Our experiments showing a genetic rescue of craniofacial defects in *Twsg1*$^{-/-}$ mice corroborate this data and suggest that this approach may have broader implications for the prevention of craniofacial defects by targeting the p53 pathway.

The end-result of increased p53 signaling in *Tcof1*$^{+/-}$ mice was proposed to be an increase in NCC apoptosis and deficient formation of NCC, leading to craniofacial defects. Similarly, increased neuroepithelial apoptosis is at the core of neural tube defects in *Pax3*-deficient embryos, which also can be rescued by a loss of p53 function (Pani et al., 2002). We have previously shown that abnormal BA1 development in *Twsg1*$^{-/-}$ mice is also associated with increased apoptosis, albeit at a later stage, once NCC have populated the branchial arches (MacKenzie et al., 2009). Thus, an increase in apoptosis is a common link between these mouse models of birth defects, which each show phenotypic rescue by suppression of p53.

In *Twsg1*$^{-/-}$ mice, this increase in apoptosis is thought to be due to disruption of a BMP gradient in BA1 (MacKenzie et al., 2009). While BMPs are known to have proapoptotic effects during embryonic development (Graham et al., 1994; Mina et al., 2002), understanding of downstream molecular mechanisms remains limited. There is

some evidence from in vitro studies that BMP4-induced apoptosis may be p53-dependent (Fukuda et al., 2006). Interestingly, BMPs have been implicated in modulating cellular responses to stress and TWSG1 as a modulator of BMPs (Oelgeschlager et al., 2000; Ross et al., 2001) would also hence be implicated in this process. For example, BMP7 can have a direct antioxidative effect in the kidneys and in neurons (Tsai et al., 2007; Yeh et al., 2009). On the other hand, BMP2 and BMP4 have been shown to have pro-oxidative stress effects in endothelial cells (Csiszar et al., 2006; Csiszar et al., 2008; Wong et al., 2010). With TWSG1's bifunctional role, being able to either promote or inhibit BMP signaling depending on context, the effects on modulation of stress may also be context dependent. We propose that the cell's variable ability to cope with stress may underlie the variable apoptosis and phenotypic variability. The effectors and drivers of this adaptability are not yet known.

A possible role for epigenetic regulation of craniofacial phenotypes cannot be excluded in view of a growing body of evidence that epigenetic phenomena contribute to phenotypic variability in humans and mice (Whitelaw and Martin, 2001; Dolinoy et al., 2007). Imprinted genes are known genomic targets of epigenetic regulation (Waterland and Jirtle, 2004). Whether they also play a role in generating craniofacial variability remains to be determined. While several imprinted genes have been previously shown to be overrepresented in the mandibular prominence compared to the maxillary prominence or the frontonasal prominence in wild type mouse embryos (Feng et al., 2009), our study suggests that altered regulation of the imprinted genes may contribute to generating phenotypic variation in *Twsg1*$^{-/-}$ mice. Notably, most of these genes show gains and

losses of expression between unaffected class A and affected class C *Twsg1*$^{-/-}$ mutants, respectively. Other genes showing this expression pattern also are known to mediate epigenetic effects during development and disease, for example *Satb2* (Gyorgy et al., 2008), *Evi1* (Spensberger and Delwel, 2008), *Eya4* (Osborn et al., 2006), and *Ptch1* (Diede et al., 2009). Several "metastable epialleles" have been described in mice (*A*^{vy}, *Axin*^{Fu}, *Cabp*^{IAP}) (Rakyan et al., 2003; Waterland and Jirtle, 2003; Druker et al., 2004; Dolinoy, 2007), although none that would confer predisposition to the development of craniofacial defects. Stress response, epigenetics, and gene expression can be interrelated. P53 can interact with both DNA methyltransferase 1 (DNMT1) and DNMT3a to alter gene methylation (Esteve et al., 2005; Wang et al., 2005; Gibney and Nolan, 2010). Cellular stress can also change the expression of imprinted genes, including *Igf2, H19*, and *Meg3*, independent of the stress-responsive tumor suppressors, for example due to *de novo* methylation in cancer cells (Pantoja et al., 2005). Cellular stress and methylation are also both impacted by shared biochemical pathways in the metabolism of folate, homocysteine and the synthesis of glutathione (Chern et al., 2001; Tchantchou, 2006) Future studies will examine global methylation patterns in various classes of *Twsg1* mutants to determine if there is indeed a role for epigenetic regulation of craniofacial phenotypes and to identify targets of such regulation.

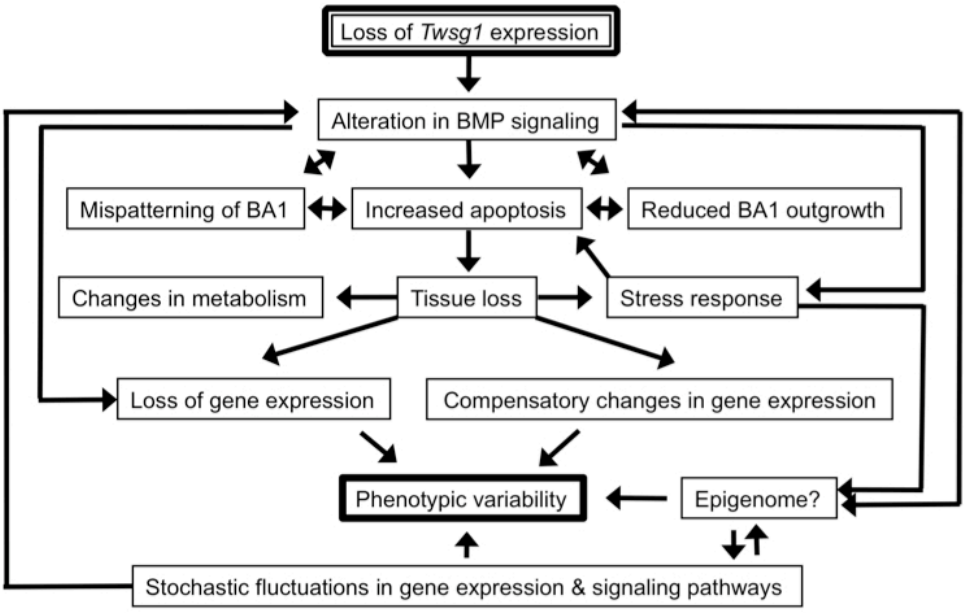

Figure 13: Model for interrelated processes leading to craniofacial phenotypes and craniofacial phenotypic variability in *Twsg1*$^{-/-}$ mice.

Loss of TWSG1 disrupts the BMP gradient within BA1, which leads to mispatterning of BA1, increased cellular stress, increased apoptosis, and reduced outgrowth. Apoptotic tissue loss and loss of peak BMP activity lead to a reduction in BMP targets and other genes expressed in the distal region of BA1 and evoke stress and metabolic responses as well as compensatory changes in gene expression. This is compounded by likely changes in the epigenome as well as stochastic fluctuations in gene expression and signaling pathways, leading to phenotypic variation.

Multifactorial model of craniofacial defects in *Twsg1*$^{-/-}$ mice

We have developed a model that integrates various processes that may be involved in establishing phenotypic variation in *Twsg1*$^{-/-}$ mutant mice (Figure 13). The most immediate effect, which has been corroborated further by transcriptome analysis described here, is the loss of the normal BMP signaling gradient, leading to mispatterning of BA1, reduced outgrowth and excessive apoptosis (MacKenzie et al., 2009). Loss of tissue by apoptosis and loss of peak BMP activity lead to a reduction in BMP targets and

other genes expressed in the distal region of BA1, and evoke compensatory changes in gene expression, changes in cellular metabolism and stress responses. These effects presumably are compounded by stochastic fluctuations in gene expression and signaling pathways (Spudich and Koshland, 1976; Melnick et al., 2006), and possibly by changes in the epigenome at various regulatory elements.

Conclusions

We show here that phenotypic classes of *Twsg1*$^{-/-}$ embryos are associated strongly with distinct patterns of differentially expressed transcripts. This suggests that the phenotypic variation observed in *Twsg1*$^{-/-}$ mice may be caused by heretofore unidentified "master regulators" which in turn would bring about coordinate changes in expression of many downstream genes. An initiating event is disruption of BMP signaling in BA1 of *Twsg1*$^{-/-}$ mice that evokes a number of cellular and molecular responses, including a cellular stress response, which appears to play a key role in the pathogenesis of craniofacial defects. Occurrence of these defects can be suppressed by a reduction in p53 dosage. Further study of transcriptional, and probably epigenetic, contributions to phenotypic variation may not merely explain the wide variation of craniofacial phenotypes in clinical craniofacial syndromes, but also suggest how craniofacial morphological diversity might be enhanced through evolutionary processes (Brugmann et al., 2006). That the face is a key site for morphological evolution is suggested by the wide diversity of craniofacial adaptations in vertebrates (Brugmann et al., 2006). To provide the phenotypic "space" for these adaptations, craniofacial development must

be particularly plastic. The changes we observe highlight the extreme plasticity of transcriptional states and likely the epigenetic states of genes involved in craniofacial development.

Chapter 4: Maternal diet supplementation with methyl donors and increased parity alter the incidence of craniofacial defects in the offspring of *Twisted gastrulation* mutant mice

Introduction

Dietary folate has proven to be a potent preventive factor against neural tube defects (NTD). The effect of folate against NTD was first proposed in the early 1980s and has been robustly confirmed by many subsequent studies in humans (Smithells and Sheppard, 1980; MRC, 1991; Czeizel and Dudas, 1992; Berry et al., 1999; Berry and Li, 2002; De-Regil et al., 2010). This has led to successful public health interventions to fortify foods with additional folate in several countries (Honein et al., 2001; Botto et al., 2006). Other nutrients that act as methyl donors such as choline, its metabolite betaine, and the enzyme co-factor vitamin B12, can facilitate folate metabolism and one-carbon metabolism (see illustration, Figure 14), (Zeisel and Blusztajn, 1994; Scott, 1999; Niculescu and Zeisel, 2002) and can also have protective effects against NTD in concert with or independent of folate (Ray and Blom, 2003; Shaw et al., 2004; Zeisel, 2009).

The dramatic success of folate in prevention of NTD raises the question of whether methyl-donor compounds might also prevent birth defects other than NTD. Their effectiveness in prevention of craniofacial defects is still unclear, with some studies demonstrating beneficial effects of methyl donor nutrients (Tolarova, 1982; Shaw et al., 1995; Tolarova and Harris, 1995; Loffredo et al., 2001) while other studies indicate no beneficial effects (Botto et al., 2006; Shaw et al., 2006; De-Regil et al., 2010; Wehby and Murray, 2010).

Figure 14: The folate and methionine cycles include key cellular reactions aided by methyl donor nutrients.
Folate enters into metabolism by conversion to tetrahydrofolate (THF). THF is, in turn, converted to methylene-THF and then to methyl THF which serves as the donor for remethylating homcysteine (HCY) back to Methionine (MET), a reaction catalyzed by methionine synthase with a vitamin B12 (B12) cofactor. HCY is also methylated to MET in a betaine-dependent reaction catalyzed by betaine-homocysteine methyltransferase. (Betaine is a metabolite of choline). MET serves as the substrate to generate S-adenosyl methionine (SAM). SAM is the primary cellular donor of methyl groups to substrates such as DNA or proteins. When SAM transfers its methyl group it becomes S-adenosyl homocysteine (SAH), which is converted back to cysteine to complete the cycle. If sufficient metabolites are available, methylene THF can also be used to generate nucleotide bases. Likewise if there is sufficient SAM, this allows the conversion of HCY to glutathione, the primary cellular antioxidant, in a Vitamin B6 (B6) dependent reaction.

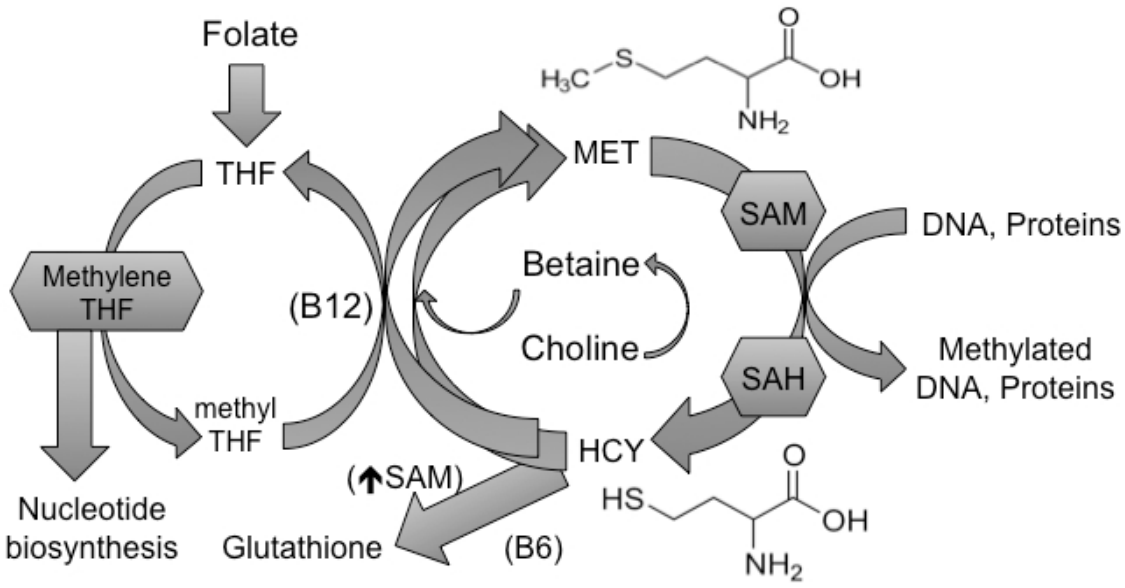

Mouse models offer an experimental advantage for studying effects of dietary supplementation on craniofacial defects because variables like environment and genetic background can be controlled and disease-causing mutations, if present, are defined and constant. For example, in the A/WySnBk mouse strain, which has a high incidence of spontaneous orofacial clefting, maternal supplementation with the folic acid derivative folinic acid reduces incidence of clefting by a factor of 4 (Paros and Beck, 1999). Mice lacking folate receptor 1 (*Folr1*, also called *Folbp1*) exhibit multiple birth defects

including not only NTD but also midline cleft lip, cleft palate, and jaw defects (micrognathia and agnathia) among others (Spiegelstein et al., 2004). Supplementation with folinic acid bypasses the folate receptor defect and ameliorates defects in a dose-dependent manner. In that study there was a trend toward reduced incidence of micrognathia and agnathia in response to folinic acid supplementation, but these defects were too rare in *Folr1*$^{-/-}$ mice to analyze statistically.

Mice deficient in Twisted gastrulation (TWSG1), on the other hand, show relatively high incidence of jaw defects (micrognathia and agnathia) with or without midline facial and brain defects characteristic of holoprosencephaly (HPE) (Petryk et al., 2004). The combination of jaw defects and HPE in humans is referred to as agnathia-HPE complex (or dysgnathia-otocephaly; OMIM #202650) (Pauli et al., 1983). In *Twsg1*$^{-/-}$ mice, these defects show incomplete penetrance and variable expressivity (Petryk et al., 2004; Billington et al., 2011a). This array of craniofacial defects in a mouse model with a defined mutation and genetic background (C57BL/6) provides an opportunity to study the effects of methyl donors on jaw and midline facial defects, which have distinct embryologic origins.

Jaw defects stem from abnormal outgrowth and patterning of the first branchial arch (BA1), an embryonic structure giving rise to the lower and upper jaws and the secondary palate (Thomas et al., 1998; Liu et al., 2010). The most striking BA1 defect seen in *Twsg1*$^{-/-}$ mice is agnathia, absence of the lower jaw (Petryk et al., 2004). Micrognathia (small jaw) represents a less severe BA1 defect (MacKenzie et al., 2009).

Orofacial clefting may also arise from defective BA1 development since clefting of both palate (Stanier and Moore, 2004; Dixon et al., 2011) and lip (Merritt, 2005; Juriloff and Harris, 2008) can derive from deficient growth of the maxillary component of BA1. Defects of midline formation, on the other hand, arise from failure of proper patterning or signaling from the prechordal plate and ventral forebrain (Muenke and Beachy, 2000; Chong et al., 2012) and the frontonasal ectodermal zone, which direct the formation of the midline of the face (Pera and Kessel, 1997; Hu and Marcucio, 2009b; Hu and Marcucio, 2009a).

This study's primary aim was to investigate whether maternal dietary methyl donors reduce the incidence of craniofacial defects in *Twsg1*$^{-/-}$ mice and whether this effect differs for jaw versus midline facial defects. Based on the trend towards reduced agnathia and micrognathia with added folate derivatives in *Folr1*$^{-/-}$ mice, we hypothesized that *Twsg1*$^{-/-}$ mice would show reduced incidence of jaw defects with dietary supplementation of methyl donors.

This study's secondary aim was to examine whether parity has any effect on the incidence or types of defects seen in *Twsg1*$^{-/-}$ mice. Increased parity has been associated with increased risk of NTD (Vieira, 2004), orofacial clefting (Vieira and Orioli, 2002), ear defects (Castilla and Orioli, 1986; Mastroiacovo et al., 1995), and congenital heart defects (Zhan et al., 1991) in humans. On the other hand, some defects, including esophageal defects, limb defects, and hypospadias show decreased incidence with increased birth order (Hay and Barbano, 1972; Duong et al., 2012). No studies of the

effect of parity on craniofacial defects in mice have been published. In fact, parity is typically not taken into account in mouse model studies. Hence, in addition to studying the effect of methyl donors on craniofacial development we have examined parity as a potential factor in *Twsg1*$^{-/-}$ birth defects. This secondary aim is important to consider along with the effect of dietary supplementation particularly given that folate, at least, has been proposed to help reduce risk of recurrence of defects such as clefting in a second pregnancy following a previously affected pregnancy in humans (Tolarova, 1982; Tolarova and Harris, 1995).

Materials and Methods

Mouse care and diet

Generation of mice carrying a deletion of exon 4 in the *Twisted gastrulation* gene (*Twsg1*$^{-}$, MGI: *Twsg1*$^{tm1.1Mboc}$) was previously described (Petryk et al., 2004). All mice were in the C57BL/6 background after backcrossing to C57BL/6NTac mice from Taconic (Hudson, NY) for at least ten generations. Mice were maintained under specific pathogen free conditions in filter-lidded, 18x29 cm cages lined with pulverized corncob bedding, with cotton fiber blocks for nesting material. Cages were changed weekly. Ambient conditions were: air temperature 20-23˚C, humidity 30-70%, with 14h/10h light/dark cycle.

Water was provided in glass bottles *ad libitum*. Mice were given a control diet (NIH31, Harlan-Teklad 7017, repelleted as TD.95262) or a previously described (Wolff et al., 1998; Cooney et al., 2002) form of this diet supplemented with methyl donor

compounds (MDS diet) including folate, vitamin B12, choline, and betaine (Harlan Teklad-TD.01308). Female mice were fed experimental diets for at least 2 weeks prior to mating. Duration of feeding experimental diets past this initial period varied depending on the time to pregnancy and whether litters were kept until weaning. This two week dietary preload period is consistent with previous studies employing these diets (Wolff et al., 1998; Cooney et al., 2002; Waterland and Jirtle, 2003). Physiological levels of nutrients like folate are able to respond to dietary changes rapidly, altering significantly within days of a dietary change (Kitami et al., 2008). Male mice were given the control diet prior to mating and then fed the control or MDS diet along with the females. Ages of females set up for matings ranged from 7 to 35 weeks. Ages of males ranged from 8 to 103 weeks old. For second pregnancies, dams were set up for mating as soon as possible after weaning of first pregnancy offspring.

To generate offspring for the present study, 47 homozygous (*Twsg1*$^{-/-}$) or heterozygous (*Twsg1*$^{+/-}$) female mice from 32 different litters were mated to 15 homozygous (*Twsg1*$^{-/-}$) males, all from different litters. Mice were monitored closely as delivery approached to prevent dams from eating dead or deformed pups before they could be assessed. In some cases pregnant dams were killed, using CO_2 euthanasia, between embryonic day 15.5 (E15.5) and E18.5, and the fetuses explanted. Pups and fetuses were genotyped by PCR amplification of DNA prepared from tail snips using primers for the wild-type allele (5'-ataggagggttgggcgttgaag-F and 5'-acctgacggctaacacagatgc-R), and for the *Twsg1* deletion allele (5'-caacctccctgttagcccac-F, 5'-actgccttgggaaaagcgcc-R). Genotypes of the mice were verified to confirm numbers

of mice in expected Mendelian ratios between +/- and -/- genotypes. Subsequent analyses considered only *Twsg1*$^{-/-}$ offspring.

The University of Minnesota Institutional Animal Care and Use Committee approved the care and use of the mice in this study.

Phenotype scoring

The study's primary outcome was occurrence of jaw and midline facial defects. Pups were assessed by inspection for craniofacial defects including cleft lip, cleft palate, micrognathia, agnathia, cyclopia, proboscis, and anterior truncation. Eye defects such as microphthalmia and anophthalmia were noted but were not included in scoring because they are seen at relatively high prevalence (4-10%) in the endogenous, wild type C57BL/6 background (Chase, 1942; Kalter, 1968). Wild type C57BL/6 mice do not show any incidence of jaw and midline defects. Pups with abnormalities were scored and photographed by one investigator and scoring was independently assessed from the photograph by a second investigator blinded to the diet and pregnancy status of the mother.

Pups with abnormalities are stillborn or die shortly after birth. Clefting of the palate was observed by dilating the jaws with a forceps and, where suspected, confirmed by surgically opening the jaw to expose the palate. Agnathia was defined by absence of a mandible with or without ventral displacement of the ears. Micrognathia was noted where some mandibular structures were present but visibly reduced in size. Proboscis was noted where there was an elongated dysmorphic nose-like structure in place of a snout.

Cyclopia was characterized by a midline eye-like structure. Embryos with no recognizable facial features at all were assessed as having anterior truncation (corresponding to human aprosopia).

Pups with no defects or with isolated eye defects were classed as "Normal" with respect to BA1-derived and midline facial structures. Mice with clefting and/or micrognathia were grouped together for statistical purposes as having mild BA1 defects while presence of isolated agnathia (without midline defects) was classified as a severe BA1 defect. For some comparisons all BA1 defects were grouped together. The additional presence of proboscis, cyclopia, or anterior truncation was counted as a midline defect. These midline phenotypes were always seen with concomitant agnathia.

Statistical analyses

The effect of diet for each pregnancy and the parity effect within each diet were assessed by permutation tests to account for clustering of pups into litters. The test statistic used in the permutation tests was the 2-sided p-value from Fisher's exact test. For permutation tests comparing diets and involving only the first pregnancy or only the second pregnancy, diet labels were permuted among litters (dams). For permutation tests comparing parity and involving only a single diet, parity labels were permuted among litters if a dam had only one pregnancy for that diet or between a dam's two pregnancies if she had both pregnancies on the same diet. The p-value of the permutation test is the proportion of test statistics from the 1000 permutation samples that were as extreme as or more extreme than the observed test statistic from the actual data.

Generalized estimating equations (GEE) accounting for clustering by dam and litter was used to investigate the effects of diet, parity, any potential interaction between diet and parity, and maternal age. These analyses had the form of a logistic regression; robust variance estimates were used in computing confidence intervals. 2-way and 3-way interactions of factors did not test significant so only the main effects of maternal age, diet, and parity are included in the analyses reported here. P-values are two-sided; those less than or equal to 0.05 were deemed statistically significant. All analyses used the SAS system (v. 9.2, SAS institute, Cary, NC, USA); GEE analyses were done using the GENMOD procedure. 27 dams had a single pregnancy in the data set, while 21 dams had two pregnancies. Of the latter, 5 dams were fed the MDS diet for both pregnancies and 16 were fed the NIH31 diet for the first pregnancy and the MDS diet for the second pregnancy.

Results

Methyl donor supplementation reduces the incidence of BA1-derived but not midline facial defects among *Twsg1*$^{-/-}$ offspring from previously nulliparous dams

Twsg1$^{-/-}$ pups born to mothers being fed each diet continued to show variable defects including pups with defects as well as unaffected pups (Figure 15A, B). Observed malformations included isolated defects of BA1-derived tissues such as clefting in the secondary palate (Figure 15 C, F), micrognathia (Figure 15 D, G), and agnathia (Figure

15 E, H). Cleft lip was also observed in a few cases (not shown). In each diet group some pups showed severe defects of the upper face, with mispatterning of midline structures, including proboscis, which was seen with cyclopia (Figure 15 I, L), or with absent eyes (Figure 15 J, M). These defects were always accompanied by agnathia in these *Twsg1*$^{-/-}$ animals.

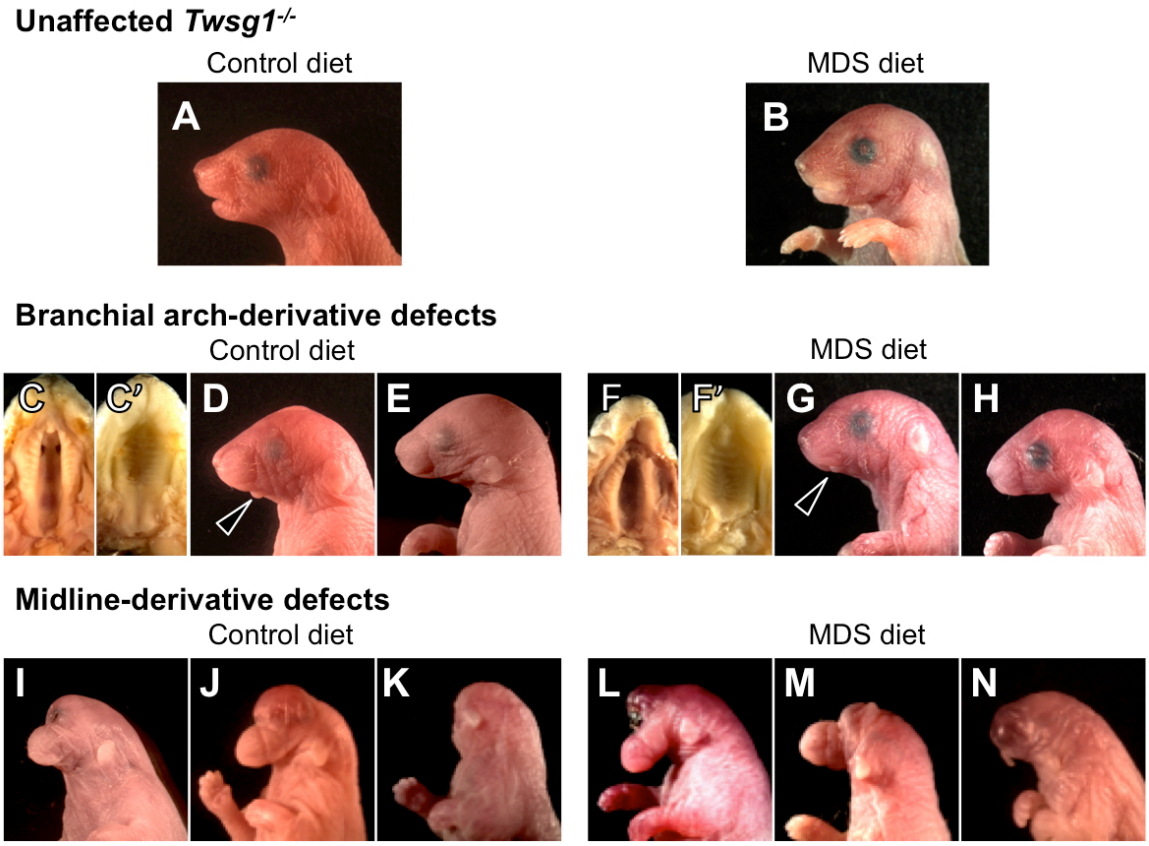

Figure 15: The full range of *Twsg1*$^{-/-}$ phenotypes is seen in mouse pups born to mothers fed either control or methyl donor supplemented diets.
With either control or MDS diet, some *Twsg1*$^{-/-}$ mice are born with no defects (A,B). Some have defects of BA1 derived structures (C-H): palatal clefting (C, F) with normal palates (C', F') included for reference; (D,G) micrognathia, with jaw rudiment indicated by the black arrowhead.; (E, H) agnathia. Some have severe midline defects (I-N); (I,L) Cyclopia with proboscis; (J,M) Proboscis; (K,N) Anterior truncation.

We first analyzed pups born to previously virgin females. In the control diet group, the rate of defects was 37.7% (29 of 77 *Twsg1*$^{-/-}$ pups from 20 litters); this rate was almost halved with the MDS diet, to 19.1% (9 of 47 pups from 11 litters) (Figure 16A, Table 6). The permutation test found this difference statistically significant (p=0.03), indicating a beneficial effect of the MDS diet for pups born from their mother's first pregnancy.

We next considered whether dietary intervention affects the variable phenotypes evenly and found that the MDS diet protected exclusively against BA1-derived defects (Table 6, Figure 16A). In the first pregnancy, clefting, micrognathia, and agnathia together decreased by more than half (12.8% in MDS vs. 32.5% in control) with the MDS diet, and this decrease alone was significant (p=0.02; Figure 16B, Table 6). Midline and anterior head defects showed no impact from the MDS diet and occurred at nearly the same frequency in each diet group, 5.2% in the control diet group and 6.4% in the MDS diet group (Figure 16C, Table 6; p=1.00).

The incidence of craniofacial defects increases in the second pregnancy.

Offspring of second pregnancies during which mothers were fed either diet had markedly more defects than offspring of first pregnancies. In the control diet group, the incidence of defects increased from 37.7% to 59.5% (p=0.04; Figure 17A, Table 6). With the MDS diet the second pregnancy was also associated with increased prevalence of defects. The incidence of craniofacial defects was 19.1% among the first MDS pregnancy offspring and 45.3% among the second MDS pregnancy offspring (p=0.045; Figure 17B, Table 6).

Figure 16: Methyl donor supplemented maternal diet protects against craniofacial defects seen in *Twsg1*$^{-/-}$ mice born from first pregnancies, specifically BA1 but not midline defects.

Bars represent the percent of each group of pups that show a given phenotype. (A) Reduced incidence of any defect with maternal MDS diet. Phenotypes of pups born to mothers given control diet (77 pups total, n=20 dams) or MDS diet (47 pups total, n=11 dams) are categorized by type and severity into severe midline defects (dark gray), and severe (mid gray) and mild (light gray) BA1 defects. (B) Reduced incidence of defects of BA1 derivatives with MDS diet. (C) Equivalent incidence of severe midline defects between control and MDS diet groups. P-value is calculated vs. control diet group by permutation test, * $p<0.05$. Significance tests are indicated for the combined total represented by a column. More complete statistics can be found in Table 6. Abbreviations: BA1, first branchial arch; MDS, methyl donor supplemented.

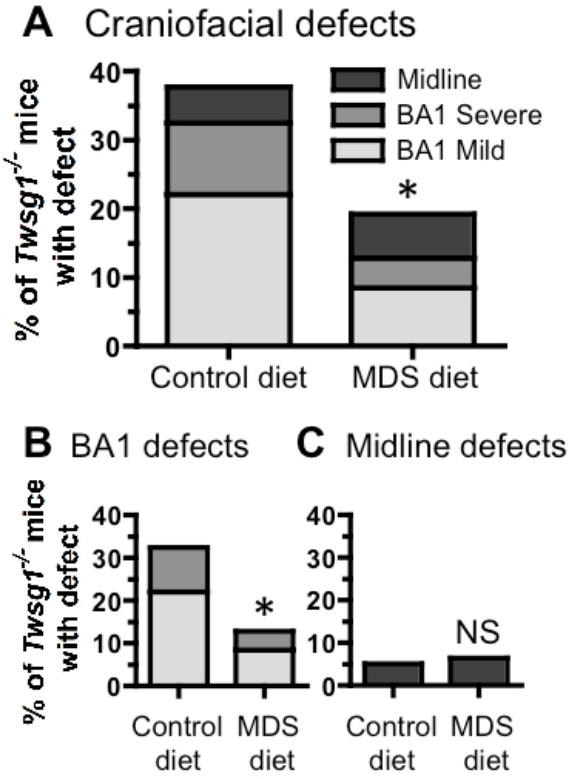

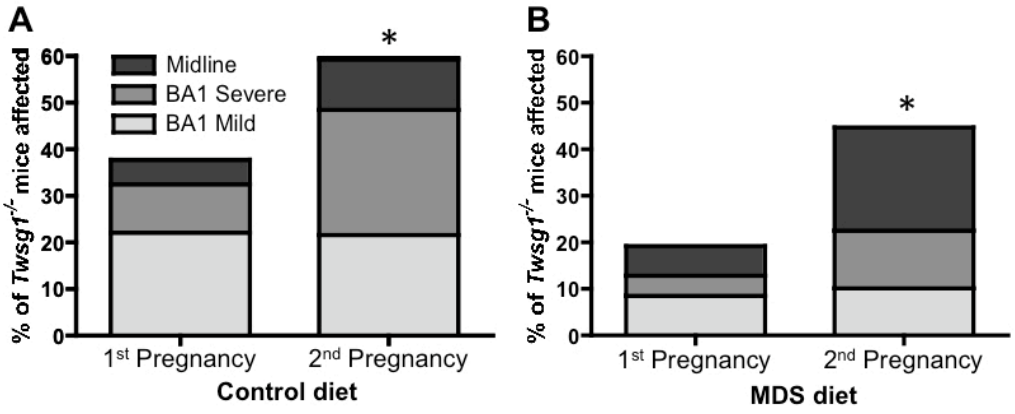

Figure 17: Parity increases defects in *Twsg1*$^{-/-}$ mice regardless of diet.
Bars represent the percent of each group of pups that show a given phenotype. (A) First and second pregnancy phenotype incidence with control diet (77 *Twsg1*$^{-/-}$ pups from first pregnancies, n=20 dams, and 37 from second pregnancies, n=14 dams). (B) First and second pregnancy phenotype incidence with MDS diet (47 *Twsg1*$^{-/-}$ pups from first pregnancies, n=11 dams, and 106 *Twsg1*$^{-/-}$ pups from second pregnancies, n=24 dams). Overall defects in (A) and (B) are subcategorized by type and severity into severe midline defects, and severe and mild BA1 defects. * $p<0.05$, by permutation test for difference from first pregnancy. Significance tests are indicated for the combined total represented by a whole column. Complete statistics can be found in Table 6. BA1, first branchial arch; MDS, methyl donor supplemented.

Table 6: Summary of craniofacial malformations seen in *Twsg1*$^{-/-}$ mouse pups, to dams given control or methyl donor supplemented diets, from both first and second pregnancies

Variable	First pregnancy		Second pregnancy		Permutation Test p-values			
	Control diet *n (%)*	MDS diet *n (%)*	Control diet *n (%)*	MDS Diet *n (%)*	1st preg[6]	2nd preg	Control diet	MDS diet
Counts of *Twsg1*$^{-/-}$ offspring phenotypes[1]	77 (100)	47 (100)	37 (100)	106 (100)	Control vs. MDS	Control vs. MDS	1st vs. 2nd preg.	1st vs. 2nd preg.
Normal[2,3,4]	48 (62.3)	38 (80.9)	15 (40.5)	58 (54.7)	–	–	–	–
BA1[6] + midline defects[2]	29 (37.7)	9 (19.1)	22 (59.5)	48 (45.3)	0.03	0.37	0.04	0.045
BA1[6] defects[3]	25 (32.5)	6 (12.8)	18 (48.6)	24 (22.6)	0.02	0.08	0.08	0.23
-Mild BA1 defects: [4]	17 (22.1)	4 (8.5)	8 (21.6)	11(10.4)				
-Micrognathia[5]	12 (15.6)	3 (6.4)	7 (18.9)	10 (9.4)				
-Orofacial clefting[5]	7 (9.1)	1 (2.1)	3 (8.1)	2 (1.9)				
–Cleft Lip[5]	3 (3.9)	0 (0)	1 (2.7)	1 (0.9)				
–Cleft Palate[5]	6 (7.8)	1 (2.1)	3 (8.1)	1 (0.9)				
-Severe BA1 defects: Agnathia[4]	8 (10.4)	2 (4.3)	10 (27.0)	13 (12.3)				
Midline defects: [3,4]	4 (5.2)	3 (6.4)	4 (10.8)	24 (22.6)	1.0	0.30	0.34	0.08
-Proboscis[5]	4 (5.2)	3 (6.4)	1 (2.7)	20 (18.9)				
-Anterior Truncation[5]	0 (0)	0 (0)	3 (8.1)	4 (3.8)				
-Cyclopia[5]	2 (2.6)	2 (4.3)	1 (2.7)	9 (8.5)				

[1] Numbers in the table are totals for each category of phenotype. In parentheses is the percent of the total with that phenotype within the group with the same parity and diet. Clefting and micrognathia are considered together as mild (BA1) defects and were frequently seen in the same mouse. Agnathia is classed as a severe BA1 defect. "Orofacial clefting" includes cleft lip and/or cleft palate. "Midline defects" includes all mice with proboscis, anterior truncation or cyclopia. Mice with midline defects also all had agnathia, but are not counted in the upper rows of the chart for having jaw defects due to overriding presence of the severe midline defect.

[2,3,4] Categories are mutually exclusive up to the same level of indentation and can be added to make up total numbers.

[5] Categories are nonexclusive and cannot be added to make totals.

[6] Abbreviations: BA1, first branchial arch; MDS Methyl donor supplemented; Preg, pregnancy.

Increased parity raised the incidence of severe BA1 phenotypes (agnathia) and midline defects, but not incidence of mild BA1 phenotypes (micrognathia and/or clefting). Pups with micrognathia and/or clefting were seen at nearly the same rate in both first and second pregnancies in both diet groups (Control: 22.1% vs. 21.6%, P=0.99, MDS: 8.5% vs. 10.8%, P=0.99, Table 6 and Figure 17). On the other hand, agnathia incidence nearly tripled among mice born from second pregnancies given control diet (10.4% up to 27.0% in the second control diet pregnancy, P=0.03), but the change in prevalence was not significantly different among mice born from second pregnancies given MDS diet (4.3% up to 12.3% in the second MDS pregnancy, P=0.25, Table 6 and Figure 17). Midline defects in second pregnancies tended to increase relative to first pregnancies from 6.4% to 22.6% with the maternal MDS diet (P=0.08) but not with the maternal control diet (5.2% to 10.4%) (P=0.34). Notably, the most severe form of the *Twsg1*$^{-/-}$ phenotype, anterior truncation, characterized by absence of any recognizable anterior head and face structures, was seen only in mice born from second pregnancies in each diet group (Figure 15 K, N).

Methyl donor supplementation has protective effects regardless of parity

Given that both diet and parity, considered separately, had significant impacts on the frequency of defects, we were interested in whether methyl donor supplementation had the same effect in the second pregnancy as in the first. We did two analyses using generalized estimating equations (GEE), including both first and second pregnancies and both diets. The first analysis, Model 1, included a test of the so-called interaction of diet

and pregnancy (Table 7). This interaction term indicates whether the effect of diet differs between the two pregnancies (1st or 2nd) or equivalently whether the effect of parity differs between the two diets (Control or MDS). The interaction of diet and parity did not test significant (p=0.59), meaning these data provide no evidence that the effect of diet differs between first and second pregnancies. Therefore, a second analytical model (Model 2) excluded the interaction term and considered diet and parity only as acting separately. Consistent with the permutation tests for first and second pregnancies separately, the MDS diet was associated with reduced risk of defects regardless of parity (Table7, Model 2). Likewise, first pregnancies had significantly lower frequency of defects after controlling for diet (Table 7, Model 2).

Table 7: Effect of diet and parity on the incidence of defects in *Twsg1*$^{-/-}$ mice.

		Model 1[1] with interaction	P-value	Model 2[1] without interaction	P-value
Comparison	Subset	OR (95% CI)	-	OR (95% CI)	-
MDS[2] vs. Control diet	1st Pregnancy 2nd Pregnancy	0.38 (0.17, 0.85) 0.54 (0.22, 1.30)	0.03	0.47 (0.26, 0.86)	0.03
1st vs. 2nd pregnancy	MS diet NIH diet	0.28 (0.12, 0.66) 0.39 (0.17, 0.90)	0.001	0.33 (0.19, 0.60)	0.002

[1] A generalized estimating equations analysis (GEE) with the form of a logistic regression and using robust variance estimates was performed for two different models and used to generate odds ratios and P-values. Model 1 proposed that diet and parity might be acting synergistically (i.e., showing a statistical interaction) on the incidence of defects. The P-value for the interaction of diet and parity was 0.59. Model 2 proposed that diet and parity acted separately and did not show a statistical interaction. Since this analysis did not include the interaction of diet and parity, only one odds ratio is estimated and tested for each factor.
[2]Abbreviation: MDS, Methyl donor supplemented.

Increased maternal age does not account for the effect of parity on craniofacial defects

Finally, we considered the possibility that increased maternal age in second pregnancies might account for the increased incidence of defects. The mouse dams in the study gave birth over a range of ages from 72 to 261 days. Not surprisingly, dams were significantly older when giving birth to their second litter, for either diet individually or considering the whole group together ($p<0.0001$, by unpaired Student's t-test). Age distribution did not differ significantly between diet groups (Student's t-test $p=0.23$ for first pregnancies, and $p=0.97$ for second pregnancies) (Figure 18). We again used a GEE-logistic regression to test whether maternal age had an effect on incidence of defects after accounting for the confounding effect of parity (Table 8). In an analysis accounting for diet and parity, the estimated age effect was extremely small, with an odds ratio of 1.02 for an increase of 50 days in maternal age ($p = 0.94$). Thus, there is no indication that maternal age had an independent effect on the incidence of defects.

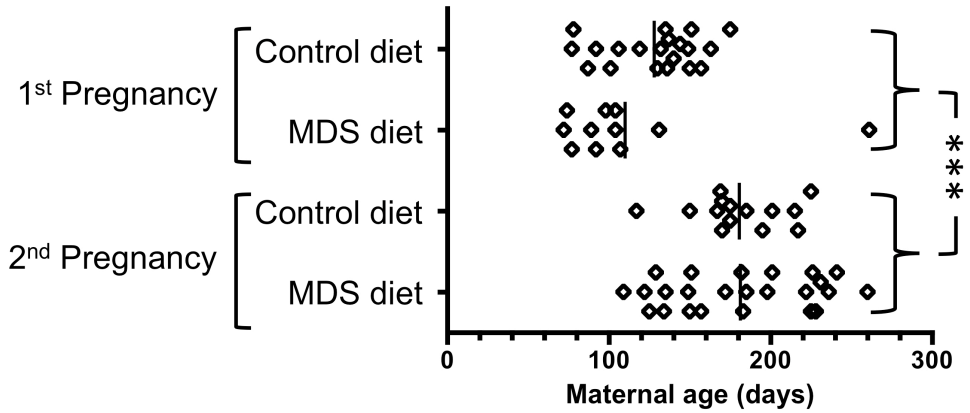

Figure 18: Distribution of maternal ages in study group.
Each point indicates a litter delivered at a given maternal age. Vertical lines indicate mean ages for the category. *** $p<0.001$.

Table 8: Effect of maternal age on incidence of defects in *Twsg1*$^{-/-}$ mice, adjusting for diet and parity

	OR[1] (95% CI)	P-value[1]
MDS Diet: Yes vs. No	0.47 (0.26, 0.86)	0.03
1st Pregnancy: Yes vs. No	0.34 (0.14, 0.82)	0.01
Maternal Age: 50-day increase	1.02 (0.65, 1.59)	0.94

[1] Odds ratios (OR) and 95% CI and p-values were calculated using a generalized estimating equations analysis with the form of a logistic regression and using robust variance estimates.

Discussion

The role of methyl donor supplementation in prevention of defects arising from the first branchial arch

Recommendations for increased folate intake during pregnancy and particularly population-level folate fortification have significantly reduced NTDs (Honein et al., 2001) but have not had such clear effects on other types of birth defects (Canfield et al., 2005; Botto et al., 2006). Experiments in animal models present a suitable way to study this potential effect and the effects of other methyl donors in a controlled experimental setting. The current study in TWSG1-deficient mice supports the role of maternal dietary methyl donor supplementation, including folate, in prevention of birth defects beyond those of the neural tube, specifically those of BA1.

The BA1 mesenchyme is populated with neural crest cells (NCC) derived from the margins of the developing neural tube. Like the neural tube, NCCs appear to be particularly sensitive to maternal dietary and plasma folate levels during development (Burgoon et al., 2002; Spiegelstein et al., 2004; Blom et al., 2006) and methyl donor

supplementation supports the role of folate in one-carbon metabolism. This may partially explain how the NCC-populated BA1 mesenchyme could be a suitable target for methyl donor action.

Methyl donor supplementation did not protect against non-BA1 craniofacial defects observed in *Twsg1*$^{-/-}$ mice, including cyclopia, proboscis, or anterior truncation. This suggests that, rather than being part of a single continuum of severity of the same pathological process, the variable phenotypes in *Twsg1*$^{-/-}$ mice are actually a constellation of pathologies with differing responses to dietary intervention. The observation that *Folr1*$^{-/-}$ mice do not show midline defects of HPE (Spiegelstein et al., 2004) supports the notion that methyl donor metabolism is not likely to play a major role in the pathogenesis or prevention of these defects.

The mechanism of dietary folate, choline or B12 actions in prevention of birth defects, including NTDs, remains unknown (Blom et al., 2006), but several potential mechanisms have been proposed. First, these nutrients are all involved in one-carbon metabolism, which is required for synthesis of nucleotides (Stover, 2004). This is particularly important for rapidly dividing cells (Botto et al., 1999) such as NCC. Thus, increased availability of these nutrients may act to promote development of an embryonic structure such as BA1 by facilitating rapid cell proliferation and growth. Second, folate and methyl donors provide methyl groups for DNA and protein methylation (Choi et al., 2005; Blom et al., 2006). Given increasing attention to the role of epigenetics in NCC regulation and action (Liu and Xiao, 2011), it is conceivable that the protective action of

dietary methyl donors is through facilitation of epigenetic gene regulation in NCC of BA1. This idea is supported by the observation that the supplemented diet used in this study is able to alter DNA methylation status and gene regulation at epigenetically labile loci, such as those seen in the agouti viable yellow (Wolff et al., 1998; Cooney et al., 2002; Waterland and Jirtle, 2003) and axin fused (Waterland et al., 2006) strains. It is currently unknown if genes important for craniofacial development can act as metastable epialleles (Rakyan et al., 2002) in the response of *Twsg1*$^{-/-}$ mice to dietary supplementation. Third, methyl donors are also required for remethylation of homocysteine to methionine (Tchantchou, 2006). Rising homocysteine levels in the absence of adequate ability to detoxify this compound can have deleterious effects on NCC (Boot et al., 2003; Li et al., 2005), so methyl donor sufficiency would have protective effect on NCC. Finally, sufficiency of methyl donors may also provide an antioxidant effect, which could protect NCC from apoptosis induced by oxidative stress (Loeken, 2004).

Parity as a potential variable in dysmorphology

Previous pregnancy has been hypothesized to increase the risk of certain types of defects in human studies, particularly NTD (specifically spina bifida) (Vieira, 2004) and orofacial clefts (Vieira and Orioli, 2002). The effect of increased parity has been controversial, however, with recent studies not finding an effect of parity on these same defects (Duong et al., 2012). We report a significant effect of parity in increasing incidence of craniofacial defects in mice, particularly severe BA1 defects (agnathia) and

severe defects of midline formation and head patterning. Our finding of an impact of a previous pregnancy on subsequent pregnancy outcome is, as far as we know, a novel finding in mouse research. *Twsg1*$^{-/-}$ mice represent a potentially important model for studying mechanisms of the effect of birth order on birth defects. Other mouse model dysmorphology studies may also need to account for parity as a potential variable.

The effect of increased parity has several potential explanations. Maternal age would be one potential confounding variable to consider. In humans, age, particularly maternal age >40 years, has been associated with increased risk for defects, for example, congenital heart defects, trisomy 21 and neural tube defects (Hay and Barbano, 1972; Vieira and Taucher, 2005). In our mouse study, we found no effect of age on craniofacial defects after accounting for parity. However, it is unclear what would be a proper mouse model of human advanced maternal age. Further studies of age-matched mice in their first and second pregnancies could provide additional direct information on the question of the extent to which age plays a role in the effect of parity in *Twsg1*$^{-/-}$ mice. Apart from age, it is possible that increased pregnancy is associated with depletion of maternal nutrients necessary for healthy gestation (Todoroff and Shaw, 2000). Notably, it has been reported that methyl donors can be depleted as a result of pregnancy in both rodents (Zeisel et al., 1995; Achón et al., 2000) and humans (McMahon and Farrell, 1985; Bailey, 1992). Iron could be another potential micronutrient subject to depletion (Sharma et al., 1991; Milman et al., 1992). Depletion of iron with increased parity has been proposed as a mechanism of increased ethanol teratogenicity with increased parity (Rufer, 2010). Since the phenotypes seen with ethanol toxicity in mice (Higashiyama et al., 2007;

Aoto et al., 2008) resemble those seen in *Twsg1*$^{-/-}$ mice, some shared pathologic mechanisms could be involved. Finally, increased maternal oxidative stress with higher parity may play a role. Increases in markers of oxidative stress have been seen in human mothers and in rats with increased parity (Tawfik et al., 2008; Mutlu et al., 2012).

Effects of folate in prevention of birth defects of the neural tube and face appear to be stage and region-specific

It is interesting that the preventive effects of methyl donors against defects are region-specific. This suggests that the embryonic origins of impacted structures and differences in underlying processes may play a role in differing responses to dietary supplementation. The findings of this and other studies (Yan et al., 2012) lead us to propose a model where the effects of methyl donor supplementation are specific to the embryonic origin of craniofacial and neural structures. Our model subdivides embryonic development of these structures into three steps (Figure 19). Each step must proceed properly to allow normal embryonic development.

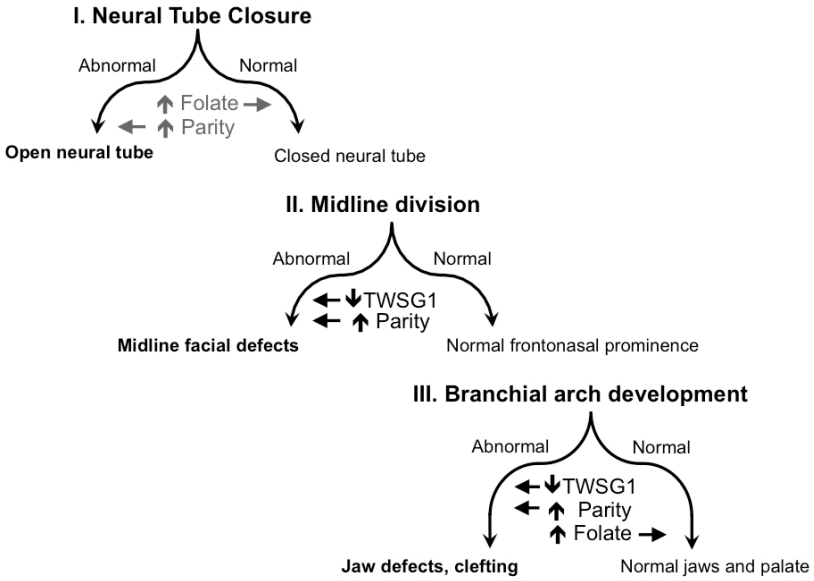

Figure 19: A multifactorial model of craniofacial defects in *Twsg1*$^{-/-}$ mice.
Craniofacial development is subdivided into three stages, neural tube development, midline division and branchial arch development. The consequence of failure is indicated at the left of each step. In each stage, three factors are considered for their inferred effects: deficiency of TWSG1, MDS (methyl donor supplementation), and increased parity. Grayed factors in the first, neural tube step indicate this portion of the model is derived from literature review and not from the results of this study: for MDS references (Smithells and Sheppard, 1980; MRC, 1991; Fisher et al., 2001; Shaw et al., 2004; Spiegelstein et al., 2004; Burren et al., 2008); for parity reference (Vieira, 2004).

Early in embryonic development, the neural tube forms as the neural folds grow together and fuse in the midline. This takes place from embryonic day 8.5 (E8.5) to (E10) in mice (Ybot-Gonzalez et al., 2002) and in the fourth week of development (Days 21-24) in humans (Northrup and Volcik, 2000; Larsen et al., 2001). Failure at this step leads to NTDs. *Twsg1*$^{-/-}$ mice do not show NTDs, indicating the dispensability of TWSG1 for neural tube development. The protective effect of methyl donors on NTD development has been previously established in both NTD-susceptible mice (Fisher et al., 2001; Spiegelstein et al., 2004; Burren et al., 2008) and in humans (Smithells and Sheppard, 1980; MRC, 1991; Shaw et al., 2004). In contrast to the effect of methyl donor

supplementation, increased parity may act to favor NTD, based on work in humans (Vieira, 2004).

Paralleling the process of neural tube closure is early head patterning and midline specification, which begins around E7.5 (Aoto et al., 2009) in mice or at stage 7-10 (weeks 3-4) of human development (Larsen et al., 2001; Muller and O'Rahilly, 2003). Failure of this process leads to HPE and associated midline facial defects, such as cyclopia or proboscis. We did not see any protection from these defects by methyl donor supplementation, suggesting that methyl donors are unable to protect normal midline patterning. Midline defects tended to appear at increased incidence in second pregnancy offspring of dams fed the MDS diet (P=0.08).

Somewhat later in development, around E9 in mouse development (Thomas et al., 1998) or around 24 days in humans (Larsen et al., 2001), the branchial arches become apparent as NCC-derived mesenchyme begins to condense. For normal development to proceed, the NCC-derived mesenchyme must maintain a proper balance between proliferation and apoptosis. This allows normal jaw outgrowth and palatal formation. Precise regulation of bone morphogenetic protein signaling is essential for mandibular outgrowth (Stottmann et al., 2001) and specifically TWSG1 is important for limiting apoptosis in BA1 (MacKenzie et al., 2009). We observed notable protection by methyl donor dietary supplementation of structures derived from BA1 in *Twsg1*$^{-/-}$ mice, possibly through facilitating NCC mesenchymal proliferation. The incidence of agnathia increased with higher parity among mice born from pregnancies given control diet (P=0.03).

In summary, we found that dietary methyl donor supplementation and maternal parity both had significant effects on *Twsg1*$^{-/-}$ pregnancy outcomes in terms of craniofacial defects. These results suggest that environmental factors can alter the incidence of phenotypes arising from the genetic susceptibility conferred by *Twsg1* mutation. Differential responses of different types of defects to diet and parity suggest that a heterogenous set of pathologies underlies the complexity and variation of the *Twsg1*$^{-/-}$ phenotype. This highlights the possibility that different defects within a given syndrome may show different responses to specific interventions. This study also highlights the importance of accounting for parity when analyzing the results of any preventive approach. It should be noted, however, that this study has several limitations, such as lack of direct measurement of folate or other methyl donor levels in the maternal serum or variable duration of feeding with experimental diets, largely due to variable time to pregnancy. Future studies should explore whether there is a correlation between maternal and/or fetal nutrient levels and the incidence or type of craniofacial defects as well as the mechanisms through which increased parity may increase the incidence of craniofacial defects.

Chapter 5: Generation of a conditional mouse model of *Twsg1* overexpression

Introduction

Twisted gastrulation (TSG or TWSG1 in mammals) is a conserved extracellular BMP binding protein. It was first identified based on the effect of mutation on dorsal-ventral patterning in the early Drosophila embryo (Zusman and Wieschaus, 1985; Mason et al., 1994; Mason et al., 1997). Homologs have been identified in other species as well, including vertebrates such as frogs, fish, chickens, mice and humans (Oelgeschlager et al., 2000; Chang et al., 2001; Graf et al., 2001; Ross et al., 2001; Scott et al., 2001). Most of the mechanistic studies of TSG action have been performed in non-mammals. TSG has been primarily reported as an antagonist of BMP action, based on studies performed in flies, frogs and fish. This antagonism takes place due to binding of TSG to BMPs and particularly through TSG potentiating the action another BMP inhibitor, Chordin (Yu et al., 2000; Chang et al., 2001; Ross et al., 2001; Scott et al., 2001; Blitz et al., 2003; Wills et al., 2006). Intriguingly, TSG can also serve in some situations to promote BMP signaling (Oelgeschlager et al., 2000; Little and Mullins, 2004). The seeming paradox of these dual activities of TSG inhibiting or promoting BMP signaling has been explained as a consequence of TSG helping facilitate BMP ligand transport and proteolytic cleavage of Chordin (Oelgeschlager et al., 2000; Harland, 2001; Larrain et al., 2001; O'Connor et al., 2006).

In mice *Twsg1* is robustly expressed in mouse embryonic and postnatal tissues

beginning as early as embryonic day 7 (E7) (Graf et al., 2001). In order to understand the role of TWSG1 in mice we generated mice deficient in TWSG1 by deleting the fourth exon of the mouse *Twsg1* gene (Petryk et al., 2004). Deletion of this exon makes TWSG1 unable to bind BMP, even if TWSG1 protein is made (Billington et al., 2011b). Other existing TWSG1-deficient mouse models have been generated by replacing exon 2 (Nosaka et al., 2003; Zakin and De Robertis, 2004), or parts of exons 2 and 3 (Gazzerro et al., 2006), of the *Twsg1* gene with neo^R or *LacZ* gene cassettes. Disruption of *Twsg1* resulted in both embryonic and postnatal phenotypes. The most striking embryonic phenotype resulting from TWSG1 deficiency is abnormal craniofacial development (holoprosencephaly and jaw defects) in the C57BL/6 background (Petryk et al., 2004). Other abnormalities of development in $Twsg1^{-/-}$ mice include improper development of the vertebrae (Nosaka et al., 2003; Petryk et al., 2004; Zakin and De Robertis, 2004; Gazzerro et al., 2006) as well as the salivary gland abnormalities (Melnick et al., 2006). In conjunction with Crossveinless 2, TWSG has also been implicated in embryonic kidney development (Ikeya et al., 2010).

Postnatally, TWSG1 has been implicated in immune cell development and function (Nosaka et al., 2003; Tsalavos et al., 2011), iron homeostasis (Tanno et al., 2009), and particularly in bone homeostasis, as indicated both by the *in vitro* studies (Gazzerro et al., 2005; Petryk et al., 2005) and by the osteopenia seen in $Twsg1^{-/-}$ mice (Nosaka et al., 2003; Petryk et al., 2004; Gazzerro et al., 2006). The lower perinatal mortality of $Twsg1^{-/-}$ mice in the 129SvEv background allowed us to study the basis of osteopenia in these mice. We found that deficiency of TWSG1 led to increased

osteoclastogenesis, manifesting as larger and more numerous osteoclasts with increased ability to resorb bone (Sotillo Rodriguez et al., 2009; Pham et al., 2011). The pleiotropic effects of TWSG1 acting in widely varying tissues and processes are not surprising given its role to modulate BMPs, which themselves regulate a wide range of embryonic and postnatal processes in normal development and disease (Wagner et al., 2010).

While the consequences of loss-of-function of *Twsg1* have been well described, a mouse model over-expressing the *Twsg1* gene has not yet been generated. The overexpression studies that have been performed so far with mouse tissues or cells have utilized exogenously applied TWSG proteins (Petryk et al., 2005; Billington et al., 2011b) or have used viral transduction (Gazzerro et al., 2005; Pham et al., 2011) to model overexpression of *Twsg1*. The goal of this study was to generate transgenic mice overexpressing *Twsg1* to examine its effects on craniofacial skeletal development and postnatal bone homeostasis. Our hypothesis was that excess TWSG1 would be protective against craniofacial defects during embryonic development and postnatally, overexpression of TWSG1 would limit osteoclast differentiation and function. It is important to understand the effect of under-and overexpression of TWSG1 on osteoclast function because of potential clinical implications. Stimulation of osteoclastogenesis is important for treatment of diseases with impaired osteoclast function, such as osteopetrosis (Marks, 1987). On the other hand, inhibition of osteoclast function would be beneficial in diseases with pathologically increased osteoclast function, such as osteoporosis (Teitelbaum and Ross, 2003). An *in vivo* model would provide an additional reagent that will facilitate further study.

Materials and Methods

Plasmids

pBigT and pROSA26PA plasmids for targeting *ROSA26* locus were a kind gift of Dr. Sankar Srinivas (Srinivas et al., 2001). The *Twsg1* coding DNA Sequence (CDS) was amplified by PCR using the primers 5'- aatgcgtcgacctttgagccaccatgaagtc-F and 5'-tccccgcggcctctttaaaacatgcagttc-R with engineered *SalI* and *SacII* restriction sites and 5' Kozak sequence (Kozak, 1987). The resultant *Twsg1* amplicon was cloned into the pCR2-Topo vector according to manufacturer's instructions (Invitrogen, Carlsbad CA) and confirmed by sequencing. The *Twsg1* insert was cut from the pCR2-Topo plasmid using *SalI* and *SacII* and ligated into pBigT using a rapid DNA ligation kit (Roche, Indianapolis, IN). The resulting pBigT-*Twsg1* plasmid was then digested with *PacI* and *AscI* and ligated into the pROSA26PA plasmid in which an *XbaI* site 1.1 kb to 3' from the 5' end of the *ROSA26* homologous sequence has been replaced by a *PacI-SwaI-AscI* linker. This insertion of the pBigT-*Twsg1* sequences into pROSA26PA yielded the targeting vector.

ES cell injection screening and mouse generation

The pROSA26PA-pBigT-*Twsg1* plasmid was linearized by digestion with *KpnI* and cleaned up by phenol-choloroform extraction for electroporation into mouse CJ7/129SV ES cells. ES cell electroporations were performed at the Mouse Genetics Laboratory at the University of Minnesota. Clones were selected for G418 resistance and

picked for screening. Genomic DNA was initially screened by PCR using a primer of P1: 5'-TAGGTAGGGGATCGGGACTC-F and P2: 5'-TCATCAAGGAAACCCTGGAC-R. Following an approach previously described (Soriano, 1999), this primer pair has one primer complimentary to the endogenous genomic locus outside the region of homology (P1) and one end in the splice acceptor sequence (P2) PCR yields an 1194 bp amplification band if targeting takes place. Primers were designed using the NCBI primer BLAST tool (http://www.ncbi.nlm.nih.gov/tools/primer-blast/) and MacVector (MacVector, Cary, NC). Positive clones by PCR were confirmed by Southern blotting after EcoRV digestion of genomic DNA samples. Restriction fragments were detected using a 559 bp ^{32}P-labeled probe complimentary to the 5' flanking region for *ROSA26*. The probe template was generated by PCR amplification of CJ7/129SV ES cell genomic DNA using the primers 5'-AATACCCAGGCAAAAAGGGGAGACC-F and 5'-GCTCAGAGACTCACGCAGCCCTAGT-R and probe labeling was performed using the Prime-a-gene labeling system (Promega, Madison, WI). This probe detects an 11kb wild type band and a 4.1 kb targeted band after *EcoRV* digestion. Selected positive clones were also further confirmed by Southern blotting after *SacI* digestion, yielding a wild type band of 17kb and a targeted band of 5.7 kb. Confirmed targeted clones were sent for cytogenetic analysis. Clones without identifiable chromosomal abnormalities were injected into blastocysts and then the blastocysts implanted into pseudopregnant dams to generate chimeras. Offspring of the chimeras were screened for germline transmission by PCR and Southern blotting as described above. After confirmation of targeted colony founders, subsequent genotyping was performed by PCR, using primers P1 and P2 to

detect the targeted allele and primers P3 5'- TTGGAGGCAGGAAGCACTTG-F, and P4 5'- CCGACAAAACCGAAAATCTGTG-R to detect the wild type allele "$R26^{+}$".

Mice

Mice were housed in SPF conditions in filter-lidded, 18x29cm cages lined with pulverized corncob bedding, with cotton fiber blocks for nesting material. Cages were changed weekly. Standard chow (Teklad) and water were provided ad libitum. Ambient conditions were maintained with air temperature 20-23˚C, humidity 30-70%, and a 14h/10h light/dark cycle. All animal procedures in this report were approved by the University of Minnesota Institutional Animal Care and Use Committee.

In addition to the targeted $R26^{(fs)Twsg1}$ allele (fs: floxed STOP) generated as described above, several other lines were used. C57BL/6 mice for backcrossing were obtained from Taconic (Hudson, NY). *EIIa-cre* mice, MGI: *Tg(EIIa-cre)C5379Lmgd*, (Lakso et al., 1996) were a gift of Dr. York Marahrens. *LysM-cre* mice (Clausen et al., 1999) were provided by Dr. Kim Mansky and Dr. Rajaram Gopalakrishnan. *EIIa-cre* and *LysM-cre* mice were genotyped using primers designed to detect the *cre* gene insertion: 5'- CTGCCACGACCAAGTGACAGC-F, 5'-CTTCTCTACACCTGCGGTGCT-R.

Generation of mice with global overexpression of Twsg1

The latent conditional *ROSA26-Twsg1* targeted allele, $R26^{(fs)Twsg1}$ was activated to generate a globally overexpressing line, $R26^{Twsg1}$, by crossing *ROSA* targeted mice with *EIIa-cre* mice (Lakso et. al., 1996). *EIIa-cre* mice express Cre recombinase in the early embryo and in the germline. Offspring of the mating of *EIIa-cre* and $R26^{(fs)Twsg1/+}$ mice

yielded mice which were *R26*$^{Twsg1/+}$*;EIIa-cre*+ The offspring of these mice were expected to have and transmit the activated form of the *ROSA26* targeted allele, *R26*^{Twsg1}, with fixed deletion of the floxed STOP cassette now independent of Cre activity. Recombination was detected by PCR using primers P3 and P4, which were expected to yield a 1619bp band after cassette deletion. Cassette deletion was confirmed by Southern blotting with the probe as described above, after *SacI* digestion. This yielded a band of 3.1kb after cassette deletion compared to 5.7 kb prior to deletion. Subsequent genotyping was performed by PCR. *LysM-cre* mice were crossed to *R26* $^{(fs)Twsg1/+}$ or *R26* $^{(fs)Twsg1/(fs)Twsg1}$ mice to generate *R26* $^{(fs)Twsg1/+}$*;LysMcre*+ or *R26* $^{(fs)Twsg1/(fs)Twsg1}$*;LysMcre*+ mice which would over-express *Twsg1* only in cells of the myeloid lineage.

Isolation, culture and characterization of osteoclast cells

Osteoclasts were cultured from bone marrow of 5-week old mice and grown in alpha-MEM with 10% fetal bovine serum with L-glutamine and antibiotics similarly to previously reported protocols (Sharma et al., 2007; Sotillo Rodriguez et al., 2009). Briefly, bone marrow was flushed with media and the resulting suspension was allowed to plate overnight in 100mm dishes. The next day, the non-adherent fraction was treated with erythrocyte lysis buffer to yield a preparation containing primarily monocytes. These cells were then moved to culture plates in growth media with the addition of 10% conditioned media from L-cells to provide m-csf. After 2 days RANKL (R&D systems, Minneapolis, MN) was added at 60 ng/mL and the osteoclasts were allowed to differentiate for 5 days. Cells were stained for TRAP using a commercially available kit

(Sigma, St. Louis, MO). Photographed osteoclasts were analyzed in Adobe Photoshop (Adobe, San Jose, CA).

Tissue harvests and overexpression confirmation

Timed matings were set up to obtain first branchial arch (BA1) tissue at E11.5 (counting the appearance of spermatic plug as E0.5). Mandibular and maxillary components of BA1 were microdissected with etched tungsten needles and flash frozen in liquid nitrogen, while remaining embryonic tissues were saved for genotyping. Adult mice were sacrificed by CO_2 inhalation and kidneys and lungs were dissected and homogenized in Trizol (Invitrogen). Osteoclast RNA was harvested by lysing cultured osteoclasts in the culture dish with Trizol. RNA was isolated from tissue or cell homogenates in Trizol according to manufacturer's instructions. cDNA was synthesized from RNA using the Thermoscript reverse transcription kit according to manufacturer's instructions (Invitrogen).

After cDNA synthesis, samples were assayed by qPCR using primers directed against the CDS or the un-translated regions (UTR) of the native *Twsg1* transcript. CDS primers used were 5'-TGAGCAAATGCCTCATTCAG-F, 5'-GGTTGCACATACCGACACAG-R which amplifies a region spanning exons 2, 3 and 4 of the *Twsg1* mRNA, UTR primers were 5'-CTCCCGATCCTCATGTGACT-F, 5'-TGCATGTTTTAAAGAGGGGG-R in the exon 5 3' UTR Expression was normalized to amplification from *Gapdh*, 5'-TGCACCACCAACTGCTTAG-F, 5'-GATGCAGGGATGATGTTC-R. PCR was performed using 2x mastermix with ROX

from SA biosciences (Valencia, CA) and performed on an Mx3000p thermocycler (Stratagene, La Jolla, CA) with analysis using the MxPro software (Stratagene).

Results

Targeting to the *ROSA26* locus inserts allows generation of a conditional *Twsg1* overexpression allele

We were able to generate a mouse that has conditional overexpression of *Twsg1* from the *ROSA26* locus. The *ROSA26-Twsg1* transgenic strategy was based on previous work (Srinivas et al., 2001) and takes advantage of ubiquitous expression of sequences inserted into the *ROSA26* locus (Soriano, 1999; Srinivas et al., 2001). A floxed triple polyadenylation sequence upstream of the inserted gene functions as a transcriptional STOP cassette and prevents expression without the action of Cre recombinase (Figure 20A). We screened 480 electroporated ES cell clones by PCR (Figure 20B) and were able to identify 8 with targeting, 5 of these were confirmed by Southern blotting. Of these, 2 were suitable for injection after karyotyping. We generated several chimeras and established a mouse line from a chimera that showed germline transmission of the conditional targeted allele $R26^{(fs)Twsg1}$. Mice from this line had a targeted insertion at the *ROSA26* locus, as indicated by PCR and by Southern Blotting (Figure 20B, 20C). PCR shows a 1194 bp band in targeted mice and no amplification in untargeted mice. Southern blotting after *EcoRV* digestion of genomic DNA shows a 4.1kb band in targeted $R26^{(fs)Twsg1/+}$ mice but only an 11.5 kb band in wild type $R26^{+/+}$ mice.

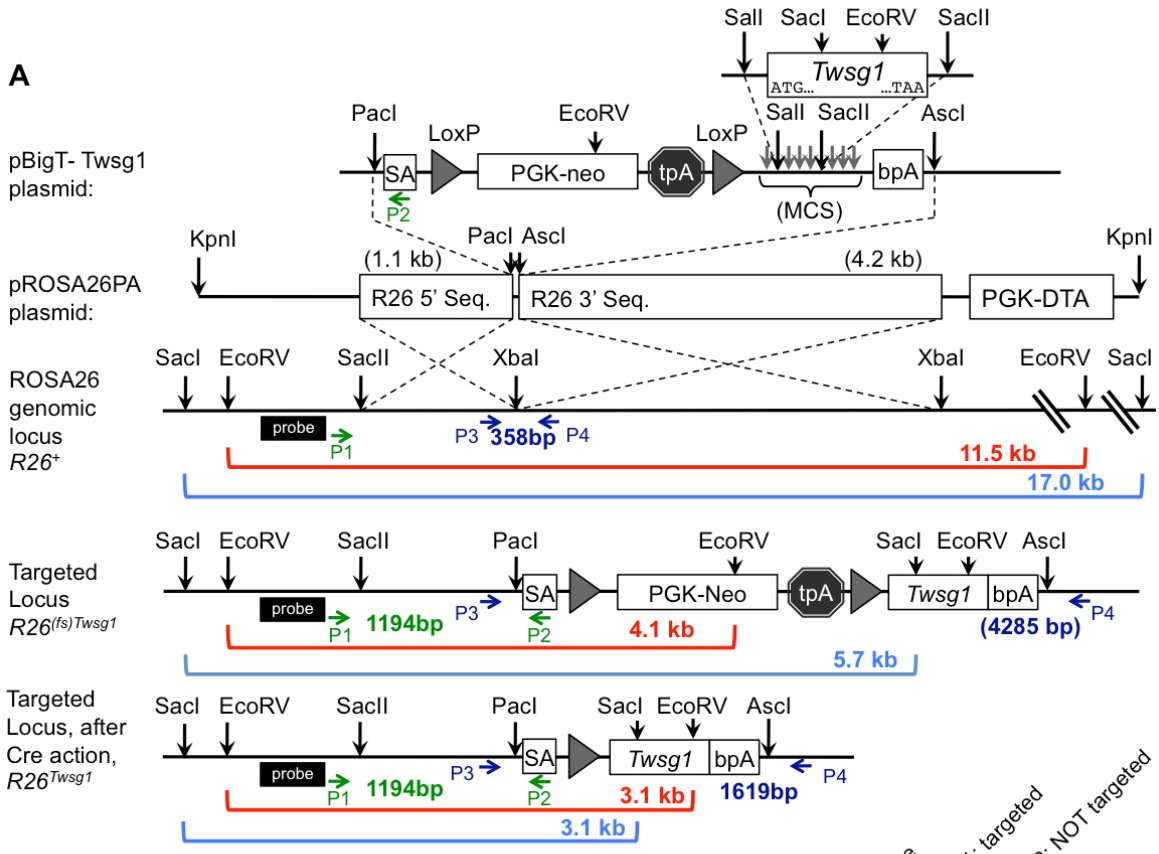

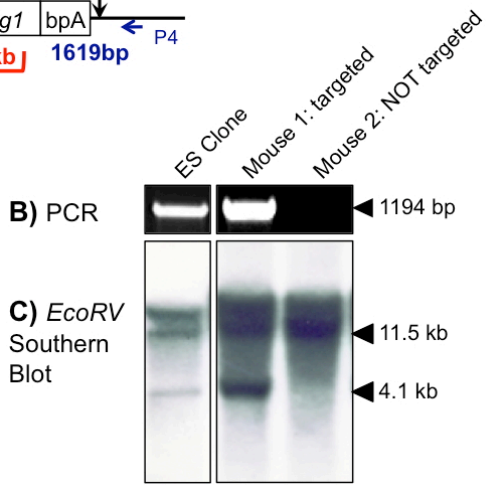

Figure 20: Targeting *Twsg1* to the *ROSA26* locus and identifying targeted clones and targeted mice.

A) Top to bottom: pBigT plasmid with a splice acceptor (SA) sequence followed by a LoxP-flanked cassette containing a phosphoglycerate kinase promoter driven Neomycin/G418 resistance marker (PGK-Neo) for positive selection and a triple SV40-polyadenylation transcriptional termination sequence (tpA). The cassette is followed by an insertion of the mouse *Twsg1* CDS into the multiple cloning site (MCS) of the plasmid with a final polyadenylation signal (bpA) derived from the bovine growth hormone gene.

pROSA26PA plasmid contains 5' and 3' genomic sequences for homologous recombination (R26 5' and 3' Seq.) The *PacI-AscI* fragment from pBigT is cloned into pROSA26PA plasmid at an engineered linker in between the 5' and 3' homology arms. The plasmid also contains a diptheria toxin negative selection gene (PGK-DTA) outside the homology arms.

The ROSA26 genomic locus is illustrated with the endogenous restriction sites. Homologous regions for pROSA26-PA are bordered by the *SacII* and *XbaI* restriction sites. Binding locations for ROSA26 primers P1 and P2 are shown in green and for primers P3 and P4 in purple. P3 and P4 make a 358 bp band with the untargeted genomic locus $R26^{+}$ as a template. P1 and P2 do not amplify without targeting due to absence of P2's target sequence. Southern blot probe binding is indicated by the black rectangle with restriction fragments from *EcoRV* in red, and *SacI* in light blue with lengths 11.5 kb and 17.0kb respectively.

Figure 20, continued:

The targeted but inactive transgenic locus $R26^{(fs)Twsg1}$ (fs: Floxed STOP) has the floxed *neo*-tpA STOP cassette and *Twsg1* CDS insertion. The primer pair P1 and P2 make a 1194 bp amplicon. P3 and P4 would be predicted to make a 4285 bp band but in practice this does not amplify. Restriction fragment lengths are 4.1kb for *EcoRV*, and 5.7kb for *SacI*.

The activated locus $R26^{Twsg1}$, following Cre-mediated STOP cassette excision. The P1-P2 PCR amplicon is still 1194 bp. P3 and P4 now make a 1619bp amplicon. Restriction fragment lengths are 3.1kb for *EcoRV*, and 3.1kb for *SacI*.

B) PCR screening using ROSA26 primer pair 1 was able to identify positive clones, including the positive clone which was used for embryo injections. Offspring from the first generation of C57Bl/6 backcrossing also show positive amplification from tail tip genomic DNA in targeted mice but not in untargeted littermates

C) Confirmation of targeting by Southern blotting for *EcoRV* restriction fragments. ES cell clone and mouse 1 show the targeted band at 4.1 kb while mouse 2 does not.

Generation of mice with global overexpression of *Twsg1*

In order to activate the latent conditional allele $R26^{(fs)Twsg1}$ we mated the conditional targeted transgenic line to mice with the *EIIa-cre* allele, which express Cre recombinase in the early embryo (Lakso et al., 1996). We reasoned that in this would yield pups that had germline deletion of the inhibitory STOP cassette, generating the active overexpression allele ($R26^{Twsg1}$). We were able to mediate cassette excision using *EIIa-cre* as indicated by PCR and confirmed by Southern blotting. The formation of a 1619 bp band with primers P3 and P4 indicates the deletion of the STOP cassette (Figure 21A). In the heterozygous state, $R26^{Twsg1/+}$, this band is weak, likely due to competition with the shorter 358 bp band amplified from the wild type $R26^{+}$ allele, but in homozygous $R26^{Twsg1/Twsg1}$ samples this 1619 bp band produces a strong signal. A predicted band at 4285bp (See figure 20A) in targeted but not cassette-deleted mice does not form (Figure 21A), likely exceeding amplification length. Southern blotting is able to

confirm the excision of the *neo*-STOP cassette by the shortening of a *SacI* restriction fragment from 5.7 to 3.1 kb (Figure 21B). Mice with STOP cassette deletion, in the homozygous or heterozygous state were viable and fertile with no gross defects apparent on examination.

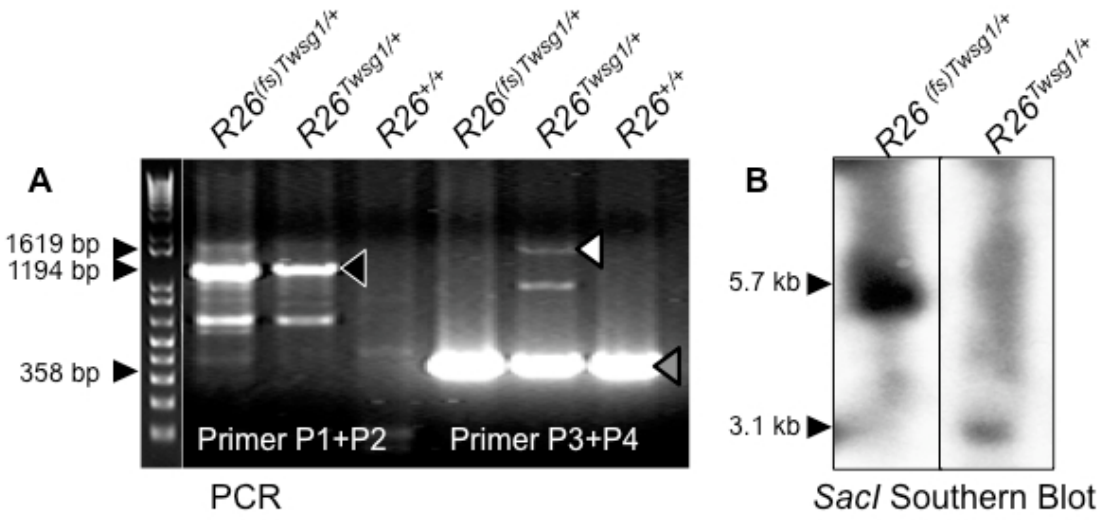

Figure 21: Deletion of floxed *neo*-transcriptional stop cassette.
A) PCR can be used screen or to genotype genomic DNA samples for both targeting and cassette excision. Inactive targeted, active targeted and wild type samples are shown with amplification products from ROSA26 primer set 1 and primer set 2. The 1194 bp band **indicative of targeting (***R26*$^{(fs)Twsg1}$*, R26*^{Twsg1}) is present in both targeted samples (Black triangle). The 1619 bp band (white triangle) is seen in the activated targeted allele (*R26*^{Twsg1}) only. The same primer set also amplifies a band from the native locus (+) 358bp amplicon (gray triangle). B) Southern blotting for *SacI* restriction fragments shows a 5.7kb band with the targeted but inactive allele. With the activation of the allele by Cre-recombinase to remove the 2.6 kb floxed STOP cassette, a 3.1kb band is seen.

Confirmation of transcript overexpression in *R26*^{Twsg1} Mice

We proceeded to confirm that the *R26*^{Twsg1} allele overexpressed the inserted *Twsg1* sequence in embryonic and adult tissues as expected. Based on previous work indicating a role for TWSG1 during embryonic development in the developing face and

specifically in BA1 (Petryk et al., 2004; MacKenzie et al., 2009; Billington et al., 2011a) we were interested in whether *Twsg1* would be overexpressed in these embryonic tissues. We found that *Twsg1* was significantly overexpressed in BA1 at E11.5. In heterozygous $R26^{Twsg1/+}$ embryos this overexpression was roughly 2.5-fold over the wild type expression, while in homozygous $R26^{Twsg1/Twsg1}$ embryos *Twsg1* transcript levels were increased by approximately 6-fold (Figure 22A). Overexpression was limited solely to CDS sequences. *Twsg1* UTR sequences showed no change in expression (Figure 22A). To confirm these results, we assayed the same BA1 cDNA samples by two more pairs of qPCR primers designed against the CDS and UTRs and found nearly identical results (data not shown).

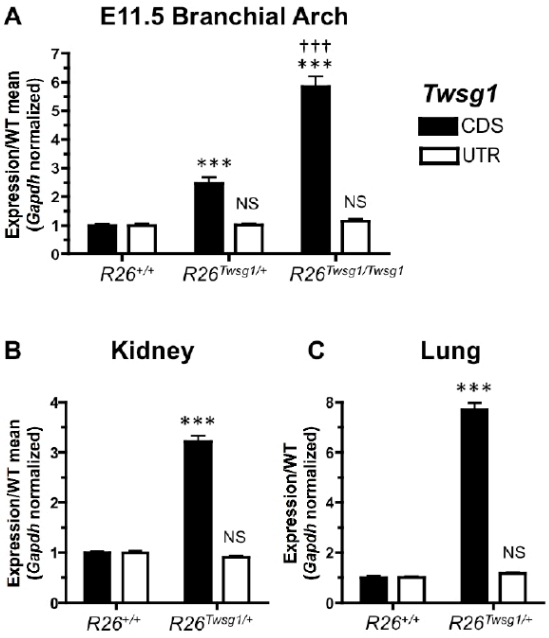

Figure 22: Increased CDS-specific *Twsg1* transcripts in adult and embryonic tissues in $R26^{Twsg1/+}$ and $R26^{Twsg1/Twsg1}$ mice:
A) cDNA was prepared from embryonic day 11.5 maxillary and mandibular branchial arch 1 (BA1) tissues was assayed for expression of both the *Twsg1* CDS (black bars) and the untranslated regions (UTR) present in the *Twsg1* native locus but not the transgene (white bars). E11.5 BA1s show increasing expression of CDS sequences with increasing gene dosage from $R26^{+/+}$ to $R26^{Twsg1/+}$ to $R26^{Twsg1/Twsg1}$. *** $p < 0.001$ by Student's t-test compared to $R26^{+/+}$. ††† $p < 0.001$ by Student's t-test compared to $R26^{Twsg1/+}$ **B)** Kidney tissue cDNA from $R26^{+/+}$ and $R26^{Twsg1/+}$ animals shows more than 3 fold increase in *Twsg1* transcripts of the CDS in $R26^{Twsg1/+}$ with no impact on the prevalence of UTR sequences. **C)** Lung tissue cDNA was assayed from $R26^{Twsg1/+}$ animals and shows a more than 7 fold increase compared to $R26^{+/+}$ specifically for CDS sequences. *** $p < 0.001$ by Student's t-test compared to $R26^{+/+}$.

We also assayed adult kidney and lung tissues from two *R26* $^{Twsg1/+}$ and two *R26*$^{+/+}$ mice and found that there were increased levels of *Twsg1* CDS sequences. *R26*$^{Twsg1/+}$ overexpressed *Twsg1* CDS transcripts by 3-fold in the kidney and by more than 7-fold in the lung, compared to the same tissues from wild type mice (Figure 22B, 22C). UTR sequences were not elevated (Figure 22B, 22C) To confirm these results, we assayed the same samples by two more pairs of qPCR primers designed against the CDS and UTRs and found similar results (data not shown).

Osteoclast specific overexpression of *Twsg1* limits size and number of osteoclasts

Based on previous work demonstrating that TWSG1 limits BMP induced osteoclastogenesis (Sotillo Rodriguez et al., 2009; Pham et al., 2011) we hypothesized that overexpression of *Twsg1* in osteoclasts should limit osteoclastogenesis. We generated myeloid lineage-specific *Twsg1* overexpressing mice by combining the conditional targeted *R26* $^{(fs)Twsg1}$ allele with a myeloid-specific Cre recombinase expressing allele, *LysM-cre*. We then isolated and cultured osteoclasts from these mice. The resulting *R26* ^{Twsg1} osteoclast cultures showed marked and significant increase in their expression of *Twsg1* transcripts depending on gene dosage (Figure 23). The cultured cells, being from the myeloid lineage, have the Cre-activated form of the allele. The osteoclast suppressive effect of *Twsg1* overexpression is apparent upon inspection of stained culture plates (Figure 24A, 24B, 24C). Increased *Twsg1* expression correlated with decreases in mature osteoclast number (Figure 24D) and in osteoclast size (Figure 24E).

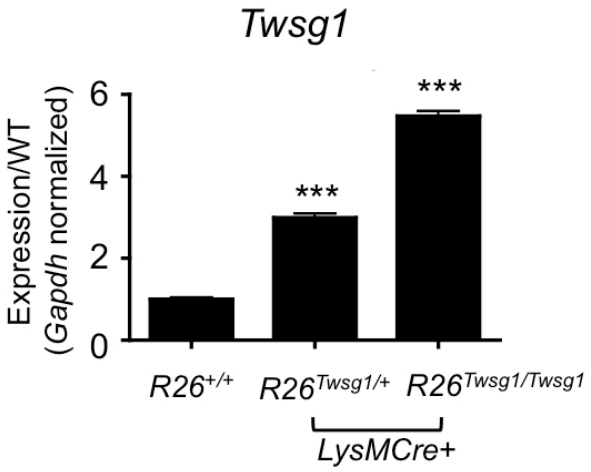

Figure 23: Cre-mediated overexpression of *Twsg1* in osteoclasts.
Osteoclasts generated from floxed or wild type mice carrying the *LysM-cre* allele show increasing expression of CDS sequences with increasing gene dosage from $R26^{+/+}$ to $R26^{Twsg1/+}$ to $R26^{Twsg1/Twsg1}$. *** $p < 0.001$ by Student's t-test compared to $R26^{+/}$

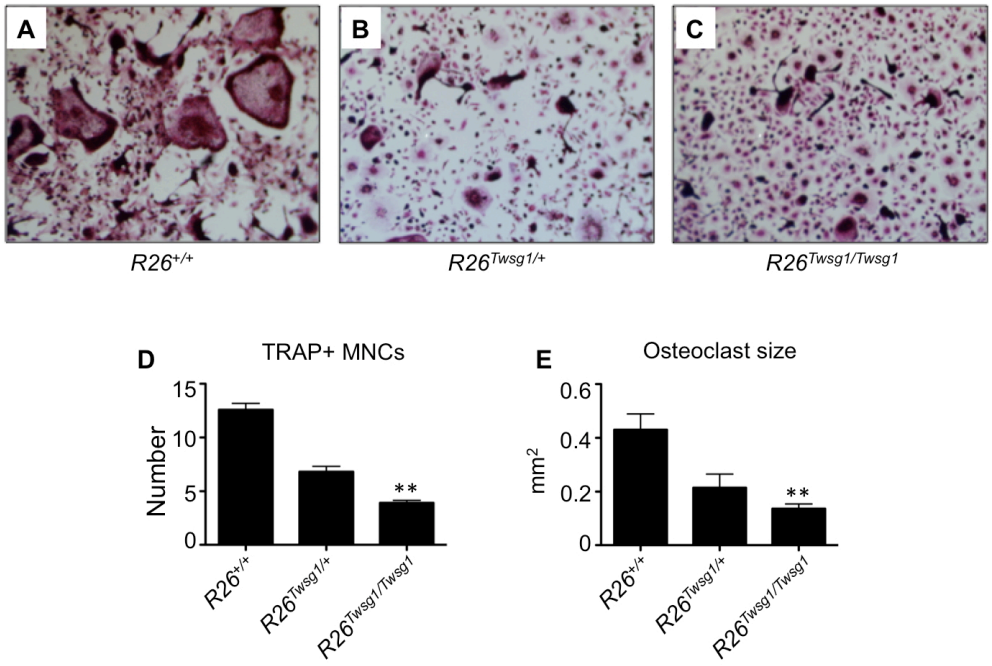

Figure 24: Deletion of floxed *neo*-transcriptional stop cassette.
$R26^{+/+}$, $R26^{(fs)Twsg1/+}$, and $R26^{(fs)Twsg1/(fs)}$Twsg1 osteoclasts were generated from floxed or wild type mice carrying the *LysM-cre* allele and stained for tartrate resistant acid phosphatase (TRAP) A) $R26^{+/+}$ osteoclasts show many large multinuclear TRAP+ cells. B, C) $R26^{Twsg1/+}$ and $R26^{Twsg/Twsg1}$ show fewer TRAP+ multinucleated cells and those present are smaller in size. D) the number of TRAP+ multinucleated cells, indicating mature osteoclasts, is decreased with increased gene dosage of the overexpressing allele E) Osteoclast size is also decreased with increasing gene dosage of the Twsg1 transgenic allele.

Discussion

The model of *Twsg1* overexpression presented here takes advantage of the ubiquitous expression of genes inserted into the *ROSA26* locus. A floxed transcriptional STOP cassette formed by a tripled SV40 derived polyadenylation sequence provided control over the overexpression of the inserted *Twsg1* sequence. This allows precise spatial control of *Twsg1* overexpression. We were able to confirm overexpression of *Twsg1* transcripts in mice with Cre-activated targeted alleles. Both embryonic tissues and adult tissues showed significant overexpression. We designed our assays to take advantage of the fact that only the CDS was inserted into the transgene. This allowed us to confirm that overexpression was coming specifically from the transgene by controlling for the untranslated regions (UTRs) in the endogenous transcript. There was no upregulation of UTR sequences compared to WT levels, indicating not only that additional *Twsg1* CDS transcripts are solely from the transgene, but also that the overexpression appears to have no impact on the endogenous expression of *Twsg1*.

Given TWSG1's role in the embryonic development of the face (Petryk et al., 2004; MacKenzie et al., 2009; Billington et al., 2011a) we were particularly interested in the ability to increase expression of *Twsg1* in the developing facial tissues. We were able to see increased *Twsg1* transcript levels in isolated BA1s suggesting the utility of this mouse model for studies of the effect of *Twsg1* overexpression on craniofacial development.

The increased susceptibility of TWSG1-deficient mice to craniofacial birth

defects after certain teratogenic exposures (Billington et al. unpublished observations) raises the possibility that TWSG1 *over*expression could prove to have an embryoprotective role during development. It is conceivable that TWSG1-overexpressing transgenic mice will show additional robustness to teratogenic insults compared to wild type mice. This hypothesis will be addressed in future studies using the mice generated in this report.

In addition to the role of TWSG1 in embryonic development, TWSG1 also plays an important role in regulation of adult tissues. Research in osteoclast models uncovered a role for TWSG1 in limiting osteoclast promoting BMP activity. Without TWSG1 osteoclasts are overactive, leading to osteopenia (Sotillo Rodriguez et al., 2009). To date however the only *in vivo* studies of TWSG1 action have been models of TWSG1 deficiency. The effect of increased TWSG1 has only been studied *in vitro* using using exogenous protein or viral transduction in cell culture (Sotillo Rodriguez et al., 2009; Pham et al., 2011). These *in vitro* studies can now be complemented by *in vivo* studies. This will allow better characterization of the action of TWSG in regulating signals that govern osteoclast development. Better understanding of osteoclast regulation will allow development of better therapies for diseases like osteopetrosis and osteoporosis that are characterized by under-or over-activity of osteoclasts.

In summary, the *ROSA26* targeted conditional *Twsg1*-overexpressing mouse will provide a valuable reagent for future studies of the action of TWSG1 in embryonic and adult tissues.

References:

Chapter 2 note of previous publication

Figures, tables and text in Chapter 2 are reprinted with minor editing from the article:

Billington, C. J., Jr., Fiebig, J. E., Forsman, C. L., Pham, L., Burbach, N., Sun, M., Jaskoll, T., Mansky, K., Gopalakrishnan, R., O'Connor, M. B. et al. (2011a). Glycosylation of Twisted Gastrulation is Required for BMP Binding and Activity during Craniofacial Development. *Front Physiol* 2, 59.

"Under … the Frontiers General Conditions for Authors, authors of articles published in Frontiers journals retain copyright on their articles, … Authors are therefore free to disseminate and re-publish their articles… subject to the original publication being fully cited." (http://www.frontiersin.org/Physiology/about)

Chapter 3 note of previous publication

Figures, tables and text in Chapter 3 are reprinted with minor editing from the article:

Billington, C. J., Jr., Ng, B., Forsman, C., Schmidt, B., Bagchi, A., Symer, D. E., Schotta, G., Gopalakrishnan, R., Sarver, A. L. and Petryk, A. (2011b). The molecular and cellular basis of variable craniofacial phenotypes and their genetic rescue in Twisted gastrulation mutant mice. *Dev Biol* 355, 21-31.

Journal Authors retain "the right to include the journal article, in full or in part, in a thesis or dissertation" (http://www.elsevier.com/wps/find/authorsview.authors/rights#whatrights)

Chapter 4 note of previous publication

Figures, tables and text in Chapter 4 are reprinted with minor editing from the article:

Billington, C. J., Jr., Schmidt, B., Zhang, L., Hodges, J. S., Georgieff, M. K., Schotta, G., Gopalakrishnan, G., Petryk, A. (2013). Maternal diet supplementation with methyl donors and increased parity affect the incidence of craniofacial defects in the offspring of *Twisted gastrulation* mutant mice. *J Nutr* 143 (3), 332-339.

"Effective upon acceptance for publication, the American Society for Nutrition will license the following nonexclusive rights back to authors: … The right to include their article in their thesis or dissertation." (http://www.nutrition.org/publications/guidelines-and-policies/permissions/#autogrant)

Works Cited:

Achón, M., Alonso-Aperte, E., Reyes, L., Ubeda, N. and Varela-Moreiras, G. (2000). High-dose folic acid supplementation in rats: effects on gestation and the methionine cycle. *Br J Nutr* **83**, 177-183.

Anderson, R. M., Lawrence, A. R., Stottmann, R. W., Bachilier, D. and Klingensmith, J. (2002). Chordin and noggin promote organizing centers of forebrain development in the mouse. *Development* **129**, 4975-4987.

Aoto, K., Shikata, Y., Higashiyama, D., Shiota, K. and Motoyama, J. (2008). Fetal ethanol exposure activates protein kinase A and impairs Shh expression in prechordal mesendoderm cells in the pathogenesis of holoprosencephaly. *Birth Defects Res A Clin Mol Teratol* **82**, 224-231.

Aoto, K., Shikata, Y., Imai, H., Matsumaru, D., Tokunaga, T., Shioda, S., Yamada, G. and Motoyama, J. (2009). Mouse Shh is required for prechordal plate maintenance during brain and craniofacial morphogenesis. *Dev Biol* **327**, 106-120.

Avsian-Kretchmer, O. and Hsueh, A. J. (2004). Comparative genomic analysis of the eight-membered ring cystine knot-containing bone morphogenetic protein antagonists. *Mol Endocrinol* **18**, 1-12.

Bailey, L. B. (1992). Evaluation of a new Recommended Dietary Allowance for folate. *J Am Diet Assoc* **92**, 463-468, 471.

Barbosa, J. A., Santos-Aguado, J., Mentzer, S. J., Strominger, J. L., Burakoff, S. J. and Biro, P. A. (1987). Site-directed mutagenesis of class I HLA genes. Role of glycosylation in surface expression and functional recognition. *J Exp Med* **166**, 1329-1350.

Benjamini, Y. and Hochberg, Y. (1995). Controlling the false discovery rate: a practical and powerful approach to multiple testing. *Journal of the Royal Statistical Society. Series B*.

Benz, I. and Schmidt, M. A. (2001). Glycosylation with heptose residues mediated by the aah gene product is essential for adherence of the AIDA-I adhesin. *Mol Microbiol* **40**, 1403-1413.

Berdal, A., Molla, M., Hotton, D., Aïoub, M., Lézot, F., Néfussi, J. R. and Goubin, G. (2009). Differential impact of MSX1 and MSX2 homeogenes on mouse maxillofacial skeleton. *Cells, tissues, organs* **189**, 126-132.

Berry, R. J. and Li, Z. (2002). Folic acid alone prevents neural tube defects: evidence from the China study. *Epidemiology* **13**, 114-116.

Berry, R. J., Li, Z., Erickson, J. D., Li, S., Moore, C. A., Wang, H., Mulinare, J., Zhao, P., Wong, L. Y., Gindler, J. et al. (1999). Prevention of neural-tube

defects with folic acid in China. China-U.S. Collaborative Project for Neural Tube Defect Prevention. *N Engl J Med* **341**, 1485-1490.

Bier, E. (2008). Intriguing extracellular regulation of BMP signaling. *Dev Cell* **15**, 176-177.

Billington, C. J., Jr., Ng, B., Forsman, C., Schmidt, B., Bagchi, A., Symer, D. E., Schotta, G., Gopalakrishnan, R., Sarver, A. L. and Petryk, A. (2011a). The molecular and cellular basis of variable craniofacial phenotypes and their genetic rescue in Twisted gastrulation mutant mice. *Dev Biol* **355**, 21-31.

Billington, C. J., Jr., Fiebig, J. E., Forsman, C. L., Pham, L., Burbach, N., Sun, M., Jaskoll, T., Mansky, K., Gopalakrishnan, R., O'Connor, M. B. et al. (2011b). Glycosylation of Twisted Gastrulation is Required for BMP Binding and Activity during Craniofacial Development. *Front Physiol* **2**, 59.

Blitz, I. L., Cho, K. W. and Chang, C. (2003). Twisted gastrulation loss-of-function analyses support its role as a BMP inhibitor during early Xenopus embryogenesis. *Development* **130**, 4975-4988.

Blom, H. J., Shaw, G. M., den Heijer, M. and Finnell, R. H. (2006). Neural tube defects and folate: case far from closed. *Nat Rev Neurosci* **7**, 724-731.

Bobola, N., Carapuco, M., Ohnemus, S., Kanzler, B., Leibbrandt, A., Neubuser, A., Drouin, J. and Mallo, M. (2003). Mesenchymal patterning by Hoxa2 requires blocking Fgf-dependent activation of Ptx1. *Development* **130**, 3403-3414.

Boot, M. J., Steegers-Theunissen, R. P., Poelmann, R. E., Van Iperen, L., Lindemans, J. and Gittenberger-de Groot, A. C. (2003). Folic acid and homocysteine affect neural crest and neuroepithelial cell outgrowth and differentiation in vitro. *Dev Dyn* **227**, 301-308.

Botto, L. D., Moore, C. A., Khoury, M. J. and Erickson, J. D. (1999). Neural-tube defects. *N Engl J Med* **341**, 1509-1519.

Botto, L. D., Lisi, A., Bower, C., Canfield, M. A., Dattani, N., De Vigan, C., De Walle, H., Erickson, D. J., Halliday, J., Irgens, L. M. et al. (2006). Trends of selected malformations in relation to folic acid recommendations and fortification: an international assessment. *Birth Defects Res A Clin Mol Teratol* **76**, 693-705.

Braybrook, C., Doudney, K., Marcano, A. C., Arnason, A., Bjornsson, A., Patton, M. A., Goodfellow, P. J., Moore, G. E. and Stanier, P. (2001). The T-box transcription factor gene TBX22 is mutated in X-linked cleft palate and ankyloglossia. *Nat Genet* **29**, 179-183.

Bruce, S., Hannula-Jouppi, K., Peltonen, J., Kere, J. and Lipsanen-Nyman, M. (2009). Clinically Distinct Epigenetic Subgroups in Silver-Russell Syndrome: The Degree of H19 Hypomethylation Associates with Phenotype Severity and Genital and Skeletal Anomalies. *Journal of Clinical Endocrinology & Metabolism* **94**,

579-587.

Brugmann, S. A., Kim, J. and Helms, J. A. (2006). Looking different: understanding diversity in facial form. *Am J Med Genet A* **140**, 2521-2529.

Buller, A. L., Hastings, G. A., Kirkness, E. F. and Fraser, C. M. (1994). Site-directed mutagenesis of N-linked glycosylation sites on the gamma-aminobutyric acid type A receptor alpha 1 subunit. *Mol Pharmacol* **46**, 858-865.

Burgoon, J. M., Selhub, J., Nadeau, M. and Sadler, T. W. (2002). Investigation of the effects of folate deficiency on embryonic development through the establishment of a folate deficient mouse model. *Teratology* **65**, 219-227.

Burren, K. A., Savery, D., Massa, V., Kok, R. M., Scott, J. M., Blom, H. J., Copp, A. J. and Greene, N. D. (2008). Gene-environment interactions in the causation of neural tube defects: folate deficiency increases susceptibility conferred by loss of Pax3 function. *Hum Mol Genet* **17**, 3675-3685.

Butchbach, M. E., Rose, F. F., Jr., Rhoades, S., Marston, J., McCrone, J. T., Sinnott, R. and Lorson, C. L. (2009). Effect of diet on the survival and phenotype of a mouse model for spinal muscular atrophy. *Biochem Biophys Res Commun*.

Canalis, E., Economides, A. N. and Gazzerro, E. (2003). Bone morphogenetic proteins, their antagonists, and the skeleton. *Endocr Rev* **24**, 218-235.

Canfield, M. A., Collins, J. S., Botto, L. D., Williams, L. J., Mai, C. T., Kirby, R. S., Pearson, K., Devine, O. and Mulinare, J. (2005). Changes in the birth prevalence of selected birth defects after grain fortification with folic acid in the United States: findings from a multi-state population-based study. *Birth Defects Res A Clin Mol Teratol* **73**, 679-689.

Caragea, C., Sinapov, J., Silvescu, A., Dobbs, D. and Honavar, V. (2007). Glycosylation site prediction using ensembles of Support Vector Machine classifiers. *BMC Bioinformatics* **8**, 438.

Castilla, E. E. and Orioli, I. M. (1986). Prevalence rates of microtia in South America. *Int J Epidemiol* **15**, 364-368.

Champy, M. F., Selloum, M., Zeitler, V., Caradec, C., Jung, B., Rousseau, S., Pouilly, L., Sorg, T. and Auwerx, J. (2008). Genetic background determines metabolic phenotypes in the mouse. *Mamm Genome* **19**, 318-331.

Chang, C., Holtzman, D. A., Chau, S., Chickering, T., Woolf, E. A., Holmgren, L. M., Bodorova, J., Gearing, D. P., Holmes, W. E. and Brivanlou, A. H. (2001). Twisted gastrulation can function as a BMP antagonist. *Nature* **410**, 483-487.

Chaoui, R., Heling, K. S., Thiel, G. and Karl, K. (2011). Agnathia-otocephaly with holoprosencephaly on prenatal three-dimensional ultrasound. *Ultrasound Obstet Gynecol* **37**, 745-748.

Chase, H. B. (1942). Studies on an Anophthalmic Strain of Mice. III. Results of Crosses

with Other Strains. *Genetics* **27**, 339-348.

Chern, C. L., Huang, R. F., Chen, Y. H., Cheng, J. T. and Liu, T. Z. (2001). Folate deficiency-induced oxidative stress and apoptosis are mediated via homocysteine-dependent overproduction of hydrogen peroxide and enhanced activation of NF-kappaB in human Hep G2 cells. *Biomed Pharmacother* **55**, 434-442.

Choi, S. W., Friso, S., Keyes, M. K. and Mason, J. B. (2005). Folate supplementation increases genomic DNA methylation in the liver of elder rats. *Br J Nutr* **93**, 31-35.

Chong, H. J., Young, N. M., Hu, D., Jeong, J., McMahon, A. P., Hallgrimsson, B. and Marcucio, R. S. (2012). Signaling by SHH rescues facial defects following blockade in the brain. *Dev Dyn* **241**, 247-256.

Clausen, B. E., Burkhardt, C., Reith, W., Renkawitz, R. and Forster, I. (1999). Conditional gene targeting in macrophages and granulocytes using LysMcre mice. *Transgenic Res* **8**, 265-277.

Cohen, M. M., Jr. and Shiota, K. (2002). Teratogenesis of holoprosencephaly. *Am J Med Genet* **109**, 1-15.

Cooney, C. A., Dave, A. A. and Wolff, G. L. (2002). Maternal methyl supplements in mice affect epigenetic variation and DNA methylation of offspring. *J Nutr* **132**, 2393S-2400S.

Csiszar, A., Labinskyy, N., Jo, H., Ballabh, P. and Ungvari, Z. (2008). Differential proinflammatory and prooxidant effects of bone morphogenetic protein-4 in coronary and pulmonary arterial endothelial cells. *Am J Physiol Heart Circ Physiol* **295**, H569-577.

Csiszar, A., Ahmad, M., Smith, K. E., Labinskyy, N., Gao, Q., Kaley, G., Edwards, J. G., Wolin, M. S. and Ungvari, Z. (2006). Bone morphogenetic protein-2 induces proinflammatory endothelial phenotype. *Am J Pathol* **168**, 629-638.

Czeizel, A. E. and Dudas, I. (1992). Prevention of the first occurrence of neural-tube defects by periconceptional vitamin supplementation. *N Engl J Med* **327**, 1832-1835.

Dale, J. K., Vesque, C., Lints, T. J., Sampath, T. K., Furley, A., Dodd, J. and Placzek, M. (1997). Cooperation of BMP7 and SHH in the induction of forebrain ventral midline cells by prechordal mesoderm. *Cell* **90**, 257-269.

Dale, L. (2000). Pattern formation: a new twist to BMP signalling. *Curr Biol* **10**, R671-673.

De-Regil, L. M., Fernandez-Gaxiola, A. C., Dowswell, T. and Pena-Rosas, J. P. (2010). Effects and safety of periconceptional folate supplementation for preventing birth defects. *Cochrane Database Syst Rev*, CD007950.

Depreux, F. F., Darrow, K., Conner, D. A., Eavey, R. D., Liberman, M. C., Seidman, C. E. and Seidman, J. G. (2008). Eya4-deficient mice are a model for heritable

otitis media. *J Clin Invest* **118**, 651-658.

Diede, S. J., Guenthoer, J., Geng, L. N., Mahoney, S. E., Marotta, M., Olson, J. M., Tanaka, H. and Tapscott, S. J. (2009). DNA methylation of developmental genes in pediatric medulloblastomas identified by denaturation analysis of methylation differences. *Proc Natl Acad Sci U S A*.

Dindot, S. V., Person, R., Strivens, M., Garcia, R. and Beaudet, A. L. (2009). Epigenetic profiling at mouse imprinted gene clusters reveals novel epigenetic and genetic features at differentially methylated regions. *Genome Res* **19**, 1374-1383.

Dixon, M. J., Marazita, M. L., Beaty, T. H. and Murray, J. C. (2011). Cleft lip and palate: understanding genetic and environmental influences. *Nat Rev Genet* **12**, 167-178.

Dolinoy, D. C. (2007). Epigenetic gene regulation: early environmental exposures. *Pharmacogenomics* **8**, 5-10.

Dolinoy, D. C., Das, R., Weidman, J. R. and Jirtle, R. L. (2007). Metastable epialleles, imprinting, and the fetal origins of adult diseases. *Pediatr Res* **61**, 30R-37R.

Donehower, L. A., Harvey, M., Slagle, B. L., McArthur, M. J., Montgomery, C. A., Jr., Butel, J. S. and Bradley, A. (1992). Mice deficient for p53 are developmentally normal but susceptible to spontaneous tumours. *Nature* **356**, 215-221.

Druker, R., Bruxner, T. J., Lehrbach, N. J. and Whitelaw, E. (2004). Complex patterns of transcription at the insertion site of a retrotransposon in the mouse. *Nucleic Acids Res* **32**, 5800-5808.

Du, Y. and Yip, H. (2009). Effects of bone morphogenetic protein 2 on Id expression and neuroblastoma cell differentiation. *Differentiation*.

Duong, H. T., Hoyt, A. T., Carmichael, S. L., Gilboa, S. M., Canfield, M. A., Case, A., McNeese, M. L. and Waller, D. K. (2012). Is maternal parity an independent risk factor for birth defects? *Birth Defects Res A Clin Mol Teratol* **94**, 230-236.

Ekanayake, S. and Hall, B. K. (1997). The in vivo and in vitro effects of bone morphogenetic protein-2 on the development of the chick mandible. *Int J Dev Biol* **41**, 67-81.

Esteve, P. O., Chin, H. G. and Pradhan, S. (2005). Human maintenance DNA (cytosine-5)-methyltransferase and p53 modulate expression of p53-repressed promoters. *Proc Natl Acad Sci U S A* **102**, 1000-1005.

Feng, W., Leach, S. M., Tipney, H., Phang, T., Geraci, M., Spritz, R. A., Hunter, L. E. and Williams, T. (2009). Spatial and Temporal Analysis of Gene Expression during Growth and Fusion of the Mouse Facial Prominences. *PLoS One* **4**, e8066.

Finley, K. R., Tennessen, J. and Shawlot, W. (2003). The mouse secreted frizzled-related protein 5 gene is expressed in the anterior visceral endoderm and foregut

endoderm during early post-implantation development. *Gene expression patterns : GEP* **3**, 681-684.

Fisher, M., Zeisel, S., Mar, M. and Sadler, T. (2001). Inhibitors of choline uptake and metabolism cause developmental abnormalities in neurulating mouse embryos. . *Teratology* **64**, 114-122.

FitzPatrick, D. R., Carr, I. M., McLaren, L., Leek, J. P., Wightman, P., Williamson, K., Gautier, P., McGill, N., Hayward, C., Firth, H. et al. (2003). Identification of SATB2 as the cleft palate gene on 2q32-q33. *Human molecular genetics* **12**, 2491-2501.

Fraser, F. C. (1970). The genetics of cleft lip and cleft palate. *Am J Hum Genet* **22**, 336-352.

Fukuda, N., Saitoh, M., Kobayashi, N. and Miyazono, K. (2006). Execution of BMP-4-induced apoptosis by p53-dependent ER dysfunction in myeloma and B-cell hybridoma cells. *Oncogene* **25**, 3509-3517.

Garrigue-Antar, L., Hartigan, N. and Kadler, K. E. (2002). Post-translational modification of bone morphogenetic protein-1 is required for secretion and stability of the protein. *J Biol Chem* **277**, 43327-43334.

Gavel, Y. and von Heijne, G. (1990). Sequence differences between glycosylated and non-glycosylated Asn-X-Thr/Ser acceptor sites: implications for protein engineering. *Protein Eng* **3**, 433-442.

Gazzerro, E., Deregowski, V., Vaira, S. and Canalis, E. (2005). Overexpression of twisted gastrulation inhibits bone morphogenetic protein action and prevents osteoblast cell differentiation in vitro. *Endocrinology* **146**, 3875-3882.

Gazzerro, E., Deregowski, V., Stadmeyer, L., Gale, N. W., Economides, A. N. and Canalis, E. (2006). Twisted gastrulation, a bone morphogenetic protein agonist/antagonist, is not required for post-natal skeletal function. *Bone* **39**, 1252-1260.

Gekas, J., Li, B. and Kamnasaran, D. (2010). Current perspectives on the etiology of agnathia-otocephaly. *Eur J Med Genet* **53**, 358-366.

Gibney, E. R. and Nolan, C. M. (2010). Epigenetics and gene expression. *Heredity (Edinb)* **105**, 4-13.

Graf, D., Nethisinghe, S., Palmer, D. B., Fisher, A. G. and Merkenschlager, M. (2002). The developmentally regulated expression of Twisted gastrulation reveals a role for bone morphogenetic proteins in the control of T cell development. *J Exp Med* **196**, 163-171.

Graf, D., Timmons, P. M., Hitchins, M., Episkopou, V., Moore, G., Ito, T., Fujiyama, A., Fisher, A. G. and Merkenschlager, M. (2001). Evolutionary conservation, developmental expression, and genomic mapping of mammalian Twisted gastrulation. *Mamm Genome* **12**, 554-560.

Graham, A., Francis-West, P., Brickell, P. and Lumsden, A. (1994). The signalling molecule BMP4 mediates apoptosis in the rhombencephalic neural crest. *Nature* **372**, 684-686.

Groppe, J., Greenwald, J., Wiater, E., Rodriguez-Leon, J., Economides, A. N., Kwiatkowski, W., Affolter, M., Vale, W. W., Belmonte, J. C. and Choe, S. (2002). Structural basis of BMP signalling inhibition by the cystine knot protein Noggin. *Nature* **420**, 636-642.

Gumienny, T. L. and Padgett, R. W. (2002). The other side of TGF-beta superfamily signal regulation: thinking outside the cell. *Trends Endocrinol Metab* **13**, 295-299.

Gyorgy, A. B., Szemes, M., de Juan Romero, C., Tarabykin, V. and Agoston, D. V. (2008). SATB2 interacts with chromatin-remodeling molecules in differentiating cortical neurons. *Eur J Neurosci* **27**, 865-873.

Hansen, M., Lucarelli, M. J., Whiteman, D. A. H. and Mulliken, J. B. (1996). Treacher Collins syndrome: Phenotypic variability in a family including an infant with arhinia and uveal colobomas. *American Journal of Medical Genetics* **61**, 71-74.

Harland, R. M. (2001). Developmental biology. A twist on embryonic signalling. *Nature* **410**, 423-424.

Hay, S. and Barbano, H. (1972). Independent effects of maternal age and birth order on the incidence of selected congenital malformations. *Teratology* **6**, 271-279.

Hehr, U., Gross, C., Diebold, U., Wahl, D., Beudt, U., Heidemann, P., Hehr, A. and Mueller, D. (2004). Wide phenotypic variability in families with holoprosencephaly and a sonic hedgehog mutation. *European Journal of Pediatrics* **163**, 347-352.

Heinecke, K., Seher, A., Schmitz, W., Mueller, T. D., Sebald, W. and Nickel, J. (2009). Receptor oligomerization and beyond: a case study in bone morphogenetic proteins. *BMC Biol* **7**, 59.

Henderson, G. E., Isett, K. D. and Gerngross, T. U. (2011). Site-Specific Modification of Recombinant Proteins: A Novel Platform for Modifying Glycoproteins Expressed in E. coli. *Bioconjug Chem* **22**, 903-912.

Hide, T., Hatakeyama, J., Kimura-Yoshida, C., Tian, E., Takeda, N., Ushio, Y., Shiroishi, T., Aizawa, S. and Matsuo, I. (2002). Genetic modifiers of otocephalic phenotypes in Otx2 heterozygous mutant mice. *Development* **129**, 4347-4357.

Higashiyama, D., Saitsu, H., Komada, M., Takigawa, T., Ishibashi, M. and Shiota, K. (2007). Sequential developmental changes in holoprosencephalic mouse embryos exposed to ethanol during the gastrulation period. *Birth Defects Res A Clin Mol Teratol* **79**, 513-523.

Honein, M. A., Paulozzi, L. J., Mathews, T. J., Erickson, J. D. and Wong, L. Y. (2001). Impact of folic acid fortification of the US food supply on the occurrence of neural tube defects. *JAMA* **285**, 2981-2986.

Hoyt, P. R., Bartholomew, C., Davis, A. J., Yutzey, K., Gamer, L. W., Potter, S. S., Ihle, J. N. and Mucenski, M. L. (1997). The Evi1 proto-oncogene is required at midgestation for neural, heart, and paraxial mesenchyme development. *Mech Dev* **65**, 55-70.

Hu, D. and Marcucio, R. S. (2009a). Unique organization of the frontonasal ectodermal zone in birds and mammals. *Dev Biol* **325**, 200-210.

Hu, D. and Marcucio, R. S. (2009b). A SHH-responsive signaling center in the forebrain regulates craniofacial morphogenesis via the facial ectoderm. *Development* **136**, 107-116.

Ikeya, M., Fukushima, K., Kawada, M., Onishi, S., Furuta, Y., Yonemura, S., Kitamura, T., Nosaka, T. and Sasai, Y. (2010). Cv2, functioning as a pro-BMP factor via twisted gastrulation, is required for early development of nephron precursors. *Dev Biol* **337**, 405-414.

Jarvis, D. L., Kawar, Z. S. and Hollister, J. R. (1998). Engineering N-glycosylation pathways in the baculovirus-insect cell system. *Curr Opin Biotechnol* **9**, 528-533.

Jaskoll, T., Abichaker, G., Witcher, D., Sala, F. G., Bellusci, S., Hajihosseini, M. K. and Melnick, M. (2005). FGF10/FGFR2b signaling plays essential roles during in vivo embryonic submandibular salivary gland morphogenesis. *BMC Dev Biol* **5**, 11.

Jeong, J., Li, X., McEvilly, R. J., Rosenfeld, M. G., Lufkin, T. and Rubenstein, J. L. (2008). Dlx genes pattern mammalian jaw primordium by regulating both lower jaw-specific and upper jaw-specific genetic programs. *Development (Cambridge, England)* **135**, 2905-2916.

Jones, N. C., Lynn, M. L., Gaudenz, K., Sakai, D., Aoto, K., Rey, J. P., Glynn, E. F., Ellington, L., Du, C., Dixon, J. et al. (2008). Prevention of the neurocristopathy Treacher Collins syndrome through inhibition of p53 function. *Nat Med* **14**, 125-133.

Juriloff, D. M. and Harris, M. J. (2008). Mouse genetic models of cleft lip with or without cleft palate. *Birth Defects Res A Clin Mol Teratol* **82**, 63-77.

Juriloff, D. M., Sulik, K. K., Roderick, T. H. and Hogan, B. K. (1985). Genetic and developmental studies of a new mouse mutation that produces otocephaly. *J Craniofac Genet Dev Biol* **5**, 121-145.

Kalter, H. (1968). Sporadic congenital malformations of newborn inbred mice. *Teratology* **1**, 193-199.

Kamimura, M., Matsumoto, K., Koshiba-Takeuchi, K. and Ogura, T. (2004). Vertebrate crossveinless 2 is secreted and acts as an extracellular modulator of the

BMP signaling cascade. *Dev Dyn* **230**, 434-445.

Kitami, T., Rubio, R., O'Brien, W., Quackenbush, J. and Nadeau, J. (2008). Gene-environment interactions reveal a homeostatic role for cholesterol metabolism during dietary folate perturbation in mice. *Physiol Genomics* **35**, 182-190.

Kontges, G. and Lumsden, A. (1996). Rhombencephalic neural crest segmentation is preserved throughout craniofacial ontogeny. *Development* **122**, 3229-3242.

Kozak, M. (1987). An analysis of 5'-noncoding sequences from 699 vertebrate messenger RNAs. *Nucleic Acids Res* **15**, 8125-8148.

Kuroiwa, Y., Kaneko-Ishino, T., Kagitani, F., Kohda, T., Li, L. L., Tada, M., Suzuki, R., Yokoyama, M., Shiroishi, T., Wakana, S. et al. (1996). Peg3 imprinted gene on proximal chromosome 7 encodes for a zinc finger protein. *Nat Genet* **12**, 186-190.

Lakso, M., Pichel, J. G., Gorman, J. R., Sauer, B., Okamoto, Y., Lee, E., Alt, F. W. and Westphal, H. (1996). Efficient in vivo manipulation of mouse genomic sequences at the zygote stage. *Proc Natl Acad Sci U S A* **93**, 5860-5865.

Larrain, J., Oelgeschlager, M., Ketpura, N. I., Reversade, B., Zakin, L. and De Robertis, E. M. (2001). Proteolytic cleavage of Chordin as a switch for the dual activities of Twisted gastrulation in BMP signaling. *Development* **128**, 4439-4447.

Larsen, W. J., Sherman, L. S., Potter, S. S. and Scott, W. J. (2001). Human Embryology, 3rd Edition. New York: Churchill Livingstone.

Li, D., Pickell, L., Liu, Y., Wu, Q., Cohn, J. S. and Rozen, R. (2005). Maternal methylenetetrahydrofolate reductase deficiency and low dietary folate lead to adverse reproductive outcomes and congenital heart defects in mice. *Am J Clin Nutr* **82**, 188-195.

Lindenthal, C. and Elsinghorst, E. A. (1999). Identification of a glycoprotein produced by enterotoxigenic Escherichia coli. *Infect Immun* **67**, 4084-4091.

Linton, K., Hey, Y., Dibben, S., Miller, C., Freemont, A., Radford, J. and Pepper, S. (2009). Methods comparison for high-resolution transcriptional analysis of archival material on Affymetrix Plus 2.0 and Exon 1.0 microarrays. *Biotechniques* **47**, 587-596.

Lipinski, R. J., Godin, E. A., O'Leary-Moore, S. K., Parnell, S. E. and Sulik, K. K. (2010). Genesis of teratogen-induced holoprosencephaly in mice. *Am J Med Genet C Semin Med Genet* **154C**, 29-42.

Little, S. C. and Mullins, M. C. (2004). Twisted gastrulation promotes BMP signaling in zebrafish dorsal-ventral axial patterning. *Development* **131**, 5825-5835.

Liu, B., Rooker, S. M. and Helms, J. A. (2010). Molecular control of facial morphology. *Semin Cell Dev Biol* **21**, 309-313.

Liu, Y. and Xiao, A. (2011). Epigenetic regulation in neural crest development. *Birth Defects Res A Clin Mol Teratol* **91**, 788-796.

Loeken, M. R. (2004). Free radicals and birth defects. *J Matern Fetal Neonatal Med* **15**, 6-14.

Loffredo, L. C., Souza, J. M., Freitas, J. A. and Mossey, P. A. (2001). Oral clefts and vitamin supplementation. *Cleft Palate Craniofac J* **38**, 76-83.

Luedi, P. P., Hartemink, A. J. and Jirtle, R. L. (2005). Genome-wide prediction of imprinted murine genes. *Genome research* **15**, 875-884.

MacKenzie, A., Ferguson, M. W. and Sharpe, P. T. (1992). Expression patterns of the homeobox gene, Hox-8, in the mouse embryo suggest a role in specifying tooth initiation and shape. *Development* **115**, 403-420.

MacKenzie, B., Wolff, R., Lowe, N., Billington, C. J., Jr., Peterson, A., Schmidt, B., Graf, D., Mina, M., Gopalakrishnan, R. and Petryk, A. (2009). Twisted gastrulation limits apoptosis in the distal region of the mandibular arch in mice. *Dev Biol* **328**, 13-23.

March-of-Dimes. (2010). March of Dimes Data Book for Policy Makers: Maternal, Infant, and Child Health in the United States. Atlanta, GA: marchofdimes.com.

Marks, S. C., Jr. (1987). Osteopetrosis--multiple pathways for the interception of osteoclast function. *Appl Pathol* **5**, 172-183.

Mason, E. D., Konrad, K. D., Webb, C. D. and Marsh, J. L. (1994). Dorsal midline fate in Drosophila embryos requires twisted gastrulation, a gene encoding a secreted protein related to human connective tissue growth factor. *Genes Dev* **8**, 1489-1501.

Mason, E. D., Williams, S., Grotendorst, G. R. and Marsh, J. L. (1997). Combinatorial signaling by Twisted Gastrulation and Decapentaplegic. *Mech Dev* **64**, 61-75.

Mastroiacovo, P., Corchia, C., Botto, L. D., Lanni, R., Zampino, G. and Fusco, D. (1995). Epidemiology and genetics of microtia-anotia: a registry based study on over one million births. *J Med Genet* **32**, 453-457.

Matsunaga, E. and Shiota, K. (1977). Holoprosencephaly in human embryos: epidemiologic studies of 150 cases. *Teratology* **16**, 261-272.

Matsuo, I., Kuratani, S., Kimura, C., Takeda, N. and Aizawa, S. (1995). Mouse Otx2 functions in the formation and patterning of rostral head. *Genes Dev* **9**, 2646-2658.

Matsuoka, T., Ahlberg, P. E., Kessaris, N., Iannarelli, P., Dennehy, U., Richardson, W. D., McMahon, A. P. and Koentges, G. (2005). Neural crest origins of the neck and shoulder. *Nature* **436**, 347-355.

McMahon, K. and Farrell, P. (1985). Measurement of free choline concentrations in

maternal and neonatal blood by micropyrolysis gas chromatography. *Clin Chim Acta* **149**, 1-12.

Melnick, M., Witcher, D., Bringas, P., Jr., Carlsson, P. and Jaskoll, T. (2005). Meckel's cartilage differentiation is dependent on hedgehog signaling. *Cells Tissues Organs* **179**, 146-157.

Melnick, M., Petryk, A., Abichaker, G., Witcher, D., Person, A. D. and Jaskoll, T. (2006). Embryonic salivary gland dysmorphogenesis in Twisted gastrulation deficient mice. *Arch Oral Biol* **51**, 433-438.

Merritt, L. (2005). Part 1. Understanding the embryology and genetics of cleft lip and palate. *Adv Neonatal Care* **5**, 64-71.

Milman, N., Kirchhoff, M. and Jorgensen, T. (1992). Iron status markers, serum ferritin and hemoglobin in 1359 Danish women in relation to menstruation, hormonal contraception, parity, and postmenopausal hormone treatment. *Ann Hematol* **65**, 96-102.

Mina, M., Wang, Y. H., Ivanisevic, A. M., Upholt, W. B. and Rodgers, B. (2002). Region- and stage-specific effects of FGFs and BMPs in chick mandibular morphogenesis. *Dev Dyn* **223**, 333-352.

Ming, J. E. and Muenke, M. (2002). Multiple hits during early embryonic development: digenic diseases and holoprosencephaly. *Am J Hum Genet* **71**, 1017-1032.

Ming, J. E., Kaupas, M. E., Roessler, E., Brunner, H. G., Golabi, M., Tekin, M., Stratton, R. F., Sujansky, E., Bale, S. J. and Muenke, M. (2002). Mutations in PATCHED-1, the receptor for SONIC HEDGEHOG, are associated with holoprosencephaly. *Hum Genet* **110**, 297-301.

Morison, I. M., Paton, C. J. and Cleverley, S. D. (2001). The imprinted gene and parent-of-origin effect database. *Nucleic Acids Res* **29**, 275-276.

Morison, I. M., Ramsay, J. P. and Spencer, H. G. (2005). A census of mammalian imprinting. *Trends Genet* **21**, 457-465.

MRC, V. S. R. G. (1991). Prevention of neural tube defects: results of the Medical Research Council Vitamin Study. MRC Vitamin Study Research Group. *Lancet* **338**, 131-137.

Muenke, M. and Cohen, M. M., Jr. (2000). Genetic approaches to understanding brain development: holoprosencephaly as a model. *Ment Retard Dev Disabil Res Rev* **6**, 15-21.

Muenke, M. and Beachy, P. A. (2000). Genetics of ventral forebrain development and holoprosencephaly. *Curr Opin Genet Dev* **10**, 262-269.

Mukhopadhyay, M., Shtrom, S., Rodriguez-Esteban, C., Chen, L., Tsukui, T., Gomer, L., Dorward, D. W., Glinka, A., Grinberg, A., Huang, S. P. et al. (2001). Dickkopf1 is required for embryonic head induction and limb

morphogenesis in the mouse. *Dev Cell* **1**, 423-434.

Muller, F. and O'Rahilly, R. (2003). The prechordal plate, the rostral end of the notochord and nearby median features in staged human embryos. *Cells Tissues Organs* **173**, 1-20.

Muller, S. M., Stolt, C. C., Terszowski, G., Blum, C., Amagai, T., Kessaris, N., Iannarelli, P., Richardson, W. D., Wegner, M. and Rodewald, H. R. (2008). Neural crest origin of perivascular mesenchyme in the adult thymus. *J Immunol* **180**, 5344-5351.

Murray, J. C. (2002). Gene/environment causes of cleft lip and/or palate. *Clin Genet* **61**, 248-256.

Mutlu, B., Bas, A. Y., Aksoy, N. and Taskin, A. (2012). The effect of maternal number of births on oxidative and antioxidative systems in cord blood. *J Matern Fetal Neonatal Med* **25**, 802-805.

Neuberger, A. and Marshall, R. D. (1968). In *Symposium on Foods - Carbohydrates and their Roles*, (eds H. W. Schultz R. F. Cain and R. W. Wrolstad), pp. 115-132: Avi Publishing Co., Westport, CT.

Niculescu, M. D. and Zeisel, S. H. (2002). Diet, methyl donors and DNA methylation: interactions between dietary folate, methionine and choline. *J Nutr* **132**, 2333S-2335S.

Nie, X., Luukko, K. and Kettunen, P. (2006). BMP signalling in craniofacial development. *Int J Dev Biol* **50**, 511-521.

Nora, J. J. (1968). Multifactorial inheritance hypothesis for the etiology of congenital heart diseases. The genetic-environmental interaction. *Circulation* **38**, 604-617.

Northrup, H. and Volcik, K. A. (2000). Spina bifida and other neural tube defects. *Curr Probl Pediatr* **30**, 313-332.

Nosaka, T., Morita, S., Kitamura, H., Nakajima, H., Shibata, F., Morikawa, Y., Kataoka, Y., Ebihara, Y., Kawashima, T., Itoh, T. et al. (2003). Mammalian twisted gastrulation is essential for skeleto-lymphogenesis. *Mol Cell Biol* **23**, 2969-2980.

Nussbaum, R. L., McInnes, R. R., Willard, H. F. and Hamosh, A. (2007). Thompson & Thompson Genetics in Medicine. Philadephia: Saunders-Elsevier.

O'Connor, M. B., Umulis, D., Othmer, H. G. and Blair, S. S. (2006). Shaping BMP morphogen gradients in the Drosophila embryo and pupal wing. *Development* **133**, 183-193.

Oelgeschlager, M., Larrain, J., Geissert, D. and De Robertis, E. M. (2000). The evolutionarily conserved BMP-binding protein Twisted gastrulation promotes BMP signalling. *Nature* **405**, 757-763.

Oelgeschlager, M., Tran, U., Grubisic, K. and De Robertis, E. M. (2004).

Identification of a second Xenopus twisted gastrulation gene. *Int J Dev Biol* **48**, 57-61.

Oelgeschlager, M., Reversade, B., Larrain, J., Little, S., Mullins, M. C. and De Robertis, E. M. (2003). The pro-BMP activity of Twisted gastrulation is independent of BMP binding. *Development* **130**, 4047-4056.

Osborn, N. K., Zou, H., Molina, J. R., Lesche, R., Lewin, J., Lofton-Day, C., Klatt, K. K., Harrington, J. J., Burgart, L. J. and Ahlquist, D. A. (2006). Aberrant methylation of the eyes absent 4 gene in ulcerative colitis-associated dysplasia. *Clin Gastroenterol Hepatol* **4**, 212-218.

Pandolfi, P. P., Roth, M. E., Karis, A., Leonard, M. W., Dzierzak, E., Grosveld, F. G., Engel, J. D. and Lindenbaum, M. H. (1995). Targeted disruption of the GATA3 gene causes severe abnormalities in the nervous system and in fetal liver haematopoiesis. *Nat Genet* **11**, 40-44.

Pani, L., Horal, M. and Loeken, M. R. (2002). Rescue of neural tube defects in Pax-3-deficient embryos by p53 loss of function: implications for Pax-3- dependent development and tumorigenesis. *Genes Dev* **16**, 676-680.

Pantoja, C., de Los Rios, L., Matheu, A., Antequera, F. and Serrano, M. (2005). Inactivation of imprinted genes induced by cellular stress and tumorigenesis. *Cancer Res* **65**, 26-33.

Paros, A. and Beck, S. L. (1999). Folinic acid reduces cleft lip [CL(P)] in A/WySn mice. *Teratology* **60**, 344-347.

Pauli, R. M., Pettersen, J. C., Arya, S. and Gilbert, E. F. (1983). Familial agnathia-holoprosencephaly. *Am J Med Genet* **14**, 677-698.

Pavlidis, P., Li, Q. and Noble, W. S. (2003). The effect of replication on gene expression microarray experiments. *Bioinformatics* **19**, 1620-1627.

Peaston, A. E. and Whitelaw, E. (2006). Epigenetics and phenotypic variation in mammals. *Mammalian genome : official journal of the International Mammalian Genome Society* **17**, 365-374.

Pera, E. M. and Kessel, M. (1997). Patterning of the chick forebrain anlage by the prechordal plate. *Development* **124**, 4153-4162.

Petryk, A., Anderson, R. M., Jarcho, M. P., Leaf, I., Carlson, C. S., Klingensmith, J., Shawlot, W. and O'Connor, M. B. (2004). The mammalian twisted gastrulation gene functions in foregut and craniofacial development. *Dev Biol* **267**, 374-386.

Petryk, A., Shimmi, O., Jia, X., Carlson, A. E., Tervonen, L., Jarcho, M. P., O'Connor M, B. and Gopalakrishnan, R. (2005). Twisted gastrulation and chordin inhibit differentiation and mineralization in MC3T3-E1 osteoblast-like cells. *Bone* **36**, 617-626.

Pfaff, S. L., Mendelsohn, M., Stewart, C. L., Edlund, T. and Jessell, T. M. (1996). Requirement for LIM homeobox gene Isl1 in motor neuron generation reveals a

motor neuron-dependent step in interneuron differentiation. *Cell* **84**, 309-320.

Pham, L., Beyer, K., Jensen, E. D., Rodriguez, J. S., Davydova, J., Yamamoto, M., Petryk, A., Gopalakrishnan, R. and Mansky, K. C. (2011). Bone morphogenetic protein 2 signaling in osteoclasts is negatively regulated by the BMP antagonist, twisted gastrulation. *J Cell Biochem* **112**, 793-803.

Podos, S. D. and Ferguson, E. L. (1999). Morphogen gradients: new insights from DPP. *Trends Genet* **15**, 396-402.

Rakyan, V. K., Blewitt, M. E., Druker, R., Preis, J. I. and Whitelaw, E. (2002). Metastable epialleles in mammals. *Trends Genet* **18**, 348-351.

Rakyan, V. K., Chong, S., Champ, M. E., Cuthbert, P. C., Morgan, H. D., Luu, K. V. and Whitelaw, E. (2003). Transgenerational inheritance of epigenetic states at the murine Axin(Fu) allele occurs after maternal and paternal transmission. *Proc Natl Acad Sci U S A* **100**, 2538-2543.

Ray, J. G. and Blom, H. J. (2003). Vitamin B12 insufficiency and the risk of fetal neural tube defects. *QJM* **96**, 289-295.

Roessler, E. and Muenke, M. (1999). The molecular genetics of holoprosencephaly: a model of brain development for the next century. *Childs Nerv Syst* **15**, 646-651.

Roessler, E., Belloni, E., Gaudenz, K., Jay, P., Berta, P., Scherer, S. W., Tsui, L. C. and Muenke, M. (1996). Mutations in the human Sonic Hedgehog gene cause holoprosencephaly. *Nat Genet* **14**, 357-360.

Ross, J. J., Shimmi, O., Vilmos, P., Petryk, A., Kim, H., Gaudenz, K., Hermanson, S., Ekker, S. C., O'Connor, M. B. and Marsh, J. L. (2001). Twisted gastrulation is a conserved extracellular BMP antagonist. *Nature* **410**, 479-483.

Rufer, E. S. (2010). Marginal maternal iron deficiency exacerbates alcohol-induced learning deficits and neurodegeneration in offspring. PhD in Molecular and Environmental Toxicology, Madison WI: University of Wisconsin.

Ruppert, R., Hoffmann, E. and Sebald, W. (1996). Human bone morphogenetic protein 2 contains a heparin-binding site which modifies its biological activity. *Eur J Biochem* **237**, 295-302.

Sah, V. P., Attardi, L. D., Mulligan, G. J., Williams, B. O., Bronson, R. T. and Jacks, T. (1995). A subset of p53-deficient embryos exhibit exencephaly. *Nat Genet* **10**, 175-180.

Saremba, S., Nickel, J., Seher, A., Kotzsch, A., Sebald, W. and Mueller, T. D. (2008). Type I receptor binding of bone morphogenetic protein 6 is dependent on N-glycosylation of the ligand. *FEBS J* **275**, 172-183.

Sasaki, H. and Hogan, B. L. (1993). Differential expression of multiple fork head related genes during gastrulation and axial pattern formation in the mouse embryo. *Development* **118**, 47-59.

Sawala, A., Sutcliffe, C. and Ashe, H. L. (2012). Multistep molecular mechanism for Bone morphogenetic protein extracellular transport in the Drosophila embryo. *Proc Natl Acad Sci U S A* **109**, 11222-11227.

Schlange, T., Arnold, H. H. and Brand, T. (2002). BMP2 is a positive regulator of Nodal signaling during left-right axis formation in the chicken embryo. *Development* **129**, 3421-3429.

Schmidl, M., Adam, N., Surmann-Schmitt, C., Hattori, T., Stock, M., Dietz, U., de Crombrugghe, B., Poschl, E. and von der Mark, K. (2006). Twisted gastrulation modulates bone morphogenetic protein-induced collagen II and X expression in chondrocytes in vitro and in vivo. *Journal of Biological Chemistry* **281**, 31790-31800.

Sclafani, A. M., Skidmore, J. M., Ramaprakash, H., Trumpp, A., Gage, P. J. and Martin, D. M. (2006). Nestin-Cre mediated deletion of Pitx2 in the mouse. *Genesis* **44**, 336-344.

Scott, I. C., Blitz, I. L., Pappano, W. N., Maas, S. A., Cho, K. W. and Greenspan, D. S. (2001). Homologues of Twisted gastrulation are extracellular cofactors in antagonism of BMP signalling. *Nature* **410**, 475-478.

Scott, J. M. (1999). Folate and vitamin B12. *Proc Nutr Soc* **58**, 441-448.

Semba, I., Nonaka, K., Takahashi, I., Takahashi, K., Dashner, R., Shum, L., Nuckolls, G. H. and Slavkin, H. C. (2000). Positionally-dependent chondrogenesis induced by BMP4 is co-regulated by Sox9 and Msx2. *Dev Dyn* **217**, 401-414.

Sharma, D. C., Pendse, V., Sahay, K. and Soni, B. L. (1991). The changing pattern of maternal and neonatal anemia at Udaipur during 2 decades in relation to poverty, parity, prematurity and vegetarianism. *Asia Oceania J Obstet Gynaecol* **17**, 13-17.

Sharma, S. M., Bronisz, A., Hu, R., Patel, K., Mansky, K. C., Sif, S. and Ostrowski, M. C. (2007). MITF and PU.1 recruit p38 MAPK and NFATc1 to target genes during osteoclast differentiation. *J Biol Chem* **282**, 15921-15929.

Shaw, G., Carmichael, S., Yang, W., Selvin, S. and Schaffer., D. (2004). Periconceptional dietary intake of choline and betaine and neural tube defects in offspring. *Am J Epidemiol* **160**, 102-109.

Shaw, G. M., Carmichael, S. L., Laurent, C. and Rasmussen, S. A. (2006). Maternal nutrient intakes and risk of orofacial clefts. *Epidemiology* **17**, 285-291.

Shaw, G. M., Lammer, E. J., Wasserman, C. R., O'Malley, C. D. and Tolarova, M. M. (1995). Risks of orofacial clefts in children born to women using multivitamins containing folic acid periconceptionally. *Lancet* **346**, 393-396.

Shimmi, O. and O'Connor, M. B. (2003). Physical properties of Tld, Sog, Tsg and Dpp protein interactions are predicted to help create a sharp boundary in Bmp signals during dorsoventral patterning of the Drosophila embryo. *Development* **130**,

4673-4682.

Shimmi, O., Umulis, D., Othmer, H. and O'Connor, M. B. (2005). Facilitated transport of a Dpp/Scw heterodimer by Sog/Tsg leads to robust patterning of the Drosophila blastoderm embryo. *Cell* **120**, 873-886.

Smithells, R. W. and Sheppard, S. (1980). Possible prevention of neural-tube defects by periconceptional vitamin supplementation. *Lancet* **1**, 647.

Soriano, P. (1999). Generalized lacZ expression with the ROSA26 Cre reporter strain. *Nat Genet* **21**, 70-71.

Sotillo Rodriguez, J. E., Mansky, K. C., Jensen, E. D., Carlson, A. E., Schwarz, T., Pham, L., MacKenzie, B., Prasad, H., Rohrer, M. D., Petryk, A. et al. (2009). Enhanced osteoclastogenesis causes osteopenia in twisted gastrulation-deficient mice through increased BMP signaling. *J Bone Miner Res* **24**, 1917-1926.

Spandidos, A., Wang, X., Wang, H. and Seed, B. (2010). PrimerBank: a resource of human and mouse PCR primer pairs for gene expression detection and quantification. *Nucleic Acids Res* **38**, D792-799.

Spensberger, D. and Delwel, R. (2008). A novel interaction between the proto-oncogene Evi1 and histone methyltransferases, SUV39H1 and G9a. *FEBS Lett* **582**, 2761-2767.

Spiegelstein, O., Mitchell, L. E., Merriweather, M. Y., Wicker, N. J., Zhang, Q., Lammer, E. J. and Finnell, R. H. (2004). Embryonic development of folate binding protein-1 (Folbp1) knockout mice: Effects of the chemical form, dose, and timing of maternal folate supplementation. *Dev Dyn* **231**, 221-231.

Spiro, R. G. (2002). Protein glycosylation: nature, distribution, enzymatic formation, and disease implications of glycopeptide bonds. *Glycobiology* **12**, 43R-56R.

Spudich, J. L. and Koshland, D. E., Jr. (1976). Non-genetic individuality: chance in the single cell. *Nature* **262**, 467-471.

Srinivas, S., Watanabe, T., Lin, C. S., William, C. M., Tanabe, Y., Jessell, T. M. and Costantini, F. (2001). Cre reporter strains produced by targeted insertion of EYFP and ECFP into the ROSA26 locus. *BMC Dev Biol* **1**, 4.

Stanier, P. and Moore, G. E. (2004). Genetics of cleft lip and palate: syndromic genes contribute to the incidence of non-syndromic clefts. *Hum Mol Genet* **13 Spec No 1**, R73-81.

Stanley, E., Biben, C., Kotecha, S., Fabri, L., Tajbakhsh, S., Wang, C. C., Hatzistavrou, T., Roberts, B., Drinkwater, C., Lah, M. et al. (1998). DAN is a secreted glycoprotein related to Xenopus cerberus. *Mech Dev* **77**, 173-184.

Stottmann, R., Anderson, R. and Klingensmith, J. (2001). The BMP Antagonists Chordin and Noggin Have Essential but Redundant Roles in Mouse Mandibular Outgrowth. *Developmental Biology* **240**, 457-473.

Stover, P. J. (2004). Physiology of folate and vitamin B12 in health and disease. *Nutr Rev* **62**, S3-12; discussion S13.

Sulik, K. K., Cook, C. S. and Webster, W. S. (1988). Teratogens and craniofacial malformations: relationships to cell death. *Development* **103 Suppl**, 213-231.

Sun, M., Forsman, C., Sergi, C., Gopalakrishnan, R., O'Connor, M. B. and Petryk, A. (2010). The expression of twisted gastrulation in postnatal mouse brain and functional implications. *Neuroscience* **169**, 920-931.

Tanno, T., Porayette, P., Sripichai, O., Noh, S. J., Byrnes, C., Bhupatiraju, A., Lee, Y. T., Goodnough, J. B., Harandi, O., Ganz, T. et al. (2009). Identification of TWSG1 as a second novel erythroid regulator of hepcidin expression in murine and human cells. *Blood* **114**, 181-186.

Tawfik, H. E., Cena, J., Schulz, R. and Kaufman, S. (2008). Role of oxidative stress in multiparity-induced endothelial dysfunction. *Am J Physiol Heart Circ Physiol* **295**, H1736-1742.

Tchantchou, F. (2006). Homocysteine metabolism and various consequences of folate deficiency. *J Alzheimers Dis* **9**, 421-427.

Teitelbaum, S. L. and Ross, F. P. (2003). Genetic regulation of osteoclast development and function. *Nat Rev Genet* **4**, 638-649.

ten Berge, D., Brouwer, A., Korving, J., Martin, J. F. and Meijlink, F. (1998). Prx1 and Prx2 in skeletogenesis: roles in the craniofacial region, inner ear and limbs. *Development* **125**, 3831-3842.

Thomas, T., Kurihara, H., Yamagishi, H., Kurihara, Y., Yazaki, Y., Olson, E. N. and Srivastava, D. (1998). A signaling cascade involving endothelin-1, dHAND and msx1 regulates development of neural-crest-derived branchial arch mesenchyme. *Development* **125**, 3005-3014.

Todoroff, K. and Shaw, G. M. (2000). Prior spontaneous abortion, prior elective termination, interpregnancy interval, and risk of neural tube defects. *Am J Epidemiol* **151**, 505-511.

Tolarova, M. (1982). Periconceptional supplementation with vitamins and folic acid to prevent recurrence of cleft lip. *Lancet* **2**, 217.

Tolarova, M. and Harris, J. (1995). Reduced recurrence of orofacial clefts after periconceptional supplementation with high-dose folic acid and multivitamins. *Teratology* **51**, 71-78.

Tomasini, R., Samir, A. A., Carrier, A., Isnardon, D., Cecchinelli, B., Soddu, S., Malissen, B., Dagorn, J. C., Iovanna, J. L. and Dusetti, N. J. (2003). TP53INP1s and homeodomain-interacting protein kinase-2 (HIPK2) are partners in regulating p53 activity. *J Biol Chem* **278**, 37722-37729.

Tomiya, N., Narang, S., Lee, Y. C. and Betenbaugh, M. J. (2004). Comparing N-glycan processing in mammalian cell lines to native and engineered lepidopteran

insect cell lines. *Glycoconj J* **21**, 343-360.

Tovitto, G. and Rodriguez, A. (2007). Otocefalia, Presentación de dos casos. *Rev Obstet Ginecol Venez* **67**, 275-280.

Trainor, P. A. (2010). Craniofacial birth defects: The role of neural crest cells in the etiology and pathogenesis of Treacher Collins syndrome and the potential for prevention. *Am J Med Genet A* **152A**, 2984-2994.

Tsai, M. J., Weng, C. F., Shyue, S. K., Liou, D. Y., Chen, C. H., Chiu, C. W., Yang, T. H., Pan, H. A., Liao, R. I., Kuo, H. S. et al. (2007). Dual effect of adenovirus-mediated transfer of BMP7 in mixed neuron-glial cultures: neuroprotection and cellular differentiation. *J Neurosci Res* **85**, 2950-2959.

Tsalavos, S., Segklia, K., Passa, O., Petryk, A., O'Connor, M. B. and Graf, D. (2011). Involvement of twisted gastrulation in T cell-independent plasma cell production. *J Immunol* **186**, 6860-6870.

Tsuda, T., Markova, D., Wang, H., Evangelisti, L., Pan, T. C. and Chu, M. L. (2004). Zinc finger protein Zac1 is expressed in chondrogenic sites of the mouse. *Developmental dynamics : an official publication of the American Association of Anatomists* **229**, 340-348.

Tucker, A. S., Matthews, K. L. and Sharpe, P. T. (1998). Transformation of tooth type induced by inhibition of BMP signaling. *Science* **282**, 1136-1138.

Utkus, A., Kazakevicius, R., Ptasekas, R., Kucinskas, V., Beckwith, J. B. and Opitz, J. M. (2001). Human anotocephaly (aprosopus, acrania-synotia) in the Vilnius anatomical collection. *Am J Med Genet* **101**, 163-171.

Varrault, A., Gueydan, C., Delalbre, A., Bellmann, A., Houssami, S., Aknin, C., Severac, D., Chotard, L., Kahli, M., Le Digarcher, A. et al. (2006). Zac1 regulates an imprinted gene network critically involved in the control of embryonic growth. *Developmental cell* **11**, 711-722.

Vieira, A. R. (2004). Birth order and neural tube defects: a reappraisal. *J Neurol Sci* **217**, 65-72.

Vieira, A. R. and Orioli, I. M. (2002). Birth order and oral clefts: a meta analysis. *Teratology* **66**, 209-216.

Vieira, A. R. and Taucher, S. C. (2005). Influence of maternal age on the risk for neural tube defects, a meta analysis. *Revista Medica De Chile* **133**, 62-70.

Vilmos, P., Gaudenz, K., Hegedus, Z. and Marsh, J. L. (2001). The Twisted gastrulation family of proteins, together with the IGFBP and CCN families, comprise the TIC superfamily of cysteine rich secreted factors. *Mol Pathol* **54**, 317-323.

Wacker, M., Linton, D., Hitchen, P. G., Nita-Lazar, M., Haslam, S. M., North, S. J., Panico, M., Morris, H. R., Dell, A., Wren, B. W. et al. (2002). N-linked glycosylation in Campylobacter jejuni and its functional transfer into E. coli.

Science **298**, 1790-1793.

Wagner, D. O., Sieber, C., Bhushan, R., Borgermann, J. H., Graf, D. and Knaus, P. (2010). BMPs: from bone to body morphogenetic proteins. *Sci Signal* **3**, mr1.

Walsh, G. and Jefferis, R. (2006). Post-translational modifications in the context of therapeutic proteins. *Nat Biotechnol* **24**, 1241-1252.

Wang, Y. A., Kamarova, Y., Shen, K. C., Jiang, Z., Hahn, M. J., Wang, Y. and Brooks, S. C. (2005). DNA methyltransferase-3a interacts with p53 and represses p53-mediated gene expression. *Cancer Biol Ther* **4**, 1138-1143.

Waterland, R. A. and Jirtle, R. L. (2003). Transposable elements: targets for early nutritional effects on epigenetic gene regulation. *Mol Cell Biol* **23**, 5293-5300.

Waterland, R. A. and Jirtle, R. L. (2004). Early nutrition, epigenetic changes at transposons and imprinted genes, and enhanced susceptibility to adult chronic diseases. *Nutrition (Burbank, Los Angeles County, Calif)* **20**, 63-68.

Waterland, R. A., Dolinoy, D. C., Lin, J. R., Smith, C. A., Shi, X. and Tahiliani, K. G. (2006). Maternal methyl supplements increase offspring DNA methylation at Axin Fused. *Genesis* **44**, 401-406.

Wehby, G. L. and Murray, J. C. (2010). Folic acid and orofacial clefts: a review of the evidence. *Oral Dis* **16**, 11-19.

Westmoreland, J. J., Takahashi, S. and Wright, C. V. (2007). Xenopus Lefty requires proprotein cleavage but not N-linked glycosylation to inhibit nodal signaling. *Dev Dyn* **236**, 2050-2061.

Whitelaw, E. and Martin, D. I. (2001). Retrotransposons as epigenetic mediators of phenotypic variation in mammals. *Nature Genetics* **27**, 361-365.

Wills, A., Harland, R. M. and Khokha, M. K. (2006). Twisted gastrulation is required for forebrain specification and cooperates with Chordin to inhibit BMP signaling during X. tropicalis gastrulation. *Dev Biol* **289**, 166-178.

Wolff, G. L., Kodell, R. L., Moore, S. R. and Cooney, C. A. (1998). Maternal epigenetics and methyl supplements affect agouti gene expression in Avy/a mice. *FASEB J* **12**, 949-957.

Wong, W. T., Tian, X. Y., Chen, Y., Leung, F. P., Liu, L., Lee, H. K., Ng, C. F., Xu, A., Yao, X., Vanhoutte, P. M. et al. (2010). Bone morphogenic protein-4 impairs endothelial function through oxidative stress-dependent cyclooxygenase-2 upregulation: implications on hypertension. *Circ Res* **107**, 984-991.

Wu, Y. I., Munshi, H. G., Sen, R., Snipas, S. J., Salvesen, G. S., Fridman, R. and Stack, M. S. (2004). Glycosylation broadens the substrate profile of membrane type 1 matrix metalloproteinase. *J Biol Chem* **279**, 8278-8289.

Xie, J. and Fisher, S. (2005). Twisted gastrulation enhances BMP signaling through chordin dependent and independent mechanisms. *Development* **132**, 383-391.

Yamaguchi, K., Akai, K., Kawanishi, G., Ueda, M., Masuda, S. and Sasaki, R. (1991). Effects of site-directed removal of N-glycosylation sites in human erythropoietin on its production and biological properties. *J Biol Chem* **266**, 20434-20439.

Yan, J., Jiang, X., West, A. A., Perry, C. A., Malysheva, O. V., Devapatla, S., Pressman, E., Vermeylen, F., Stabler, S. P., Allen, R. H. et al. (2012). Maternal choline intake modulates maternal and fetal biomarkers of choline metabolism in humans. *Am J Clin Nutr* **95**, 1060-1071.

Ybot-Gonzalez, P., Cogram, P., Gerrelli, D. and Copp, A. J. (2002). Sonic hedgehog and the molecular regulation of mouse neural tube closure. *Development* **129**, 2507-2517.

Yeh, C. H., Chang, C. K., Cheng, M. F., Lin, H. J. and Cheng, J. T. (2009). The antioxidative effect of bone morphogenetic protein-7 against high glucose-induced oxidative stress in mesangial cells. *Biochem Biophys Res Commun* **382**, 292-297.

Yu, K., Srinivasan, S., Shimmi, O., Biehs, B., Rashka, K. E., Kimelman, D., O'Connor, M. B. and Bier, E. (2000). Processing of the Drosophila Sog protein creates a novel BMP inhibitory activity. *Development* **127**, 2143-2154.

Zakin, L. and De Robertis, E. M. (2004). Inactivation of mouse Twisted gastrulation reveals its role in promoting Bmp4 activity during forebrain development. *Development* **131**, 413-424.

Zakin, L., Reversade, B., Kuroda, H., Lyons, K. M. and De Robertis, E. M. (2005). Sirenomelia in Bmp7 and Tsg compound mutant mice: requirement for Bmp signaling in the development of ventral posterior mesoderm. *Development* **132**, 2489-2499.

Zeisel, S. (2009). Importance of methyl donors during reproduction. *Am J Clin Nutr* **89**, 673S-677S.

Zeisel, S. H. and Blusztajn, J. K. (1994). Choline and human nutrition. *Annu Rev Nutr* **14**, 269-296.

Zeisel, S. H., Mar, M. H., Zhou, Z. and da Costa, K. A. (1995). Pregnancy and lactation are associated with diminished concentrations of choline and its metabolites in rat liver. *J Nutr* **125**, 3049-3054.

Zhan, S. Y., Lian, Z. H., Zheng, D. Z. and Gao, L. (1991). Effect of fathers' age and birth order on occurrence of congenital heart disease. *J Epidemiol Community Health* **45**, 299-301.

Zhao, Q., Behringer, R. R. and de Crombrugghe, B. (1996). Prenatal folic acid treatment suppresses acrania and meroanencephaly in mice mutant for the Cart1 homeobox gene. *Nat Genet* **13**, 275-283.

Zhao, Y., Guo, Y. J., Tomac, A. C., Taylor, N. R., Grinberg, A., Lee, E. J., Huang, S. and Westphal, H. (1999). Isolated cleft palate in mice with a targeted mutation of the LIM homeobox gene lhx8. *Proc Natl Acad Sci U S A* **96**, 15002-15006.

Zusman, S. B. and Wieschaus, E. F. (1985). Requirements for zygotic gene activity during gastrulation in Drosophila melanogaster. *Dev Biol* **111**, 359-371.